

# SSRMP Annual Scientific Meeting 2009

University Hospital Basel 19<sup>th</sup> and 20<sup>th</sup> of November 2009



Schweizerische Gesellschaft für Strahlenbiologie und Medizinische Physik  
Société Suisse de Radiobiologie et de Physique Médicale  
Società Svizzera di Radiobiologia e di Fisica Medica  
Swiss Society for Radiobiology and Medical Physics



# **SSRMP Annual Scientific Meeting 2009**

University Hospital Basel 19<sup>th</sup> and 20<sup>th</sup> of November 2009

Abstracts & Proceedings

ISBN 3 908 125 49 9

available on <http://www.sgsmp.ch/2009/proceedings-2009.pdf>

## **Preface**

The Annual Scientific Meeting 2009 of the Swiss Society of Radiobiology and Medical Physics was held in Basel on the 19<sup>th</sup> and 20<sup>th</sup> of November 2009. It was great having so many colleagues and friends from Switzerland and abroad visiting our congress.

The program of the annual meeting was structured into six sessions with five invited talks. As usual we tried to cover the whole range of medical ionizing radiation physics. And once more we also attempted to make a few courageous steps into other fields of medical physics beyond our traditional activities.

We take up the initiative launched last year in Chur and publish the proceedings in electronic form only in the internet and on CD. The sequence of the proceedings as they are published is in accordance with the scientific program of the meeting.

We want to thank all the people that contributed to the success of the meeting, in particular the industrial exhibitors and sponsors for their support and our colleagues for their scientific contributions.

On behalf of the local organizing committee  
Hans W. Roser

# Program

## Thursday November 19<sup>th</sup> 2009

- 9:00 - 10:00 **Registration and Welcome Coffee**
- 10:00 - 10:20 **Welcome and Opening**
- Luca Cozzi (President of SSRMP)
  - Grusswort des Regierungsrates Basel-Stadt, überbracht durch PD Dr. Philipp Hübner, Kantonschemiker Basel-Stadt
  - Hans W. Roser (Conference President)
- 10:20 - 12:00 **Session 1**  
Chairpersons: Anja Stüssi (Bern), Wolf Seelentag (St. Gallen)
- 10:20 - 10:50 **Invited Talk**  
Role change in Medical Physics: Medical Physicists in Diagnostic Radiology and Nuclear Medicine  
*W Zeller, Abteilung Strahlenschutz, Bundesamt für Gesundheit, Bern*
- Topic: Radiation Protection and Dosimetry**
- 10:50 - 11:00 Shielding of Multi-Detector CT rooms: comparison of DIN, NCRP and BIR approaches  
*F R Verdun<sup>1</sup>, A Aroua<sup>1</sup>, S Baechler<sup>1</sup>, Ph R Trueb<sup>2</sup>, F Bochud<sup>1</sup>*  
*<sup>1</sup>University Institute for Radiation Physics (IRA), CHUV - UNIL, Lausanne; <sup>2</sup>Federal Office for Public Health, Bern*
- 11:00 - 11:10 Diagnostic Reference Levels (DRLs) in projection radiography  
*Th Theiler, R Treier, Ph R Trueb*  
*Federal Office of Public Health, Bern*
- 11:10 - 10:20 Clinical Audits - a concept for their implementation in Switzerland  
*R Treier, W Zeller, Ph R Trueb*  
*Federal Office of Public Health, Bern*
- 11:20 - 11:30 Quality Assurance of X-Ray Protection Clothing at the University Hospital Basel  
*D Oppliger-Schäfer, H W Roser*  
*Radiological Physics, University Hospital Basel, Basel*
- 11:30 - 11:40 Radiation therapy dosimetry in Switzerland  
*D Twerenbold*  
*Bundesamt für Metrologie METAS, Wabern*
- 11:40 - 11:50 The first IMRT dosimetry intercomparison of the SGSMP using a thorax phantom with inhomogeneities  
*H Schiefer<sup>1</sup>, G Nicolin<sup>2</sup>, A Fogliata<sup>2</sup>, W W Seelentag<sup>1</sup>, M K Fix<sup>3</sup>*  
*<sup>1</sup>Klinik für Radio-Onkologie, Kantonsspital St. Gallen, St. Gallen; <sup>2</sup>Oncology Institute of Southern Switzerland, Bellinzona; <sup>3</sup>Division of Medical Radiation Physics, Inselspital and University of Bern, Bern*
- 11:50 - 12:00 Discussion
- 12:00 - 13:30 **Lunch and Industrial Exhibition**

## Thursday November 19<sup>th</sup> 2009

### 13:30 - 15:30 **Session 2**

Chairpersons: Ulrike Melnyk (Basel), Peter Manser (Bern)

### 13:30 - 14:00 **Invited Talk**

Transcranial MR-guided High Intensity Focused Ultrasound for Non-Invasive Functional Neurosurgery

*B Werner, MR-Zentrum, Universitäts-Kinderkliniken Zürich, Zürich*

### **Topic: The Scope of Medical Physicist's Activities - from Magnetic Resonance to Antiprotons**

### 14:00 - 14:10 Passive Tracking of the Devices during MR-guided Interventions

*S Patil, O Bieri, K Scheffler*

*Radiological Physics, University Hospital Basel, Basel*

### 14:10 - 14:20 Assessing Extracranial Tumors using Diffusion-Weighted Whole-Body MRI

*C Lenz<sup>1</sup>, M Klarhöfer<sup>1</sup>, K Scheffler<sup>1</sup>, L Winter<sup>2</sup>, G Sommer<sup>2</sup>*

*<sup>1</sup> Radiological Physics, University Hospital Basel, Basel; <sup>2</sup> Department of Radiology, University Hospital Basel, Basel*

### 14:20 - 14:30 What is the Benefit of an Adaptive Statistical Iterative Reconstruction Method over Conventional CT Reconstruction Approaches?

*F Miéville<sup>1</sup>, E Rizzo<sup>2</sup>, F Gudinchet<sup>2</sup>, F Bochud<sup>1</sup>, F R Verdun<sup>1</sup>*

*<sup>1</sup> University Institute for Radiation Physics (IRA), CHUV - UNIL, Lausanne; <sup>2</sup> Radiology Department, CHUV - UNIL, Lausanne*

### 14:30 - 14:40 Mathematical observers applied to breast tomosynthesis

*I Diaz<sup>1</sup>, P Timberg<sup>2</sup>, C Abbey<sup>3</sup>, M Eckstein<sup>3</sup>, F R Verdun<sup>1</sup>, C Castella<sup>1</sup>, F O Bochud<sup>1</sup>*

*<sup>1</sup> University Institute for Radiation Physics (IRA), CHUV - UNIL, Lausanne; <sup>2</sup> Department of Medical Radiation Physics, Lund University, Malmö University Hospital, Malmö, Sweden; <sup>3</sup> Dept. of Psychology, University of California, Santa Barbara, CA, USA*

### 14:40 - 14:50 A novel calibration approach to clinical PET/CT imaging

*T Weitzel<sup>1</sup>, T Beyer<sup>2</sup>, F Corminboeuf<sup>1</sup>, T Krause<sup>1</sup>*

*<sup>1</sup> University Clinic for Nuclear Medicine, Inselspital and University of Bern, Bern; <sup>2</sup> cmi-experts GmbH, Pestalozzistr. 3, Zürich*

### 14:50 - 15:00 The influence of the bow tie filtration on the dose and image quality for the Elekta XVI coneBeam CT

*L Wissmann<sup>1</sup>, S Peters<sup>2</sup>, W W Seelentag<sup>2</sup>*

*<sup>1</sup> Department of Physics, ETH Zürich, Zürich, <sup>2</sup> Klinik für Radio-Onkologie, Kantonsspital St. Gallen, St. Gallen*

### 15:00 - 15:10 Recurrence landscapes of uterine cervix carcinoma - A 3-D analysis of topography and spatial frequency distribution

*U-D Braumann<sup>1</sup>, J Einenkel<sup>2</sup>, N Manthey<sup>2</sup>, U Wolf<sup>3</sup>, G Hildebrandt<sup>3</sup>, A Liebmann<sup>3</sup>, M Höcke<sup>2</sup>*

*<sup>1</sup> Interdisziplinäres Zentrum für Bioinformatik, Universität Leipzig, Leipzig, Germany; <sup>2</sup> Universitäts-frauenklinik (Triersches Institut), Universität Leipzig, Leipzig, Germany; <sup>3</sup> Klinik und Poliklinik für Strahlentherapie, Universität Leipzig, Leipzig, Germany*

### 15:10 - 15:20 AD-4 / ACE: Antiproton Cell Experiment

*P Weber<sup>1,2</sup>*

*<sup>1</sup> Service de radiothérapie du DPO, Hôpital neuchâtelois HNE, La Chaux-de-Fonds; <sup>2</sup> PH Division, CERN, Geneva*

### 15:20 - 15:30 Discussion

### 15:30 - 16:00 **Coffee Break and Industrial Exhibition**

### 16:00 - 17:15 **Annual General Assembly SSRMP**

### 17:15 - 18:00 **SSRMP-SPAMP Joint Session**

### 18:30 - 19:30 **Visit to Pharmazie-Historisches Museum Basel**

### 20:00 **Social Evening and Dinner at "Job Factory"**

## Friday November 20<sup>th</sup> 2009

### 9:00 - 10:20 **Session 3**

Chairpersons: Regina Müller (Villigen PSI), Raphaël Moeckli (Lausanne)

### 9:00 - 9:30 **Invited Talk**

Speedy vs. conformal: Multi-objective tradeoffs in IMRT and VMAT  
*T Bortfeld, Massachusetts General Hospital, Boston, USA*

### **Topic: IMRT, Electrons and Monte Carlo Simulation**

9:30 - 9:40 Independent 2D dose calculation of IMRT fields using MapCALC  
*A-C Schulte, M Fix, P Manser, R Mini, D Terribilini, D Vetterli, D Frauchiger*  
*Division of Medical Radiation Physics, Inselspital and University of Bern, Bern*

9:40 - 9:50 Influence of an Air Gap between Bolus and Patient Skin on Electron Beam Dose Characteristics

*G Kohler,*  
*Institut für Radioonkologie, Universitätsspital Basel, Basel*

9:50 - 10:00 Low energy electron beam dose calculation using eMC  
*M K Fix<sup>1</sup>, D Frei<sup>1</sup>, W Volken<sup>1</sup>, H Neuenschwander<sup>2</sup>, E J Born<sup>1</sup>, P Manser<sup>1</sup>*  
*<sup>1</sup> Division of Medical Radiation Physics, Inselspital and University of Bern, Bern; <sup>2</sup> Clinic for Radiation-Oncology, Lindenhofspital, Bern*

10:00 - 10:10 Monte Carlo Dose Calculation on Deforming Anatomy  
*M Peterhans<sup>1</sup>, P Manser<sup>2</sup>, D Frei<sup>2</sup>, M K Fix<sup>2</sup>*  
*<sup>1</sup>Institute for Surgical Technology and Biomechanics ISTB, University of Bern, Bern; <sup>2</sup>Division of Medical Radiation Physics, Inselspital and University of Bern, Bern*

10:10 - 10:20 Discussion

### 10:20 - 10:50 **Coffee Break and Industrial Exhibition**

### 10:50 - 12:00 **Session 4**

Chairpersons: Jatta Berberat (Aarau), Ernst Born (Bern)

### 10:50 - 11:20 **Invited Talk**

Molecular Imaging: State of the Art and Future Directions  
*J Prior, Service de Médecine Nucléaire, CHUV - UNIL, Lausanne*

### **Topic: Monte Carlo Simulation (continued)**

11:20 - 11:30 Dose Calculation for Orthovoltage Radiotherapy using Swiss Monte Carlo Plan  
*D Frauchiger, D Terribilini, B Isaak, P Manser, D Frei, W Volken, M K Fix*  
*Division of Medical Radiation Physics, Inselspital and University of Bern, Bern*

11:30 - 11:40 Investigation of 6 MV static beams within the Swiss Monte Carlo Plan  
*V Magaddino<sup>1,2</sup>, P Manser<sup>2</sup>, D Frei<sup>2</sup>, W Volken<sup>2</sup>, D Schmidhalter<sup>2</sup>, L Hirsch<sup>2</sup>, M K Fix<sup>2</sup>*  
*<sup>1</sup>University of Naples "Federico II", and INFN, Naples, Italy; <sup>2</sup>Division of Medical Radiation Physics, Inselspital and University of Bern, Bern*

11:40 - 11:50 Validation of a Monte Carlo model for peripheral dosimetry and dose calculations in a full-body voxelised phantom with regards to secondary cancers  
*A Joosten<sup>1</sup>, F Levi<sup>2</sup>, S Baechler<sup>1</sup>, O Matzinger<sup>3</sup>, W Jeanneret-Sozzi<sup>3</sup>, R-O Mirimanoff<sup>3</sup>, F Bochud<sup>1</sup>, R Moeckli<sup>1</sup>*  
*<sup>1</sup>University Institute for Radiation Physics (IRA), CHUV - UNIL, Lausanne; <sup>2</sup>Cancer Epidemiology Unit and Cancer Registries of Vaud and Neuchâtel, Institute of Social and Preventive Medicine, CHUV, Lausanne; <sup>3</sup>Department of Radiation Oncology, CHUV, Lausanne*

11:50 - 12:00 Discussion

### 12:00 - 13:15 **Annual General Assembly SPAMP**

### 13:15 - 13:50 **Lunch (sponsored by SPAMP) and Industrial Exhibition**

## Friday November 20<sup>th</sup> 2009

### 13:50 - 14:50 Session 5 - Poster Presentations

Chairpersons: Shelley Bulling (Genève), Roman Menz (Basel)

13:50 - 13:55 Interventional radiology: management of high patient dose procedures

P 1

*E T Samara<sup>1</sup>, A Aroua<sup>1</sup>, P Bize<sup>2</sup>, S Binaghi<sup>2</sup>, F R Verdun<sup>1</sup>*

*<sup>1</sup>University Institute for Radiation Physics (IRA), CHUV - UNIL, Lausanne; <sup>2</sup>Department of Radiology, CHUV - UNIL, Lausanne*

13:55 - 14:00 Exposure of the Swiss population from radiological examinations: a prospective study to estimate the examination frequency

P 2

*R Le Coultré<sup>1</sup>, R Schnyder<sup>2</sup>, S Coendoz<sup>3</sup>, E Samara<sup>2</sup>, A Aroua<sup>2</sup>, F Bochud<sup>2</sup>, F R Verdun<sup>2</sup>*

*<sup>1</sup>School of Health Sciences - Technique in medical radiology, HES-SO / University of Applied Sciences Western Switzerland, Lausanne; <sup>2</sup>University Institute for Radiation Physics (IRA), CHUV - UNIL, Lausanne; <sup>3</sup>Department of Radiology, CHUV - UNIL, Lausanne*

14:00 - 14:05 Comparison of image quality between a digital panorama X-ray unit with a CdTe-CMOS detector and panorama X-ray units with other types of digital detectors

P 3

*S Scheidegger*

*Centre for Applied Mathematics and Physics, Zurich University of Applied Sciences, Winterthur*

14:05 - 14:10 Qualification of PET-CT scanners for use in SAKK 56/07 multicentre trial

P 4

*F Camus<sup>1,2</sup>, J O Prior<sup>2</sup>, G Allenbach<sup>2</sup>, L Modolo<sup>1,2</sup>, T Hany<sup>4</sup>, J Müller<sup>5</sup>, J Coulot<sup>6</sup>, A Bischof Delaloye<sup>2</sup>, S Leyvraz<sup>3</sup>, M Montemurro<sup>3</sup>, F R Verdun<sup>1</sup>*

*<sup>1</sup>University Institute for Radiation Physics (IRA), CHUV - UNIL, Lausanne; <sup>2</sup>Nuclear Medicine, CHUV - UNIL, Lausanne; <sup>3</sup>Lausanne Cancer Centre, CHUV - UNIL, Lausanne; <sup>4</sup>Klinik für Nuklearmedizin, Universitätsspital Zürich, Zürich; <sup>5</sup>Nuklearmedizin, Kantonsspital St. Gallen, St. Gallen; <sup>6</sup>Médecine Nucléaire, Institut de Cancérologie Gustave Roussy, Villejuif, France*

14:10 - 14:15 Understanding tumour dynamics in vivo: The potential of kinetic models in radio-oncology

P 5

*S Scheidegger<sup>1</sup>, G Lutters<sup>2</sup>, S Bodis<sup>2</sup>*

*<sup>1</sup>Centre for Applied Mathematics and Physics, Zurich University of Applied Sciences, Winterthur; <sup>2</sup>Institut für Radioonkologie, Kantonsspital Aarau, Aarau*

14:15 - 14:20 Volumetric modulated arc therapy in stereotactic body radiation therapy for metastases to abdominal lymph-nodes

P 6

*L Cozzi<sup>2</sup>, M Bignardi<sup>1</sup>, A Fogliata<sup>2</sup>, G Nicolini<sup>2</sup>, E Vanetti<sup>2</sup>, A Clivio<sup>2</sup>, M Scorsetti<sup>1</sup>*

*<sup>1</sup>Istituto Clinico Humanitas, Rozzano, Italy; <sup>2</sup>Oncology Institute of Southern Switzerland, Bellinzona*

14:20 - 14:25 First year of clinical rapidarc treatments at iosi: status report

P 7

*A Fogliata, G Nicolini, E Vanetti, A Clivio, A Richetti, L Cozzi*

*Oncology Institute of Southern Switzerland, Bellinzona*

14:25 - 14:30 Hippocampal avoidance with rapid arc and helical tomotherapy for base of skull tumors

P 8

*A Clivio<sup>1</sup>, S Yartsev<sup>2</sup>, A Fogliata<sup>1</sup>, E Vanetti<sup>1</sup>, G Nicolini<sup>1</sup>, L Cozzi<sup>1</sup>*

*<sup>1</sup>Oncology Institute of Southern Switzerland, Bellinzona; <sup>2</sup>London Regional Cancer Program, London, Canada*

14:30 - 14:35 Pre-treatment verification of RapidArc treatment plans: comparison between Epiqa and Seven29 2D ion chamber array with Octavius phantom

P 9

*J Hrbacek, M Zamburlini, J Krayenbühl, S Klöck*

*Abteilung für Medizinphysik, Klinik für Radio-Onkologie, Universitätsspital Zürich, Zürich*

14:35 - 14:40 QA for rapid arc treatment using the SGSMP IMRT - dose intercomparison facility

P 10

*K Loewenich<sup>1</sup>, J Hrbacek<sup>1</sup>, H Schiefer<sup>2</sup>, T Streller<sup>1</sup>, J Krayenbühl<sup>1</sup>, S Klöck<sup>1</sup>*

*<sup>1</sup>Abteilung für Medizinphysik, Klinik für Radio-Onkologie, Universitätsspital Zürich, Zürich; <sup>2</sup>Klinik für Radio-Onkologie, Kantonsspital St. Gallen, St. Gallen*

14:40 - 14:50 Discussion

## Friday November 20<sup>th</sup> 2009

14:50 - 16:40 **Session 6**

Chairpersons: Maria M. Aspradakis (Chur), Daniel Vetterli (Biel)

14:50 - 15:20 **Invited Talk**

Modern QA in Radiation Therapy

G Lutters, Institut für Radioonkologie, Kantonsspital Aarau, Aarau

**Topic: Treatment Planning, RapidArc, Tomotherapy and Quality Assurance**

15:20 - 15:30 Absorption measurements for a carbon fibre couch top and its modelling in a treatment planning system

*G Kunz, F Hasenbalg, P Pemler*

*Klinik für Radio-Onkologie und Nuklearmedizin, Stadtspital Triemli Zürich*

15:30 - 15:40 On the impact of treatment couch modelling on rapidarc

*E Vanetti, A Clivio, A Fogliata, G Nicolini, L Cozzi*

*Oncology Institute of Southern Switzerland, Bellinzona*

15:40 - 15:50 Implementing RapidArc on the Novalis Tx

*P Manser<sup>1</sup>, E J Born<sup>1</sup>, D Schmidhalter<sup>1</sup>, D Aebersold<sup>2</sup>, R Mini<sup>1</sup>, M K Fix<sup>1</sup>*

*<sup>1</sup>Division of Medical Radiation Physics, Inselspital and University of Bern, Bern; <sup>2</sup>University Clinic for Radio-Oncology, Inselspital and University of Bern, Bern*

15:50 - 16:00 Quality assurance of RapidArc treatments with portal dosimetry: multicentric clinical practice experience

*G Nicolini<sup>1</sup>, A Clivio<sup>1</sup>, E Vanetti<sup>1</sup>, A Fogliata<sup>1</sup>, G Urso<sup>2</sup>, P Fenoglietto<sup>3</sup>,*

*E Parietti<sup>4</sup>, J Hrbacek<sup>5</sup>, S Kloeck<sup>5</sup>, L Cozzi<sup>1</sup>*

*<sup>1</sup>Oncology Institute of Southern Switzerland, Bellinzona; <sup>2</sup>Istituto Clinico Humanitas, Radiation Oncology, Rozzano, Italy; <sup>3</sup>CRLC Val d'Aurelle-Paul Lamarque Montpellier, France; <sup>4</sup>Istituti Ospedalieri di Cremona, Italy; <sup>5</sup>Radiation Oncology Dept., University Hospital Zurich, Zurich*

16:00 - 16:10 Reliability and use of the HiArt detector for 3D dose reconstruction in tomotherapy

*K Schombourg, F O Bochud, R Moeckli*

*University Institute for Radiation Physics (IRA), CHUV - UNIL, Lausanne*

16:10 - 16:20 How sensitive is the collapsed plan?

*J Hrbacek<sup>1</sup>, J Bocanek<sup>2</sup>, T Dossenbach<sup>1</sup>, G Nicolini<sup>3</sup>, A Fogliata<sup>3</sup>, S Klöck<sup>1</sup>*

*<sup>1</sup>Klinik für Radio-Onkologie, Universitätsspital Zürich, Zürich; <sup>2</sup>Varian Medical Systems, Zug; <sup>3</sup>Oncology Institute of Southern Switzerland, Bellinzona*

16:20 - 16:30 Improving the QA for geometric accuracy for stereotactic radiotherapy with a Linac

*H Petermann*

*Institut für Radioonkologie, Universitätsspital Basel, Basel*

16:30 - 16:40 Discussion

16:40 **End of Meeting**

# Diagnostic Reference Levels (DRLs) in projection radiography

Th. Theiler<sup>1</sup>, B. Ott<sup>1</sup>, R. Treier<sup>1</sup>, Ph. R. Trueb<sup>1</sup>

<sup>1</sup>Federal Office of Public Health, Bern

mail: [thomas.theiler@bag.admin.ch](mailto:thomas.theiler@bag.admin.ch)

## Introduction

Standard radiology procedures in projection radiography (plain film or digital equipment) account for 48% of the total number of examinations in diagnostic radiology and contribute 41% to the collective dose [1]. This implies that justification and optimization is not only important for high-dose applications like computed tomography or fluoroscopy but also for projection radiography. One of the main targets with the introduction of the DRL concept is to investigate situations, where patient doses are unusually high. Thus, DRLs provide a valuable method for dose optimization processes [2]. With the aim to establish and ‘familiarize’ the published reference levels and to customize them into national DRLs, a nationwide survey of applied patient dose in projection radiography was performed. The complete analysis of the study will be compared with an international compilation of DRLs in common radiography [3].

## Material and Methods

The quantity of interest in routine measurements of the patient dose in projection radiography is the Entrance Surface Dose (ESD). 38 hospital radiology departments evenly distributed across Switzerland were involved in the survey. Because plain film radiography has fully been replaced by digital radiography systems, the scope of the units was limited to non film-screen equipment (CR or DR). – For each institute, three types of common radiographs were evaluated (chest, lumbar spine and pelvis in ap or pa projection). The geographic allocation is represented as follows: 24 of the participating institutes are located in the german speaking part, 11 in the french speaking part and 3 institutes in the italian speaking part of Switzerland.

For the determination of the Entrance Surface Dose on the table ( $ESD_{Table}$ ), a calibrated X-ray multimeter (Barracuda, RTI Electronics, Mölndal, Sweden), equipped with a solid state detector (R-100B) was used.

First, the local tube output  $K_L$  of the unit was calculated by measuring the  $ESD_{Table}$ , using the equation (1). Thereafter, using the equation (2), the ESD was calculated for standard patients by applying the calculated local tube output, the used exposition parameters tube voltage, tube current and focus-skin-distance, and a well accepted backscatter factor (BSF) of 1.35 [1, 5].

$$(1) \quad K_L = ESD_{Table} \cdot \left(\frac{100}{U}\right)^2 \cdot \left(\frac{1}{Q}\right) \cdot FDD^2 \cdot \left(\frac{1}{f}\right)$$

$$(2) \quad ESD = K_L \cdot \left(\frac{U}{100}\right)^2 \cdot Q \cdot \left(\frac{1}{FOD}\right)^2 \cdot BSF$$

$K_L$  = characteristic constant of the tube (tube output), including filtration [ $mGy \cdot m^2 \cdot mAs^{-1}$ ]

$U$  = tube voltage [kV]

$Q$  = tube current [mAs]

$FOD$  = focus-skin-distance [m]

$FDD$  = focus-detector-distance [m]

$BSF$  = backscatter factor (1.35)

$f$  = intrinsic scatter factor of solid state detector (1.15)

The distribution of the ESD values (mean, minimum, maximum, 25<sup>th</sup> percentile, 75<sup>th</sup> percentile) was calculated for each unit and examination and compared to the current published DRLs, which are based on the European directive [4, 6]. National DRLs will subsequently be adapted, if necessary.

## Results

An overall data amount of total 38 institutes was analysed. The final results showed that the derived ESD values are far below the existing DRLs (*Fig. 1*). For the chest region, the 75<sup>th</sup> percentile of the ESD distribution amounts 0.16 mGy (53.3% of the DRL which is 0.3 mGy). For the pelvis, the calculated 75<sup>th</sup> percentile of the ESD distribution is 3.19 mGy (31.9% of 10 mGy) and the lumbar spine shows a 75<sup>th</sup> percentile of 6.58 mGy (65.8% of 10 mGy).

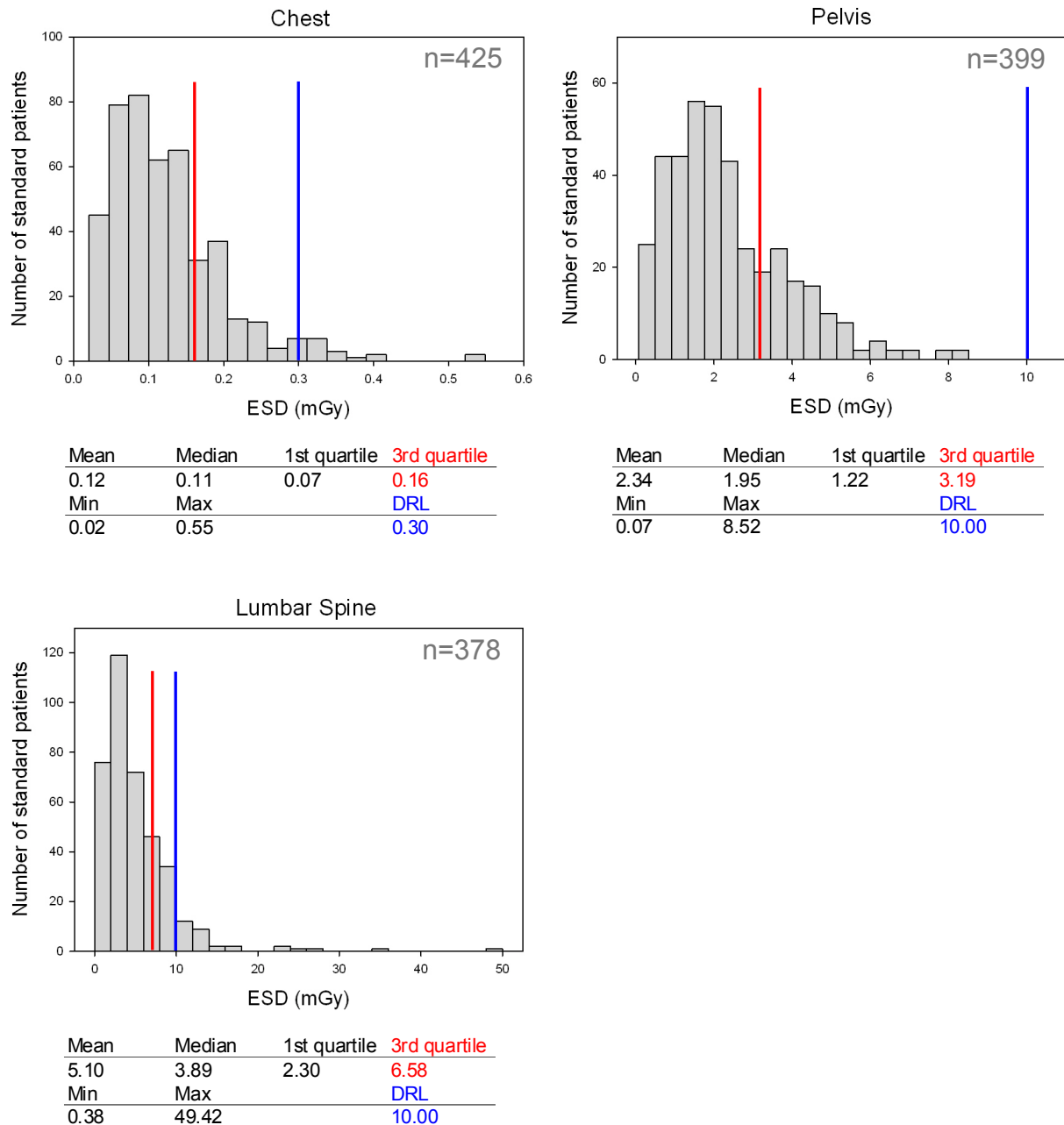


*Fig. 1.* Statistics of the three explored organ regions. The existing DRLs and the 75<sup>th</sup> percentiles of the study are represented by blue and red vertical lines, respectively.

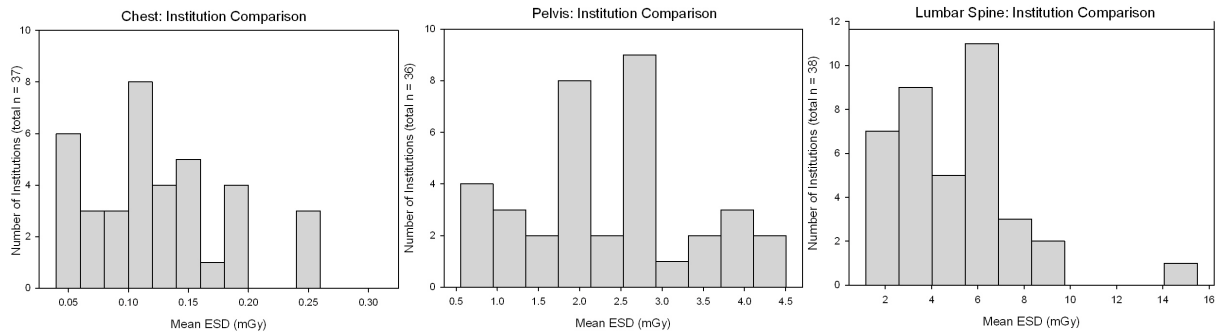


Fig. 2. Distribution histograms of the mean ESD values (institution comparison)

In the institution comparison (Fig. 2) a wide distribution of the mean ESD values was observed for all three organ regions (chest 0.05-0.25 mGy, pelvis 0.5-4.5 mGy, lumbar spine 1-15 mGy).

A combined illustration of both the inter-institutional comparison between CR and DR image receptor systems and the ranking of the calculated mean ESD values of all institutions is shown in Fig. 3. It is obvious, that the majority of the DR-systems (green bars) are in a significant lower dose range than the CR receptors (blue bars). The reason for this is based on the intrinsic lower dose requirements of DR-systems as a result of the higher detective quantum efficiency (DQE).

### Discussion

The results showed a significant potential of reducing entrance surface doses for patients in typical diagnostic imaging situations.

One of the reasons for the remarkably lower values of the 75<sup>th</sup> percentiles in this survey (compared to the existing DRLs) is explained by the high optimization potential of digital imaging modalities (particularly with direct radiography systems as mentioned above). In several places an optimization of the image receptor doses ( $K_B$ -values) was recommended. This request can be achieved by adapting the local AEC switch-off doses (organ-related automatic exposure control) of the unit.

According to the actual analysis, the present results will allow to reduce the national diagnostic reference levels significantly (approximately by a factor 1.5-2 for chest and lumbar spine and even by a factor of 3 for pelvis). To validate the results for the other organ regions where DRLs have been published, an additional small study was launched (including chest lateral and lumbar spine lateral).

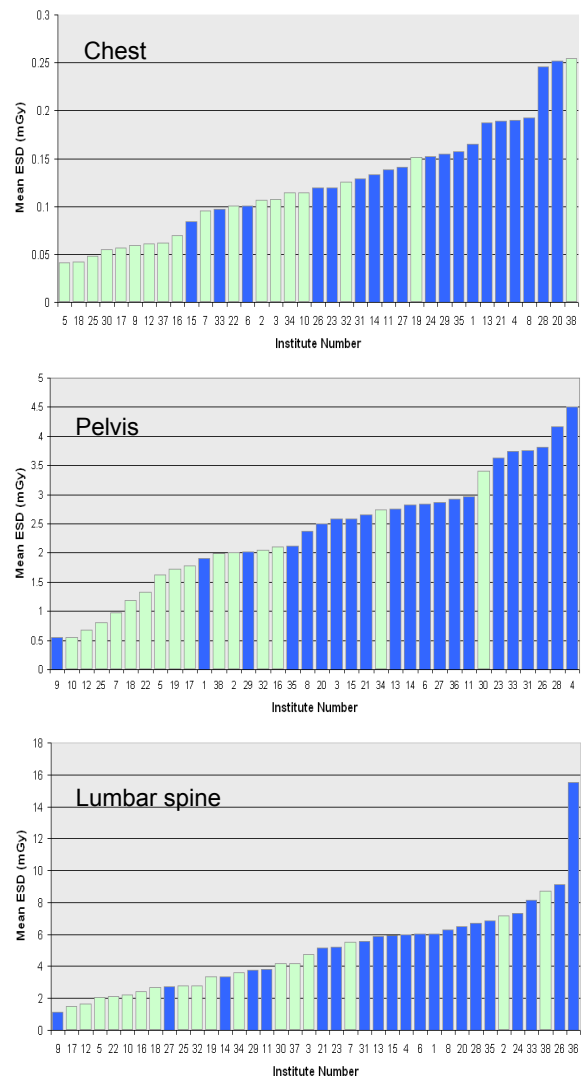


Fig. 3. Ranking and CR/DR comparison  
 blue: CR-systems  
 computed radiography (storage plates)  
 green: DR-systems  
 direct radiography systems (flatpanel detectors)

The main objective of optimization procedures is to achieve diagnostic image quality using appropriate patient doses (according to ALARA). The introduction of new techniques should involve radiologists, medical physicists and radiographers to establish QA- and dose management programmes. The survey has shown that DRLs can act as effective comparison indicators for patient dose management in the field of projection radiography, helping to avoid unnecessary high doses.

## References

- [1] Aroua A.; Vader J.P.; Valley J.F.: A survey on exposure by radiodiagnostics in Switzerland in 1998. Lausanne IRA/IMSMP (2000), pp. 44-45.
- [2] Guidance on the Establishment and Use of Diagnostic Reference Levels for Medical X-Ray Examinations. IPEM Report 88. York UK (2004).
- [3] Hart D.; Hillier M.C.; Wall B.F.: National reference doses for common radiographic, fluoroscopic and dental X-ray examinations in the UK. BJR, (January 2009), Table 7, p. 11.
- [4] BAG-Weisung R-06-04: Diagnostische Referenzwerte (DRW) in der Radiologie. Bern, BAG (2006)
- [5] Roth J.; Strahlenschutz in der Medizin. 1. Aufl., Bern, Verlag Hans Huber (2008) p. 43.
- [6] European Commission; Radiation protection 109, Guidance on diagnostic reference levels (DRLs) for medical exposures. Luxembourg (1999).

# Clinical audits – a concept for their implementation in Switzerland

R. Treier<sup>1</sup>, W. Zeller<sup>1</sup>, Ph. R. Trueb<sup>1</sup>

<sup>1</sup>Abteilung Strahlenschutz, Bundesamt für Gesundheit, Bern

Email: [reto.treier@bag.admin.ch](mailto:reto.treier@bag.admin.ch)

## Introduction

The use of ionizing radiation in medicine has increased enormously in the past few years. Annually worldwide, more than 3'600 million X-ray examinations are performed, more than 37 million nuclear medicine procedures are carried out and more than 7.5 million cancer patients are treated by radiotherapy [1]. Due to these impressive numbers and the fact that there exist no dose limits for patients it is of particular importance to fulfil the two basic principles of radiation protection – justification and optimization. While in the past much effort has been made to optimize radiological procedures, the aspect of justification has been almost completely neglected. This is critical since recent publications have shown that up to one third of all diagnostic examinations are not justified [2, 3]. The International Atomic Energy Agency (IAEA) estimates a dose reduction of 50 % by eliminating all unjustified radiological procedures.

Clinical Audits allow a systematic and continuous assessment of processes in diagnostic radiology, nuclear medicine, and radiotherapy that are performed during the clinical pathway of a patient. Thereby, unjustified processes are identified and eliminated and justified processes are optimized. This finally results in a substantial improvement in patient care and a reduction of both patient doses and health care costs. Since 1997, the member states of the European Union are obliged to carry out Clinical Audits in accordance with their national procedures [4]. To provide guidance on how to implement Clinical Audits in practice a guideline was developed by a project team consisting of members of different professional radiological associations and from different countries [5]. In Switzerland, Clinical Audits are not yet statutory but will be implemented in the fully revised legislation on radiation protection. In the meantime, Switzerland adopts international recommendations and guidelines.

The aim of this project is to develop a concept for the implementation of Clinical Audits in Switzerland.

## Material and Methods

The organizational structure of Clinical Audits in Switzerland is illustrated in Figure 1. The key position in that organization is filled by a group of experts. These experts are representatives of the stakeholders involved in the radiological processes such as radiologists, nuclear medicine professionals, radio-oncologists, medical physicists, radio-pharmacists, radiographers, and members of insurers and patient organizations. The group of experts is provided with the required authority by the Federal Office of Public Health (FOPH). Its tasks are manifold: to define the guidelines for good clinical practice, to plan and coordinate audit programs and to instruct and advise the auditors.

In practice, Clinical Audits are carried out by a team of auditors or by a professional audit company. Auditors should ideally be qualified, experienced and independent of the audited hospital. The formation of the team and the total duration of the audit depend on the complexity of the process to be audited. Typically, an audit lasts 2-5 days and covers the overall assessment of the radiological procedure. Data are collected and treated as strictly confidential since confidence is a basic prerequisite for a successful audit. The results together with recommendations of potential optimization methods will be summarized in a report which is presented and discussed at the end of

the audit with the representatives of the hospital. The report will also be sent to the group of experts and the FOPH for their information. Potential requirements concerning the optimization methods must be fulfilled by the hospital within a certain deadline. The FOPH only regulates in case of disagreement.

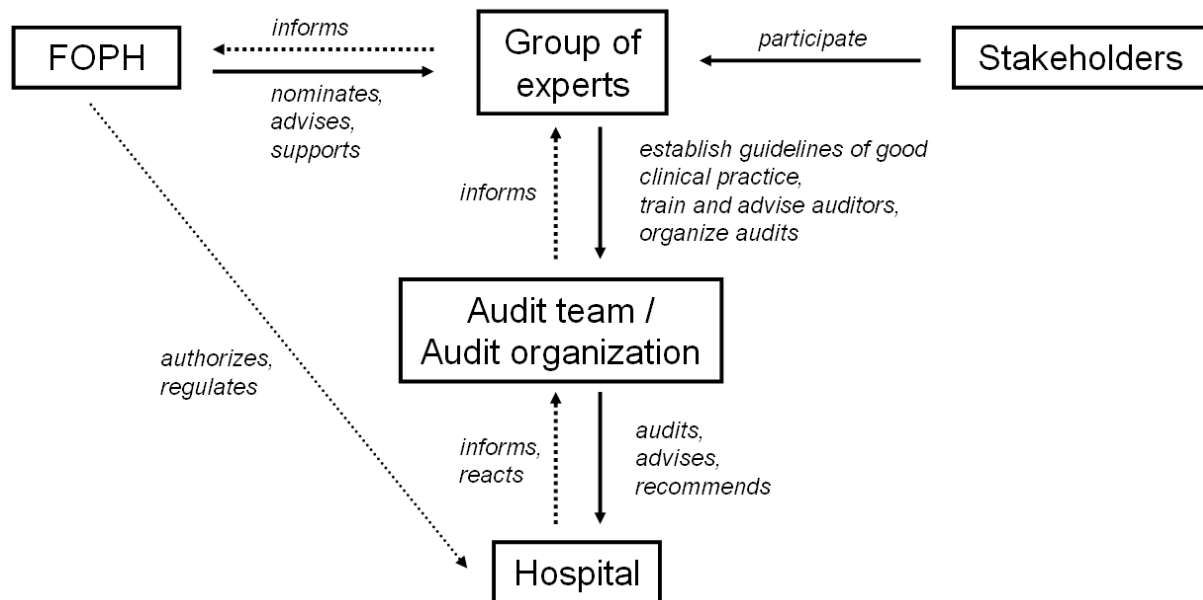


**Figure 1.** Schematic representation of the Clinical Audit organization. Audits are organized by a group of experts and carried out by an audit team or a professional audit company. The Federal Office of Public Health (FOPH) regulates only if needed.

## Results

A successful implementation of Clinical Audits in Switzerland results in an Audit cycle as shown in Figure 2. An audit cycle always starts with the selection of the radiological process of interest according to specific criteria, for example processes with high potential for quality improvement, processes generating high doses, risks, or costs, or processes with existing guidelines. After the process has been selected, standards of good clinical practice must be defined by the group of experts. Thereby, already existing guidelines and recommendations of professional associations could provide a basis for Switzerland. When the audit was performed and the data collected the results are compared with the standards. In case of serious deviations from the standards recommendations are proposed to optimize the radiological process. A plan of action is developed describing the responsibilities and tasks. After a certain time period of less than five years the process will be re-audited. If in the meantime the local practice has changed this must be taken into account by modifying the standards of good clinical practice. Ultimately, with each audit cycle, quality in patient care improves.

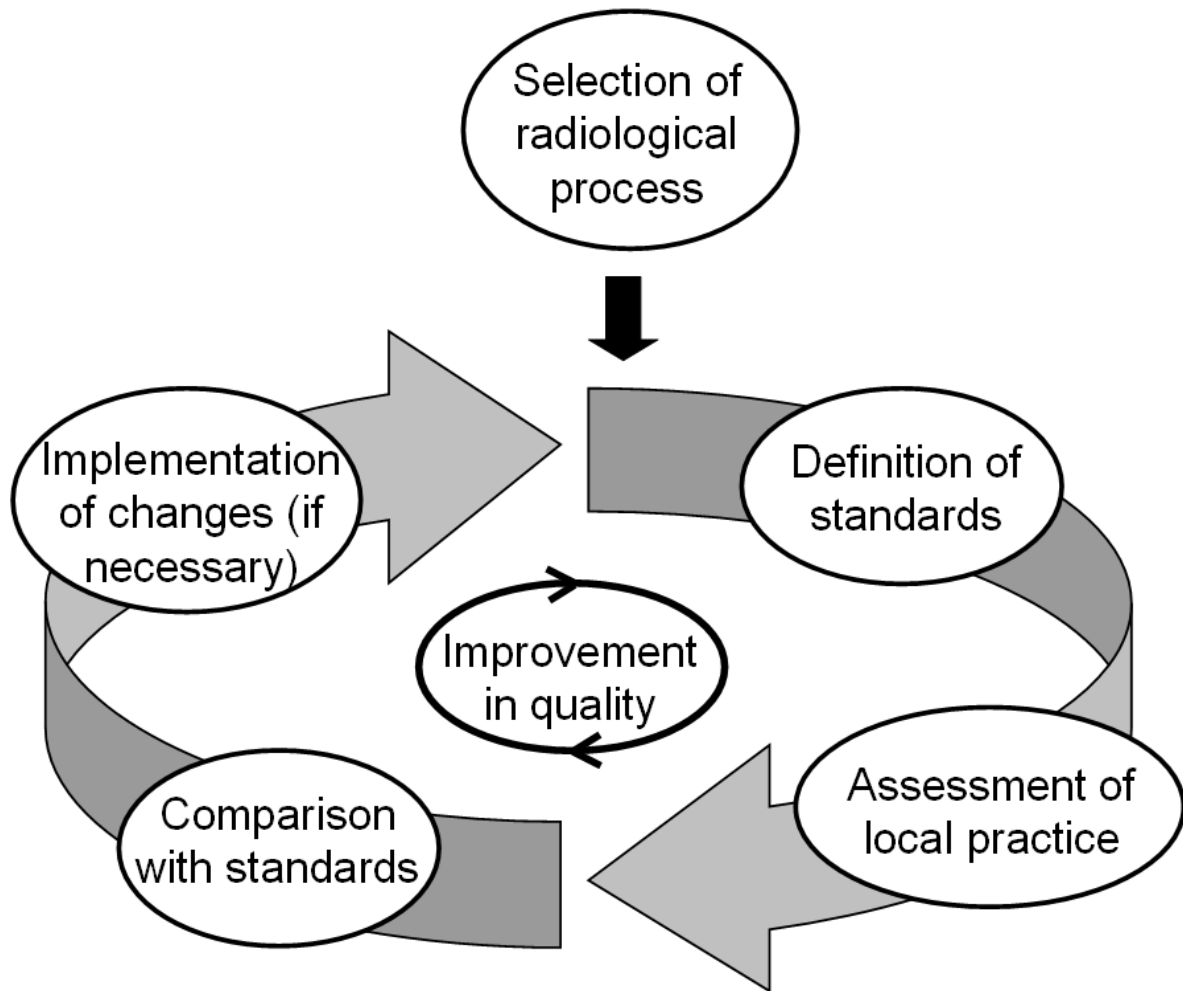


**Figure 2.** Audit cycle consisting of the selection of a specific radiological process together with the definition of the guidelines for good clinical practice, assessment of the local practice, comparison with the standards, implementation of changes when necessary, and re-auditing after a certain time.

## Discussion

The continuous increase in the frequency of medical radiological examinations using ionizing radiation (and thus the rise of accumulated patient doses and health care costs) pose a big challenge to all the involved stakeholders. Clinical Audits prove to be an essential tool to increase significantly quality in patient care by identifying and eliminating unjustified radiological processes and optimizing justified radiological processes. However, a successful implementation in Switzerland is only feasible if hospitals are aware of this problem and are willing to participate constructively in Clinical Audits. In times of increased competition between hospitals it is in their own interest to provide the best possible quality in patient care.

## References

- [1] World Health Organization: WHO Global Initiative on Radiation Safety in Health Care Settings, 2009. [http://www.who.int/ionizing\\_radiation/about/med\\_exposure/en/index.html](http://www.who.int/ionizing_radiation/about/med_exposure/en/index.html)

- [2] Swedish Radiation Safety Authority: National Survey on Justification of CT-examinations in Sweden, 2009.
- [3] America's Health Insurance Plans: Ensuring Quality through Appropriate Use of Diagnostic Imaging, 2008.
- [4] European Commission: Energy Directives EURATOM, 1997/0043.  
[http://ec.europa.eu/energy/infringements/directives/euratom\\_en.htm](http://ec.europa.eu/energy/infringements/directives/euratom_en.htm)
- [5] European Commission: European Commission guidelines on clinical audits for medical radiological practices (diagnostic radiology, nuclear medicine and radiotherapy), 2009.

# Shielding of Multi-Detector CT rooms : comparison of DIN, NCRP and BIR approaches

F.R. Verdun<sup>1</sup>, A. Aroua<sup>1</sup>, S. Baechler<sup>1</sup>, P.R. Trueb<sup>2</sup>, F. Bochud<sup>1</sup>,

<sup>1</sup>University Institute for Radiation Physics (IRA), CHUV –UNIL, Lausanne

<sup>2</sup>Federal Office for Public Health, Radiological Protection Division, Bern

mail: [francis.verdun@chuv.ch](mailto:francis.verdun@chuv.ch)

## Introduction

When designing the proper shielding of a CT room, the accurate determination of the spatial distribution of scattered radiation is necessary and various models have been proposed and of particular interest are the models proposed by the US National Council on Radiation Protection and Measurements (NCRP)<sup>1</sup>, the German Institute for Standardization (DIN)<sup>2</sup> and the British Institute of Radiology and Institute of Physics in Engineering in Medicine (BIR-IPEM)<sup>3</sup>. The aim of this work is to compare the DIN model (thus the formalism used in Switzerland) with the NCRP and BIR-IPEM models, to investigate the limits of using the tube loading in mA.min as the working parameter for new CT units and to explore the appropriateness of using the DLP instead

## Material and Methods

Dose measurements were performed on a 64-detector row CT system (VCT, GEMS, Milwaukee, WI) at the Lausanne University Hospital (CHUV). Two CTDI test objects ( $\varnothing 32$  cm and  $\varnothing 16$ ) were scanned in helical mode. The ambient dose equivalent,  $H^*(10)$ , was measured at various distances from the isocenter of the CT unit at various angles to establish an isodose cartography. Following this experiment, ten sets of thermoluminescent dosimeters (LiF 100 TDLs) were placed for two weeks at various positions in the three rooms where a CT is present (two CT units used for elective examinations (a 64-detector row and 8-detector row CT system (respectively Lightspeed and VCT from GEMS) and one CT used for emergency situations running 24 hours a day, a 64-detector row CT system VCT, GEMS) in order to measure the ambient dose delivered in a two-week period representing the normal use of the CT units.

## Results

The NCRP model differs from the DIN model by a factor of about five leading to a large overestimation of the shielding estimation when using the DIN approach.

## Discussion

In Switzerland, the tube loading needed for a CT slice, expressed in mA.min, for a given anatomical region to be examined is used to establish the dose of scattered radiation and thus to design the necessary shielding of a CT installation. If this method was already questionable for single-detector row computed tomography with sequential scanning (inadequate beam quality and tube leaking values), it becomes even more problematic with the introduction of spiral mode acquisition, since with a volume scanning as many slices as desired can be reconstructed. With the steady increase of the X-ray beam collimation width in modern CT units, the current method needs to be replaced with a more robust one in order to assure sufficient shielding. The DLP should be used since it leads to results independent of the collimation and the high voltage, and which depend only on the size of the scanned object.

## References

- [1] National Council on Radiation Protection and Measurements (NCRP). Structural Shielding Design for Medical X-Ray Imaging Facilities. NCRP Report No. 147, Bethesda (2004).
- [2] Deutsches Institut für Normung. Medizinische Röntgenanlagen bis 300 kV - Regeln für die Auslegung des baulichen Strahlenschutzes. DIN 6812 Entwurf 2006-09
- [3] Cole JA and Platten DJ. A comparison of shielding calculation methods for multi-slice computed tomography (CT) systems. J Radiol Prot 28:511-523 (2008).

# Understanding tumour dynamics in vivo: The potential of kinetic models in radio-oncology

Stephan Scheidegger<sup>1</sup>, Gerd Lutters<sup>2</sup>, Stephan Bodis<sup>2</sup>

<sup>1</sup>Centre for Applied Mathematics and Physics, Zurich University of Applied Sciences  
Winterthur

<sup>2</sup>Institut für Radio-Onkologie, Kantonsspital Aarau

## Abstract

To facilitate the investigation of the tumour response onto radiation therapy in vivo, a modified kinetic LQ-model is developed. It is based on a dose quantity which is considered as proportional to cellular damage. The resulting differential equations are implemented in a computer program and solved numerically. The model is in agreement with the kinetic model of Carlone. In contrast to the model of Carlone and other models focussing DNA lesion kinetics, different aspects of tissue dynamics (e.g. repopulation, oxygenation) can be integrated directly in the proposed LQ-based model.

## 1. Introduction

In vivo tumour response to ionizing radiation can differ remarkably from the response observed in vitro. This difference may be based on several processes related to the interaction of tumour cells with tumour environment (e.g. endothelial cells and tumour vasculature [1]). Also immune reactions and the related inflammatory processes may have an important influence. The adaption of radiobiological models based on the observation of clonogenic survival in vitro (e.g. the LQ model) to the situation in vivo is difficult. Repair, repopulation, interaction with host tissue, influence of radiotherapy onto vasculature and oxygenation can be described by the rates of changes of the related quantities (population size, cell densities, concentrations etc.). This approach directly leads to kinetic models using differential equations. Kinetic models are used for modeling DNA-lesion kinetics and repair [2,3], early tissue reactions [4] or the risk of radiation induced cancer [5]. Probably, it may be difficult to solve the resulting differential equations analytically under certain conditions. This problem can be avoided by using numerical integration. We investigated a modified kinetic LQ model which has a high degree of flexibility for extensions and may therefore be a basis for better understanding of tumour dynamics in vivo. Two different models for tumour cell repopulation were compared here.

## 2. Materials and Methods

The proposed model is based on an ordinary differential equation for tumour population size, which is corresponding to the LQ-model. Assuming no change of cellular repair (low dose rate) and no repopulation of tumour cells, the change (reduction) of the size of an irradiated population is depending on the numbers of tumour cells  $N_1 = N_1(t)$  itself, the dose rate  $R = \dot{D}$  (which is the first derivative of the dose  $D = D(t)$  in respect to the time) and a radio-sensitivity coefficient  $\alpha$  :

$$\frac{dN_1}{dt} = -\alpha N_1 \cdot R = -\alpha N_1 \cdot \frac{dD}{dt} \quad (1)$$

The solution of Eq. (1) is  $N_1(D) = N_0 \cdot e^{-\alpha D}$ . The extension to higher doses and higher dose rates can be realised by a second, dose-dependent term using a coefficient  $2\beta$ :

$$\frac{dN_1}{dt} = -(\alpha + 2\beta D) \cdot R \cdot N_1 \quad (2)$$

Separation and integration over dose results in  $N_1(D) = N_0 \cdot e^{-(\alpha D + \beta D^2)}$ . The natural logarithm of surviving fraction  $S = N_1 / N_0$  is given by  $\ln S = -(\alpha D + \beta D^2)$ . This is corresponding to the LQ-model.

Regarding the tumour volume, lethally damaged cells are not eliminated immediately. Therefore, a second cell population  $N_2$  is introduced, which is reduced by first order kinetics using the kinetic constant  $k_{res}$ :

$$\frac{dN_2}{dt} = \frac{dN_1}{dt} - k_{res} N_2 \quad (3)$$

For inclusion of dose and time dependent change of cellular repair and repopulation, Eq. (2) is modified. First, the (physical) dose is substituted by a biological dose quantity  $\Gamma_{i1}$ , which is representing a biological active proportion of the applied dose. The index  $i$  corresponds to the biological process which is linked to the biological dose quantity  $\Gamma_{i1}$ . Here,  $i = 1$  is corresponding to cellular repair processes. The second modification is concerning the inclusion of repopulation by an additional term describing the tumour growth model using a dose and population size depending function  $f(N, \Gamma_{21})$ :

$$\frac{dN_1}{dt} = -(\alpha + 2\beta \Gamma_{11}) \cdot R \cdot N_1 + f(N_1, \Gamma_{21}) \quad (4)$$

In a first step, it is assumed, that  $\Gamma_{11}$  is different to  $\Gamma_{21}$ . The two quantities may not be independent from each other since repair of cellular damages and cell division are coupled processes.

The quantities  $\Gamma_{i1}$  are determined by the following kinetic model when assuming first order repair kinetics:

$$\frac{d\Gamma_{i1}}{dt} = R - \gamma_i \cdot \Gamma_{i1} \quad (5)$$

$$\frac{d\Gamma_{i2}}{dt} = \gamma_i \cdot \Gamma_{i1} \quad (6)$$

The kinetic constants  $\gamma_i$  may be different for repair ( $i = 1$ ) and repopulation ( $i = 2$ ), but the two constants may be coupled. Regarding Eq.(5) and (6), the following condition is fulfilled:  $\lim_{t \rightarrow \infty} [\Gamma_{i2}(t)] = \lim_{t \rightarrow \infty} [D(t)] = D_{tot}$ . The impact of hypothetical quantities  $\Gamma_{i1}$  onto the cells is mediated by the radiosensitivity constant  $\beta$  at one hand and by  $f(N, \Gamma_{21})$  at the other hand. Here, a repopulation model using a dose independent repopulation term  $k_N \cdot N_1$  with constant  $k_N$  is compared with the following dose dependent function describing the radiation induced inhibition of the rate of growth:

$$f(N, \Gamma_{21}) = \frac{k_{R1}}{(1 + k_{R2} \cdot \Gamma_{21})} \cdot N = k_N(\Gamma_{21}) \cdot N \quad (7)$$

For an irradiation with constant dose rate  $R$ , the dose quantities  $\Gamma_{i1}$  reach a steady state level  $\Gamma_{ieq}$ . The condition for steady state is given by:

$$\Gamma_{ieq} = \frac{R}{\gamma_i} \quad (8)$$

If the repopulation term is neglected, the logarithm of surviving fraction becomes constant at high doses (when reaching the equilibrium):

$$\left[ \frac{d \ln S}{dD} \right]_{\Gamma_1 \rightarrow \Gamma_{ieq}} = -(\alpha + 2\beta \Gamma_{ieq}) \quad (9)$$

Therefore, the model is exhibiting a linear-quadratic-linear behaviour as observed for high fraction doses [6]. The model was compared to existing kinetic radiobiological models. The proposed kinetic LQ-model without repopulation leads to identical results as the model of Carlone [3], when the kinetic constant  $\gamma_1$  is adapted to the dose rate using the relation  $\gamma_1 = \mu + p\varepsilon R$ . The constant  $p$  is defined as the yield per unit dose of sub-lethal lesions [7] and  $R$  is the dose rate (as above). In the model of Carlone, pre-existing sublethal lesions can interact with the formation of new lesions with the interaction probability  $\varepsilon$ . The relation to the constant for radiosensitivity  $\beta$  is given by  $\beta = p^2 \varepsilon$ .

The differential equations Eq. (3), (4), (5) and (6) were implemented in a computer program using a Runge-Kutta algorithm. Also the kinetic model of Carlone et al. [3] was implemented. The surviving fractions as function of dose or time and the resulting TCP's for both models can be compared directly. Different therapy modalities were investigated. Also different approaches for repopulation were tested.

### 3. Results

For biologically targeted radionuclide therapy, the kinetic LQ-model is in agreement to classical LQ calculations [8]. For fractionated RT, the proposed model also is in agreement with the compartmental model of Carlone, even when the quantity  $\Gamma_{11}$  is far away from the equilibrium. Fig.1 shows the impact of  $\Gamma_{11}$  onto the logarithm of surviving fraction. The case  $\gamma_1 = 0 \text{ d}^{-1}$  is corresponding to the common LQ formalism. With increasing value for  $\gamma_1$ , the final slope becomes flatter and a linear-quadratic-linear behavior is exhibited.

For all simulations, the parameters for radio-sensitivity are chosen as  $\alpha = 0.3 \text{ Gy}^{-1}$  and  $\beta = 0.05 \text{ Gy}^{-2}$  respectively.

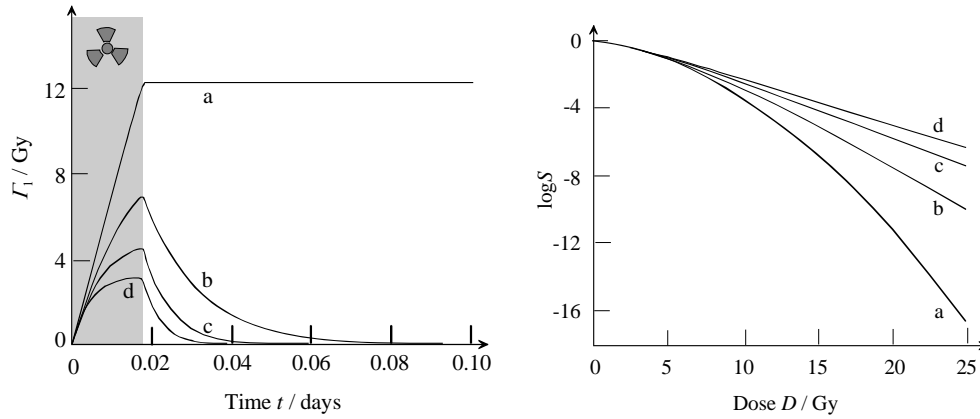


Fig.1. Relation between  $\Gamma_{11}$  and  $\log S$ : Left Diagram shows the temporal development of  $\Gamma_1 = \Gamma_{11}$  for a fraction of  $D = 12.5 \text{ Gy}$ . Right diagram shows the logarithm of surviving fraction for a single fraction. The parameters are the following: (a)  $\gamma_1 = 0 \text{ d}^{-1}$ ; (b)  $\gamma_1 = 70.22 \text{ d}^{-1}$ ; (c)  $\gamma_1 = 140.45 \text{ d}^{-1}$ ; (d)  $\gamma_1 = 210.67 \text{ d}^{-1}$ ; no repopulation ( $k_N = 0 \text{ d}^{-1}$ ), calculated with Runge-Kutta method with  $\Delta t = 0.5 \cdot 10^{-6} \text{ d}$ .

Referring to Eq. (7), the influence of  $\Gamma_{21}$  onto  $k_N(\Gamma_{21})$  is showed in Fig.2 for different values of  $k_{R2}$ . The comparison between the different models for repopulation is demonstrating the effect of growth delay due to radiation (Fig.3). In this model, a remarkable growth delay can be produced only by a reasonably large value for  $k_{R2}$  (above  $4.0 \text{ Gy}^{-1}$ , Fig.2. curve  $e$ ). In addition, the effect is only prominent for a relatively slow repair process and therefore for a small constant  $\gamma_2$  (comparable to  $k_{R1}$ , which may be considered as intrinsic growth constant). For the illustrated case in Fig.3,  $\gamma_2$  is set to  $2 \text{ d}^{-1}$ . The volume reduction (Fig.3) is also depending on the rate of tissue resorption. The larger the value for  $k_{res}$  the stronger the visible effect onto the difference curves of the tumour volume and the logarithm of surviving fraction (Fig.3).

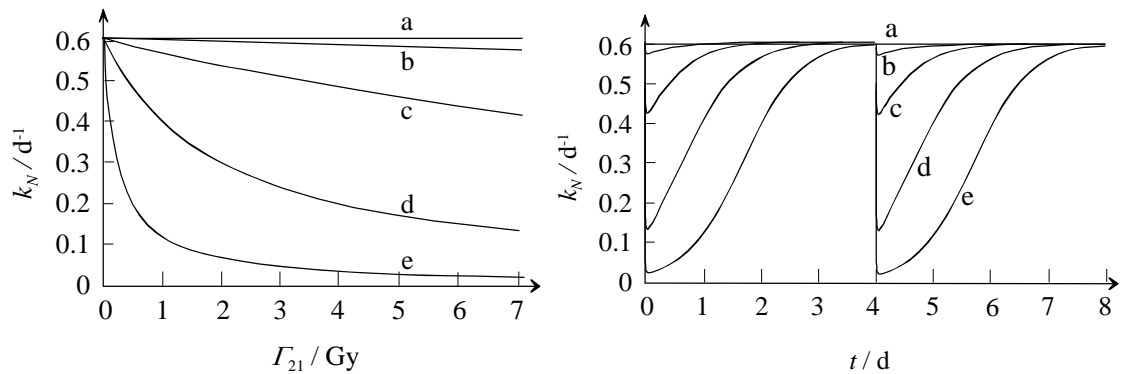


Fig.2. Dose-dependency of  $k_N$ : Left Diagram shows the  $\Gamma_{21}$  - dependency of  $k_N$ ; Right diagram shows the temporal development of  $k_N(\Gamma_{21})$  for two fractions of 7 Gy. Parameters:  $k_{R1} = 0.6 \text{ d}^{-1}$ ;  $\gamma_1 = 163.2 \text{ d}^{-1}$ ,  $\gamma_2 = 2 \text{ d}^{-1}$ ; (a)  $k_{R2} = 0.0 \text{ Gy}^{-1}$  (corresponding to the model with a constant value for  $k_N$ ); (b)  $k_{R2} = 1.0 \text{ Gy}^{-1}$ ; (c)  $k_{R2} = 2.0 \text{ Gy}^{-1}$ ; (d)  $k_{R2} = 3.0 \text{ Gy}^{-1}$ ; (e)  $k_{R2} = 4.0 \text{ Gy}^{-1}$

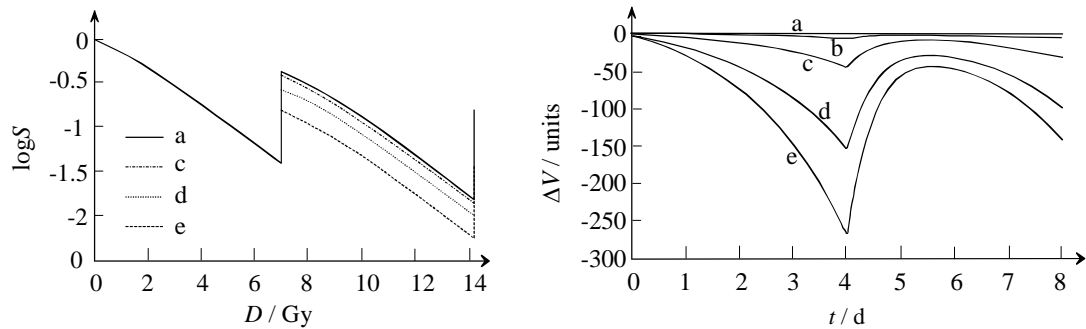


Fig.3. Impact of radiation depending  $k_N$  onto tumour size: Left Diagram is showing the logarithm of survival as function of dose  $D$ , same parameters as in Fig.2. Right: Temporal development of the difference  $\Delta V$  of tumour volume  $V$  (normalized to 1000 units) between dose independent and dose dependent growth constant  $k_N$ , the necrotic cells  $N_2$  are also included ( $k_{res} = 2 \text{ d}^{-1}$ ).

#### 4. Conclusions

The kinetic formulation of the LQ-model offers a high degree of flexibility for extensions to repair, repopulation and different therapy modalities. For the tested cases, the proposed model is in agreement with existing radiobiological models also for high dose rates and doses. Extensions to arbitrary dose distributions can be implemented in a very efficient way and provide additional information for optimizing radiotherapy. The proposed model allows the quantitative analysis of

growth delay of tumours under treatment. Calculations using the presented model suggest that a growth delay is only observable in the experiment for a strong dose dependence of the growth constant  $k_N$ .

The system can be explored by plotting the logarithm of surviving fraction and the tumour volume versus dose or time. Therefore, the computer simulation also may be used for educational purpose (e.g. to learn about effects of hyper- or hypofractionation).

#### References

- [1] Denekamp, J. (1992): Angiogenesis, neovascular proliferation and vascular pathophysiology as targets for cancer therapy. *Br. J. Radiol.* **66**, 181-196
- [2] Curtis, S. B. (1986): Lethal and potentially lethal lesions induced by radiation – A Unified Repair Model. *Radiat. Res.* **106**, 252-270
- [3] Carlone, M.C., Wilkins D., Raaphorst, G.P. (2003): An extension to the linear-quadratic model aimed at improving the description of the high dose portion of the cell survival curve. Proc. 49th Annual Meeting of the COMP, *Med. Phys.* 30, 1948
- [4] Fenwick, J. D. (2006): Delay differential equations and the dose-time dependency of early reactions. *Med. Phys.* **33**, 3526-3540
- [5] Schneider, U. (2008): Mechanistic model of radiation-induced cancer after fractionated radiotherapy using the linear-quadratic formula. *Med. Phys.* **36**, 1138-1143
- [6] Guerrero, M., Li, X.A. (2004): Extending the linear-quadratic model for large fraction doses pertinent to stereotactic radiotherapy. *Phys. Med. Biol.* 49, 4825-4835
- [7] Dale, R. G. (1985): The application of the linear-quadratic dose-effect equation to fractionated and protracted radiotherapy. *Br. J. Radiol.* **58**, 515-528
- [8] Donoghue, J.A., Hopkins K (2007): Biologically targeted radionuclide therapy. *In: Radiobiological Modelling in Radiation Oncology, Dale, R., Bledlyn J. (Ed.). The British Institute of Radiology.* 246-264

# What is the Benefit of an Adaptive Statistical Iterative Reconstruction Method over Conventional CT Reconstruction Approaches?

F. Miéville<sup>1</sup>, E. Rizzo<sup>2</sup>, F. Gudinchet<sup>2</sup>, F. Bochud<sup>1</sup> and F. R. Verdun<sup>1</sup>

<sup>1</sup> University Institute for Radiation Physics – CHUV & UNIL – Lausanne – Switzerland

<sup>2</sup> Radiology Department – CHUV & UNIL – Lausanne – Switzerland

mail: [francis.verdun@chuv.ch](mailto:francis.verdun@chuv.ch)

## Introduction

Adaptive Statistical Iterative Reconstruction (ASIR) is a new imaging reconstruction technique recently introduced by General Electric (GE) in last generation computed tomography (CT) scanner units. This technique, when combined with a conventional filtered backprojection (FBP) approach [1], allows in particular to taking into account the statistical fluctuation of noise [2]. To quantify the benefits provided on the image quality by the ASIR method with respect to the FBP one, the standard deviation (SD), modulation transfer function (MTF), noise power spectrum (NPS), signal-to-noise ratio (SNR) and low contrast detectability were determined from phantom images.

## Material and Methods

A multidetector-row CT (MDCT) was employed. Measurements were performed on a Catphan600 phantom when varying the CT dose index ( $CTDI_{vol}$ ) and the reconstruction kernels. Images were reconstructed on a CT console for different percentage of ASIR (0% pure FTB, 100% pure ASIR). To evaluate the iterative method, metrics were computed and compared using an in-house program written in MatLab 7.7 (Mathworks, USA).

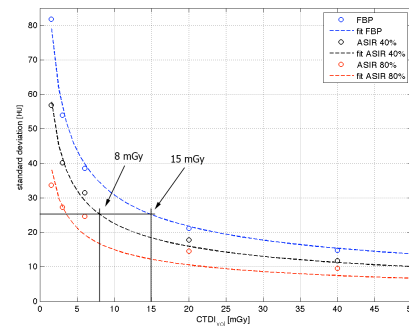


Figure 1: The standard deviation as a function of  $CTDI_{vol}$  for different percentages of ASIR.

## Results

Figure 1 shows the decrease of SD, when  $CTDI_{vol}$  increases. For a fixed value of SD ( $\sigma = 25$  HU),  $CTDI_{vol}$  can be divided by 2 and up to 3.5 if 40% and 80% of ASIR are used, respectively. It can be shown that SD decreases linearly when increasing the percentage of ASIR and the benefit is higher at lower doses. For all reconstruction kernels, MTF medium frequencies were slightly improved whereas low frequencies and the cutoff frequency were not modified. Modifications of the NPS shape curve were observed as well. However, in spite of the global improvement of the image quality metrics, clinical images with more than ~50%-60% of ASIR were considered by radiologists to be unacceptable for diagnosis establishments. This is due to the global aspect of the image that tends to be artificial (image less realistic) for high ASIR percentage.

## Discussion

The results of the present study indicated that the combination of the FBP and ASIR methods improve the image quality on phantoms by decreasing SD and increasing MTF as well as NPS. In clinical environment, however, 50% of ASIR is used because it produces the best trade-off between noise reduction and image aspect.

## References

- [1] L. A. Feldkamp, L. C. Davis, and J. W. Kress, "Practical cone-beam algorithm," J. Opt. Soc. Am. A, Vol. 1, No. 6, pp. 612–619, 1984.
- [2] J.-B. Thibault, K. D. Sauer, C. A. Bouman, and J. Hsieh, "A three-dimensional statistical approach to improved image quality for multislice helical CT," Med. Phys., Vol. 34, No. 11, pp. 4526–4544, 2007.

# Interventional radiology: management of high patient dose procedures

E.T. Samara<sup>1</sup>, A. Aroua<sup>1</sup>, P. Bize<sup>2</sup>, S. Binaghi<sup>2</sup>, F.R. Verdun<sup>1</sup>

<sup>1</sup> University Institute for Radiation Physics (IRA), CHUV – UNIL, Lausanne

<sup>2</sup> Department of Radiology, CHUV – UNIL, Lausanne

mail: [eleni-theano.samara@chuv.ch](mailto:eleni-theano.samara@chuv.ch)

## Introduction

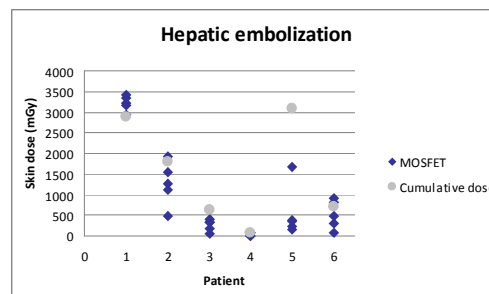
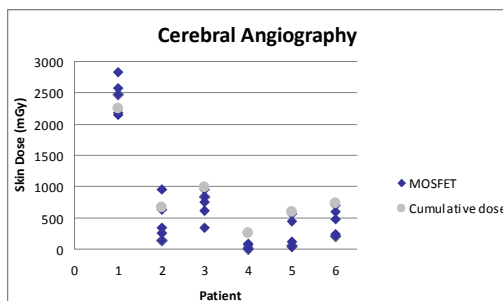
The number of interventional radiology procedures is increasing over the years due to their clinical safety and efficacy. However, these procedures may be related to high radiation doses to the patient [1, 2]. Management of the stochastic risks can be performed by monitoring the dose-area product (DAP) and comparing it to available Diagnostic Reference Levels (DRL). Anticipation of deterministic effects can be predicted by monitoring the cumulative dose [3] at the Intervention Reference Point (IRP). The aim of the study is to demonstrate the reliability of the IRP concept and to provide interventionists with a method to control risks associated with the use of ionizing radiation.

## Material and Methods

Patient data for a six-month period were collected and analyzed for hepatic embolization and cerebral angiography. Data included the dose-area product, the fluoroscopy time (T), the number of images (N) and the cumulative dose at the interventional reference point ( $D_{IRP}$ ). Patient dosimetry was also performed with the use of MOSFET dosimeters. The statistical software SPSS was employed for data analysis.

## Results

A good correlation was found between the MOSFET dosimeters and  $D_{IRP}$ . Maximum skin dose reached 9.6 and 5.7 Gy during hepatic embolization and cerebral angiography, respectively. The 75-percentile of the patient dose was calculated and compared with the national DRLs.



## Discussion

The use, validity and limitations of  $D_{IRP}$  and DRL will be discussed during the presentation. Actions have to be taken to improve patient dose management. In particular, post-procedure follow-ups should be part of the radiological procedure when the skin dose is suspected to be over 2 Gy [4].

## References

- [1] International Commission on Radiological Protection Avoidance of Radiation Injuries from Medical Interventional Procedures. ICRP Publication 85, Annals of the ICRP, 30 (2). Pergamon Press, Oxford and New York (2000).
- [2] European Union, Council Directive 97/43 Euratom, on health protection of individuals against the dangers ionizing radiation in relation to medical exposure, and repealing Directive 84/466 Euratom, Official Journal of the European Communities vol. L 180 (1997 (9th July)), pp. 22–27.
- [3] Balter S: Methods for measuring fluoroscopic skin dose. *Pediatr. Radiol.* (2006) 36 Suppl 2:136-40
- [4] Verdun FR, Bochud F, Gundinchet F, Aroua A, Schnyder P, Meuli R.: Quality initiatives radiation risk: what you should know to tell your patient. *Radiographics.* (2008) 28(7):1807-16

# Mathematical observers applied to breast tomosynthesis.

I. Diaz<sup>1</sup>, P. Timberg<sup>2</sup>, C. Abbey<sup>3</sup>, M. Eckstein<sup>3</sup>, F. R. Verdun<sup>1</sup>, C. Castella<sup>1</sup>, F.O. Bochud<sup>1</sup>

<sup>1</sup> University Institute for Radiation Physics, DUMSC, CHUV and University of Lausanne, CH-1007 Lausanne, Switzerland

<sup>2</sup> Department of Medical Radiation Physics, Lund University, Malmö University Hospital, Malmö, Sweden

<sup>3</sup> Dept. of Psychology, University of California, Santa Barbara, CA, USA 93106-9660  
mail: [francois.bochud@chuv.ch](mailto:francois.bochud@chuv.ch)

## Introduction

For breast tomosynthesis (BT) there is a large space of acquisition parameters that can be optimized both in terms of image quality and dose from the point of view of radiation protection. To attempt this optimization only using human observers would be very costly and time-consuming. Model observers have been developed to mimic the response of humans in order to test on much larger sets of images in a shorter time than would be possible otherwise. The aim of this study was to adapt existing model observers to be used with irregularly shaped breast tomosynthesis (BT) signals.

## Material and Methods

This paper expands upon a previous study where different circularly symmetric model observers were used to compare digital mammography to BT. The present study is based on a more realistic version of the signal considered at three different sizes (from microcalcification to tumor masses) and three different contrast levels.

In the previous study, we observed that the channelized Hotelling observers (CHO) with Gabor and Difference-of-Gaussians channels were always outperformed by the human observers. In this study, we decided to modify the channels in order to accommodate the fact that the targets were not radially symmetric. Instead of treating the channels as a simple linear templates, we calculated them as filters which were then convolved with the target profile. These were then tested on the signals which were embedded in real breast tomosynthesis backgrounds.

## Results

Once this modification was made, the model observers outperformed the human observers in 4-AFC trials by at least a factor of 1.5 in every case except for the smallest one, that of an observer with channels not sufficiently tuned to the high spatial frequencies necessary to detect microcalcifications. The very high performance obtained was degraded by the addition of internal noise to match the human performance.

## Discussion

Getting model observer performance to exceed that of humans is the first step in obtaining observers which can be confidently used on trials with vast numbers of parameter variations. These CHOs, better adapted to irregular signals, combined with the information gained from adding more sizes and contrasts than previously available will aid in refining the model observers which are to be used in automating the optimization of BT acquisition parameters.

## References

- [1] C. Castella, et al : Masses detection in breast tomosynthesis and digital mammography: a model observer study: Proc. SPIE Medical Imaging, 2009
- [2] Ruschin, M, et al: Improved in-plane visibility of tumors using breast tomosynthesis: Proc. SPIE Medical Imaging, 2007
- [3] Eckstein, M; Abbey, C; Bochud, F: A practical guide to model observers for visual detection in synthetic and natural noisy images: Handbook of Medical Imaging. Volume I. Physics and Psychophysics, 2000

# AD-4 / ACE : Antiproton Cell Experiment

P.Weber<sup>1, 2</sup>

<sup>1</sup> Service de radiothérapie du DPO, Hôpital neuchâtelois HNE, 2300 La Chaux-de-Fonds

<sup>2</sup> PH Division, CERN, Geneva

mail: [patrick.weber@ne.ch](mailto:patrick.weber@ne.ch)

## Introduction

A pioneering experiment at CERN studying the potential use of antimatter for cancer therapy has produced its first results [1-6]. Exploiting the unique capability of CERN's Antiproton Decelerator to produce a narrow monoenergetic antiproton beam at the right energy, the Antiproton Cell Experiment (ACE) has shown that antiprotons have been shown to be more effective than protons for neutralizing cancer cells by irradiation. [7]

## Material and Methods

The LEAR (Low Energy Antiproton Ring) facility at CERN is able to produce a bunch of  $3E7$  antiprotons with 500 MeV/c every 90 seconds. The antiprotons are extracted into a target volume filled with a gel, into which leaving V79 WNRE Chinese hamster cells are disposed. The experimental hall is equipped for dosimetry measurements, i.e with liquid ionization chambers, alanine pellets and radiochromic films. Silicon particles detectors measure the secondary leaving particles in order to perform a real time imaging of the antiproton interactions.

## Results

Antiprotons and protons exhibit near identical stopping powers and radiobiology when they penetrate into matter, in the plateau region. But when antiprotons come to rest, their behaviour is completely different as they annihilate with matter, and thus, release an energy of 1.88 GeV. Most of this energy is carried away by secondary particles (principally pions), but the energy deposited at the Bragg peak is 20-30 MeV per antiproton. The absorbed dose in this regions is 4 times higher compared to protons. Moreover, one can also measure an increase of the relative biological effect, explained by the fact that part of the emitted secondary particles have high LET properties. Dosimetry experiments are performed and the radiobiological effects on leaving cells is investigated.

## Discussion

The ACE experiment shows that when comparing antiprotons with protons, the relative biological effect in the plateau region is reduced by a factor 4 for the same biological dose deposited in the Bragg peak region.

The weekly interacting pions, leaving the target volume will be used to perform a real time imaging of the interaction vertex.

The biological effect of secondary particles leaving the target volume have to be studied in order to investigate the possible clinical use of antiproton beams.

## References

- [1] M.Holzschelter et al; Biological effectiveness of antiproton annihilation, NIM B 221 (2004), 210-214
- [2] N.Bassler et al; Bubble detector measurements of a mixed radiation field from antiproton annihilation; NIM B 251 (2006), 269-273
- [3] N.Bassler et al; Antiproton radiotherapy; Radiotherapy and Oncology 86 (2008), 14-19
- [4] N.Bassler et al; Calculated LET spectrum from antiproton beams stopping in water; Acta Oncologica (2008)
- [5] N.Bassler et al; The antiproton depth-dose curve in water ; Phys. Med. Biol. 53 (2008), 793-805
- [6] N.Bassler et al; The antiproton depth-dose curve measured with alanine detectors, NIM B 266 (2008), 929-936
- [7] H.V.Knudsen et al; Antiproton therapy; NIM B 266 (2008), 530-534

# **Exposure of the Swiss population from radiological examinations: a prospective study to estimate the examination frequency**

R. Le Coultre<sup>1</sup>, R. Schnyder<sup>2</sup>, S. Coendoz<sup>3</sup>, E. Samara<sup>2</sup>, A. Aroua<sup>2</sup>, F. Bochud<sup>2</sup>, F. R. Verdun<sup>2</sup>

<sup>1</sup>School of Health Sciences – Technique in medical radiology, HES-SO /

University of Applied Sciences Western Switzerland, Lausanne, Switzerland <sup>2</sup>University

Institute for Radiation Physics (IRA), CHUV – UNIL, Lausanne

<sup>3</sup> Department of Radiology, CHUV – UNIL, Lausanne

mail: [francis.verdun@chuv.ch](mailto:francis.verdun@chuv.ch)

## **Introduction**

Surveying the population exposure by medical x-rays is a useful tool in radiation protection. Among the main objectives of population dose assessments are: “1) to observe trends in the annual collective dose and the annual average per caput dose from medical x-rays in a country with time; 2) to determine the contributions of different imaging modalities and types of examination to the total collective dose from all medical x-rays.” In Switzerland a survey on the exposure of the population by medical x-rays in 2008 is being conducted. It updates the results obtained in 1998 [1] and 2003 [2]. The aim of this work is to explore the appropriateness of the Tarmed coding system as an automatic tool for surveying the frequency of diagnostic and interventional examinations in Switzerland.

## **Material and Methods**

The subset of invoices corresponding to a two month period activity (oct. and nov. 2008) of the Radiological Department of the Lausanne University Hospital (CHUV) has been analyzed (16'000 invoices). For each Tarmed code or group of Tarmed codes a radiological examination was defined.

## **Results**

The use of Tarmed code allows to obtain the frequency of the radiography examinations with a reasonable precision. In adults for 19'500 radiographies the percentages of abdomen, chest and lower limbs were 37%, 28% and 16% respectively. The interpretation of the CT examination statistics is more cumbersome but the use of several codes to define a CT acquisition allows also establishing the frequency of this type of examinations. Concerning fluoroscopy examinations, an almost case per case analysis is required to identify precisely the examination performed.

## **Discussion**

The use of Tarmed codification is a very convenient way to establish the frequency of the most common examinations (radiography and CT). For fluoroscopy special care must be taken to ensure the reliability of the approach. However, these preliminary results demonstrate that the tools developed to establish invoices in medicine may be used to monitor the exposure of the Swiss population from the radiological examinations.

## **References**

- [1] Aroua A, Burnand B, Decka I, Vader JP and Valley JF. (2002) Nationwide Survey on Radiation Doses in Diagnostic and Interventional Radiology in Switzerland in 1998. Health Phys 83(1):46-55.
- [2] Aroua A, Vader JP, Valley JF and Verdun FR. (2007) Exposure of the Swiss population by radiodiagnosics: 2003 review. Health Phys 92(5):442-8.

# Quality Assurance of X-Ray Protection Clothing at the University Hospital Basel

D. Oppliger-Schäfer, H.W. Roser  
Radiological Physics, University Hospital Basel  
mail: [oppligerd@uhbs.ch](mailto:oppligerd@uhbs.ch)

## Introduction

It is required that for each X-ray unit there are enough X-ray protection clothing and patient covers available and they must be employed sensibly [1] (Note: for what follow we will subsume the patient covers under the term clothing). The protection effect depends on the lead equivalence of the material and the energy of the radiation. It also depends strongly on the condition of the material involved. To evaluate the safety of protective clothing we have been performing regular and standardized quality checks at the University Hospital Basel since 2003. The results demonstrate that about 20% of all tested clothing show defects of the protective layers. The total number of pieces of protective clothing checked has grown from about 200 in 2002 to more than 400 as of today. All protective clothing is prone to such defects irrespective of age and type of material used.

## Material and Methods

We set up a two-stage method by defining two distinctly different methods for testing the material, which are performed consecutively:

1. combining visual inspection and palpation
2. using a fluoroscopy unit

According to our judgment as critical positions we established well defined spots for testing on the different pieces of clothing (like e.g. vests, skirts, surgical aprons, patient covers). These spots are emphasized as crosshairs and numbered yellow circles in Figure 1. Additionally the seams are considered as mandatory test points. By clearly defining the test positions on the clothing the development of an incipient defect can be traced from one to the next testing cycle.

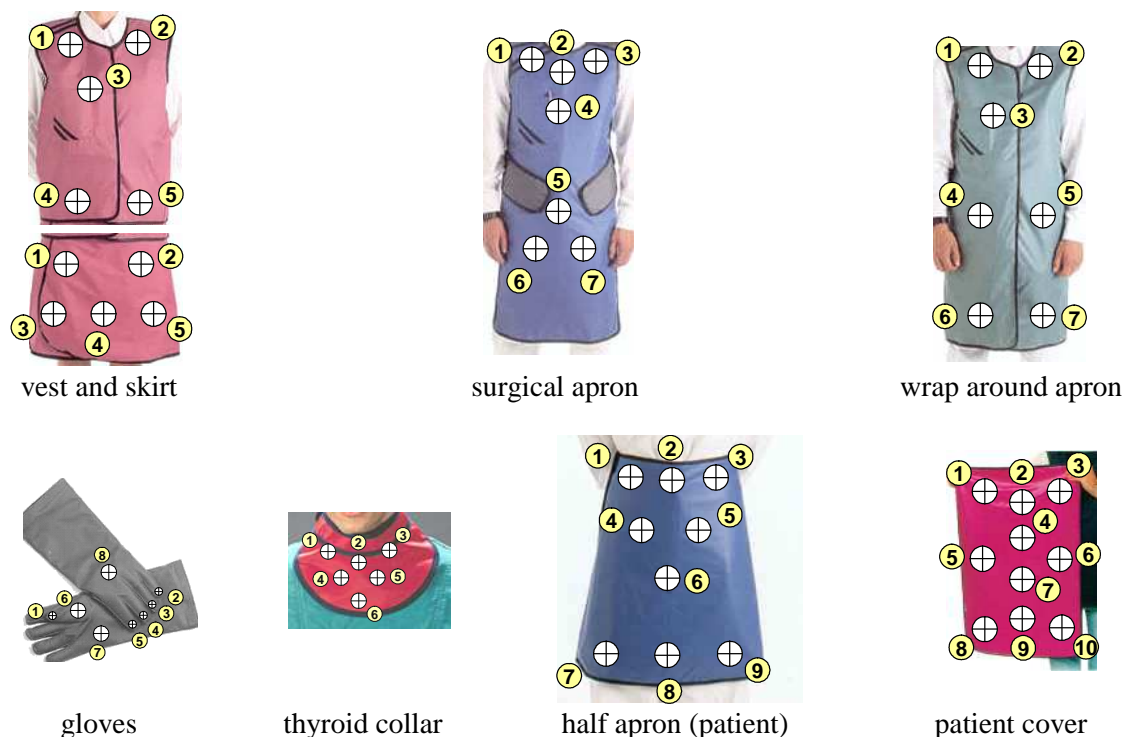


Figure 1: Types of X-Ray protective clothing and locations of mandatory testing spots

### *Visual inspection and palpation*



Figure 2: Testing X-Ray protection clothing by visual inspection and palpation

The considered piece of protective clothing is spread out on a flat surface and is checked visually for defects. It is then also examined for breaks, tears and discontinuities by palpating with the hands. This way defects not directly visible from the outside can be detected "manually". The questionable positions are marked as suspicious spots for further verification.

### *Test using a fluoroscopy unit*



Figure 3: Testing X-Ray protection clothing using a fluoroscopy unit

The suspicious locations and the predefined testing spots are X-rayed under fluoroscopy. If fluoroscopy shows locations of increased transparency or even holes and tears, the defects are captured with an X-ray, the locations are clearly marked on the outer fabric cover of the tested object and the results are archived.

The following parameters are suggested for the test procedure:

- use remote controllable fluoroscopy unit
- don't use automatic dose rate control
- do not exceed 70 kV
- use maximum focus-film or focus-detector distance
- select large focus
- recommended field size is 20 cm x 20 cm
- center points of interest with light field (if available)
- use short fluoroscopy time (e.g. not more than 0.3 min), only exception: tracking seams



Year	Number of checked protective items	Number of defective items	Number of defective items [%]
2006	281	81	28.8%
2007	387	90	23.3%
2008	357	84	23.5%
2009	401	74	18.5%

Table 1: Total number and number of detected defects for the X-Ray protection clothing at the University Hospital Basel

As mentioned before we detected a wide variety of defects from virtually undetectable and correspondingly insignificant to really "horrific", where the protection has gone completely. In Figure 5 we give a "picture gallery" of what we have seen.

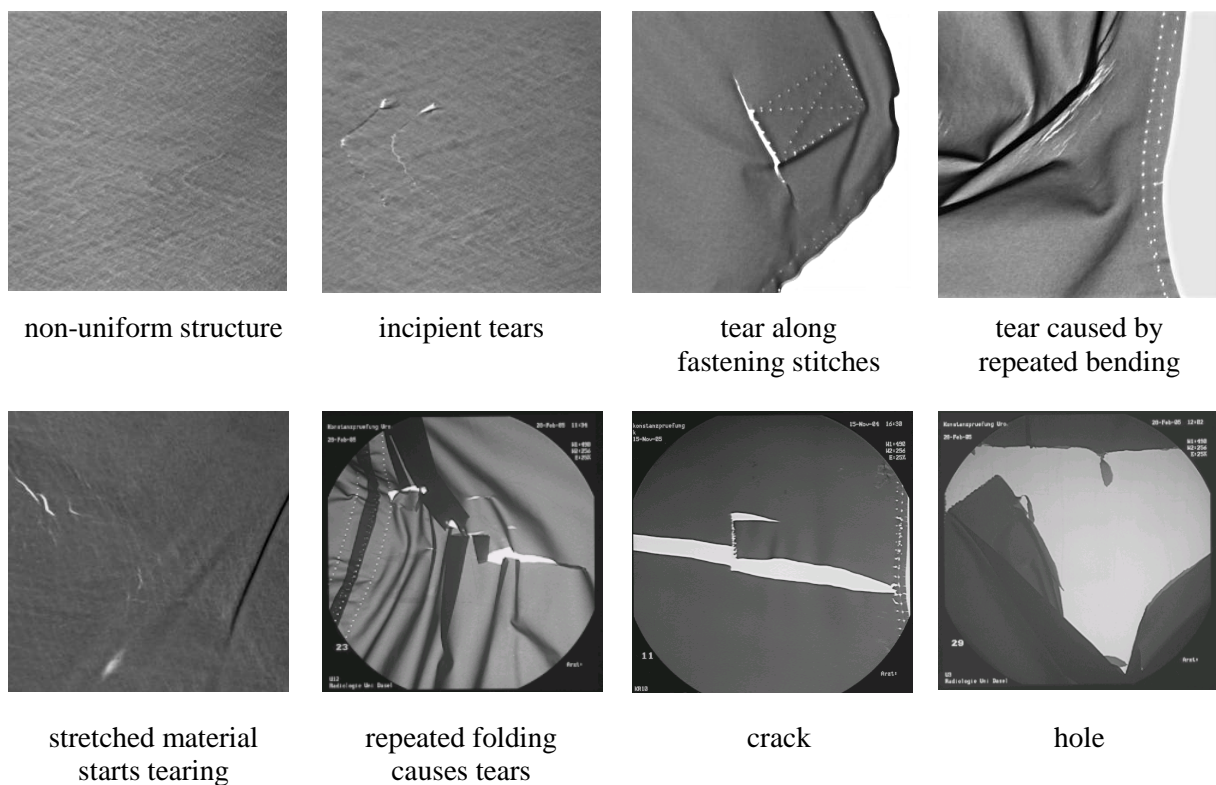


Figure 5: The "picture gallery" of defects on the X-Ray protection clothing at the University Hospital Basel

In the last couple of years not only the design and the types of protection clothing have changed but also the materials used. The weight of the clothing with clearly relates to the wearing comfort and the disposal problem for the lead material both gave clear reasons to move toward lead-free material. Consequently basically two types of material are in regular use in our hospital: lead-vinyl and Xenolite<sup>®</sup> (lead-free material, originally developed by DuPont) [2]. We therefore tried to compare the relative appearance of defects for the two types of material. The items made from Xenolite have been reduced in number by approximately one third over the last years and the remaining Xenolite items now show more than 50% defects. The corresponding number for lead-vinyl is less than 20%. The visual inspections show an increasing number of defects over the inspection period. We also find increasing numbers of defects that can be detected only under fluoroscopy. In some cases we could clearly follow the development of defects in the course of time, i.e. the affected regions became thinner and thinner at the observed regions and tears showed in exactly these locations.

Protective material	2006			2007			2008			2009		
	All	Def.	%									
Lead	204	47	23.0	292	61	20.9	312	60	19.2	353	50	14.2
Xenolite	60	18	30.0	51	24	47.1	39	21	53.8	44	24	54.5
unknown	17	16	94.1	44	5	11.4	6	3	50.0	4	-	-
Total	281	81	28.8	387	90	23.3	357	84	23.5	401	74	18.5

Table 2: Number of detected defects for different materials used in X-Ray protection clothing at the University Hospital Basel for the years 2006 through 2009

All = Number of checked protective items

Def. = Number of defective items

% = relative Number of defective items [%]

## Discussion

The result of around 20% defects for all X-ray protective items clearly show the necessity for regular quality checks. Although all departments using protective gear are affected, those departments where the equipment is in regular use (angiography, cardiology, urology and surgical disciplines) detect the most defects. Vests, skirts and wrap around aprons are in quite widespread and frequent use and correspondingly show the heaviest wear and tear problems. The number of visual damages to the equipment has increased over the inspection period. The number of defects classified as "Tolerable and under Observation" (T) and/or "Severe" (S) has slightly decreased but we see an increase in the group of problems classified as "Insignificant" (I).

The seams definitely have to be watched very carefully, they often seem to be the origin for tears. The seams appear to be weak points from start since they might coincide with zones of reduced or no protective material and the production process itself might already weaken the pieces of equipment in exactly these locations. It is particularly noteworthy that already relatively new items show regions of increased transparency and irregular thickness.

It is also noticeable that locations with increased radiation transparency more frequently show for the Xenolite material. But we want to emphasize that a statement about the toughness of the protective items comparing lead-free versus lead containing material might be premature. Firstly the number of lead-free objects has been reduced over the last couple of years and secondly the lead-free option has mainly been selected because of its reduced weight at comparable protection level in those departments where frequent and heavy use is standard. Our experience therefore indicates a typical lifetime of two to three years for the lead-free items as compared to a range of five to ten years for lead objects. Irrespective of the protective material used one of the main reasons for the development of defects is the careless handling of the objects what leads to demonstrable tears and breaks.

It can be assumed that the results are not specific for the Basel hospital and a comparison with corresponding results from other hospitals would be desirable. Nevertheless we will continue to perform the necessary quality checks on our x-ray protection clothing at the University Hospital Basel to give proper emphasis to this particular aspect of radiation protection for the patient and the personnel. We think the methods used definitely are a useful tool to detect problems early on and withdraw and replace the protective equipment timely if indicated.

## References

- [1] Bundesamt für Gesundheit: Schutzmittel für Patienten, Personal und Dritte in der Röntgendiagnostik, Merkblatt R-09-02 vom 29.1.2003
- [2] Finnerty M, Brennan PC. Protective aprons in imaging departments: manufacturer stated lead equivalence values require validation. EUR Radiol 2005; 15: 1477-1484

# First year of clinical rapidarc treatments at iosi: status report

A. Fogliata<sup>1</sup>, G. Nicolini<sup>1</sup>, E. Vanetti<sup>1</sup>, A. Clivio<sup>1</sup>, A. Richetti<sup>1</sup>, L. Cozzi<sup>1</sup>

<sup>1</sup>Oncology Institute of Southern Switzerland, Bellinzona, Switzerland

mail: [afc@ios.ch](mailto:afc@ios.ch)

## Introduction

The clinical activity and a summary of statistics of patients treated with RapidArc technique at IOSI in the first year from its clinical implementation.

## Material and Methods

Clinical indications, number of patients, stratified for pathology and district, basic treatment plan characteristics will be presented according to updated statistics at time of presentation. Pretreatment quality assurance procedures and results will be discussed. Treatment modality and efficiency in terms of time to perform IGRT and beam on time will be addressed. Future perspectives will be outlined

## Results

Since its introduction in september 2008, at time of abstract submission, 130 patients (for a total of 158 plans) have been treated or on treatment: 63 prostate, 33 anal canal, rectum or pancreas, 10 gynaecologic, 2 chordoma, 3 brain, 3 bilateral breast, 1 cranio-spinal irradiation for medulloblastoma, 1 paediatric Hodgkin lymphoma, 14 other sites. This corresponds to 27% of the total number of IMRT patients at IOSI since 2001. Dose prescription ranged from 5.4 to 78 Gy with or without SIB strategies. An average of  $24 \pm 10$  fractions were applied with an average of  $1.1 \pm 0.3$  arcs per plan. Mean collimator angle used for individual arcs was  $23 \pm 8$  degrees. Mean number of MU per fraction were  $416 \pm 136$ . Target coverage in average is  $D98 > 93\%$  with high sparing of organs at risk which will be detailed with the final analysis. Looking at the prostate subpopulation of the first 63 patients, with a dose prescription ranging from 66 to 78 Gy and a PTV  $V95\% = 96.1 \pm 2.4\%$ , the mean dose to the rectum was  $40.2 \pm 4.0$  Gy with  $V50Gy = 20.1 \pm 9.1\%$ ; the mean dose to the bladder was  $46.5 \pm 12.0$  Gy with  $V50Gy = 30.2 \pm 20.7\%$ . Mean beam on time is:  $1:18'' \pm 19''$ . Mean IGRT time is:  $7:37'' \pm 2:43''$ . Concerning pre-treatment QA with portal dosimetry (with GLAaS method) Gamma Agreement Index is:  $97.7 \pm 2.3\%$  (with a tolerance threshold of 95%, criteria of DTA=3mm, DeltaDose=3%).

## Discussion

RapidArc was smoothly introduced in clinical practice, results are confirming expectations and the new modality will progressively replace IMRT in most of the clinical indications at IOSI.

## References

- [1] Otto, K.: Volumetric Modulated Arc Therapy: IMRT in a single arc. *Med. Phys.* 2008;35: 310-317
- [2] Cameron C. Sweeping-window arc therapy: an implementation of rotational IMRT with automatic beam-weight calculation. *Phys Med Biol* 2005; 50:4317-4336.
- [3] Palma D, Vollans E., James K., Nakano S., Moiseenko V., Shaffer R., McKenzie M., Morris J., Otto K.: Volumetric modulated arc therapy for delivery of prostate radiotherapy. Comparison with intensity modulated radiotherapy and three-dimensional conformal radiotherapy. *Int. J. Radiat. Oncol. Biol. Phys.* 2008
- [4] Nicolini G, Vanetti E, Clivio A, Fogliata A, Korreman S, Bocanek J, Cozzi L.: The GLAaS algorithm for portal dosimetry and quality assurance of RapidArc, an intensity modulated rotational therapy. *Radiat. Oncol.* 2008; 9:3-24
- [5] Nicolini G, Clivio A., Fogliata A., Vanetti E., Cozzi L.: Simultaneous integrated boost radiotherapy for bilateral breast. A treatment planning and dosimetric comparison for volumetric modulated arc and fixed field intensity modulated therapy. *Radiat. Oncol. In press*

# Quality assurance of RapidArc treatments with portal dosimetry: multicentric clinical practice experience.

G. Nicolini<sup>1</sup>, A. Clivio<sup>1</sup>, E. Vanetti, A Fogliata<sup>1</sup>, G. Urso<sup>4</sup>, Fenoglietto<sup>2</sup>, E. Parietti<sup>5</sup>, Hrbacek<sup>3</sup>, S. Kloeck<sup>3</sup>, L. Cozzi<sup>1</sup>

<sup>1</sup>Oncology Institute of Southern Switzerland, Medical Physics Unit, Bellinzona, Switzerland

<sup>2</sup>Istituto Clinico Humanitas, Radiation Oncology, Rozzano, Italy

<sup>3</sup>CRLC Val d'Aurelle-Paul Lamarque Montpellier, France

<sup>4</sup>Istituti Ospedalieri di Cremona, Italy

<sup>5</sup>Radiation Oncology Dept., University Hospital Zuerich, Switzerland

mail: [afc@iosi.ch](mailto:afc@iosi.ch)

## Introduction

Quality assurance data from five centers were analysed to assess reliability of RapidArc delivery method in terms of machine and dosimetric performances.

## Material and Methods

i) General treatment data were reported to describe the RapidArc delivery features on a large collective of patients. ii) machine quality assurance was performed according to C. Ling et al [IJROBP. 2008;72:575-81]. In addition, single arcs, representing a typical clinical case, was delivered with biweekly frequency. iii) Pretreatment dosimetric validation of plan delivery is performed for each patient. All measurements and computations were performed at the depth of maximum dose in water (~15 mm for 6MV beams) according to the GLAaS method [Nicolini et al Radiat Oncol 2008;3:24] using EPID measurements;  $\gamma$  evaluation with  $\Delta d = 3\%$  and DTA=3mm scoring the gamma agreement index (GAI, % of field area passing the test).

## Results

:i) 275 patients (395 arcs) were included in the study. Averages for main delivery parameters were: collimator angle:  $35.2 \pm 17.2^\circ$ ; gantry speed:  $46.8 \pm 0.3$  cm/s; dose rate:  $361 \pm 169$  MU/min; beam on time:  $1.5 \pm 0.4$  min for a prescription ranging from 1.8 to 16.7 Gy/fraction. ii) mean deviations from baseline for reproducibility of dose rate and gantry speed variation ranged from -0.61 to 1.75%, the same value for leaf speed variation ranged from -0.73 to 0.41%. Mean GAI of repeated (8 months) clinical field was  $99.2 \pm 0.2\%$ . iii) mean GAI was  $96.3 \pm 2.3\%$  ranging from 84.7 to 100%.

## Discussion

RapidArc delivery was analysed in a variety of clinical conditions and proved to be reliable and dosimetrically accurate.

## References

- [1] Ling C, Zhang P, Archambault Y, Bocanek J, Tang G, Losasso T. Commissioning and quality assurance of RapidArc radiotherapy delivery system Int. J. Radiat. Oncol. Biol. Phys. 2008;72:575-81 [4] Gagne IM, Ansbacher W, Zavgorodni S, Popescu C, Beckham WA. A Monte Carlo evaluation of RapidArc dose calculations for oropharynx radiotherapy. Phys Med Biol. 2008; 53: 7167-85
- [2] Nicolini G, Vanetti E, Clivio A, Fogliata A, Korreman S, Bocanek J, Cozzi L. The GLAaS algorithm for portal dosimetry and quality assurance of RapidArc, an intensity modulated rotational therapy. Radiat Oncol 2008;3:24
- [3] Popple R, Brezovich I, Duan J, Shen S, Wu X. RapidArc patient specific quality assurance: comparison with DMLC IMRT. Med. Phys. 2009;36:2422
- [4] Korreman S, Medin J, Kjaer-Kristoffersen F. Dosimetric verification of RapidArc treatment delivery. Acta Oncologica 2009;48:185-91

# On the impact of treatment couch modeling on rapidarc

E. Vanetti<sup>1</sup>, A. Clivio<sup>1</sup>, A Fogliata<sup>1</sup>, G Nicolini<sup>1</sup>, L Cozzi<sup>1</sup>

<sup>1</sup>Oncology Institute of Southern Switzerland, Medical Physics Unit, Bellinzona, Switzerland

mail: [afc@ios.ch](mailto:afc@ios.ch)

## Introduction

A planning and dosimetric study was carried out on a cohort of six CT dataset from patients treated for prostate cancer to assess the impact of couch modelling on accuracy of dose calculation for the volumetric modulated arc technique RapidArc.

## Material and Methods

For each patient RapidArc plans were optimised using the couch while final dose calculation was performed with different conditions (thin, medium, thick and no couch). Analysis was performed in terms of dose volume histograms, dose difference histograms and 3D-g tests. Pre-treatment verification measurements were performed using the PTW 729 array in conjunction to the Octavius phantom; similarly, HU characterisation of couch was performed with the same phantom and ion chamber measurements comparing calculations and experimental data.

## Results

A set of HU valid for low and high energy and the entire couch length was found as: internal structure HU=-960, surface shell HU=-700. Analysis of dose plans showed that differences larger than 1.5 Gy might be observed on significant fractions of PTVs (more than 30% at low energy, 5% at high energy) when the couch is either modelled or not in the dose calculation. Smaller differences are visible in the medium low dose regions. 3D-g evaluation showed that these differences are not recoverable within 3% or 3mm thresholds leading to gamma agreement index (GAI) as low as 85% in the high dose PTV for 6MV. Pre-treatment verification on composite delivery confirmed these observations and, at the same time, showed a good accuracy of dose calculations in the presence of couch modelling compared to delivery in the same conditions (GAI ranging from 95% to 100%).

## Discussion

Results, globally confirmed that the geometrical model build-in the planning system Eclipse is reliable and: i) there is no measurable effect if the wrong segment of the couch is used in the calculations ii) there are significant and of potential clinical impact discrepancies at the level of the target volumes if calculations are performed without couch and delivery is performed with couch; iii) the effect is particularly relevant at low energy (6 MV in this case) that is the configuration clinically used by most of the centres adopting IMAT or VMAT technologies.

## References

- [1] Otto, K.: Volumetric Modulated Arc Therapy: IMRT in a single arc. *Med. Phys.* 2008;35: 310-317
- [2] Fogliata A, Vanetti E, Albers D, et al. On the dosimetric behaviour of photon dose calculation algorithms in the presence of simple geometric heterogeneities: comparison with Monte Carlo calculations. *Phys Med Biol* 2007; 52:1363-1385.
- [3] Palma D, Vollans E., James K., Nakano S., Moiseenko V., Shaffer R., McKenzie M., Morris J., Otto K.: Volumetric modulated arc therapy for delivery of prostate radiotherapy. Comparison with intensity modulated radiotherapy and three-dimensional conformal radiotherapy. *Int. J. Radiat. Oncol. Biol. Phys.* 2008
- [4] Gagne IM, Ansbacher W, Zavgorodni S, Popescu C, Beckham WA. A Monte Carlo evaluation of RapidArc dose calculations for oropharynx radiotherapy. *Phys Med Biol.* 2008; 53: 7167-85

# Hippocampal avoidance with rapid arc and helical tomotherapy for base of skull tumors

A. Clivio<sup>1</sup>, S. Yartsev<sup>2</sup>, A. Fogliata<sup>1</sup>, E. Vanetti<sup>1</sup>, G. Nicolini<sup>1</sup>, L. Cozzi<sup>1</sup>

<sup>1</sup>Oncology Institute of Southern Switzerland, Bellinzona, Switzerland

<sup>2</sup>London Regional Cancer Program, London, Canada

mail: [afc@ios.ch](mailto:afc@ios.ch)

## Introduction

The presence of radiosensitive neurogenic stem cells in the hippocampal area suggests identification and avoidance of the hippocampi may reduce the potential risks of radiation related cognitive and memory impairment.

## Material and Methods

Six patients treated for base of skull tumors (4 pituitary adenoma, 2 meningioma) were re-planned with specific hippocampus sparing using co-planar helical tomotherapy (HT) as well as co-planar and non-coplanar volumetric arc techniques: Rapid Arc (RA). Two options (10 and 2 mm) of PTV margins were considered to evaluate the impact of on-board image guidance/stereotaxis enabling tighter margins. The PTV dose was set for all plans to 50 Gy. The hippocampal areas were identified and contoured as avoidance structures with the specific goal of minimizing the planned dose to the hippocampus while respecting other organ at risk dose limits.

## Results

Comparison of the hippocampus avoidance plans with HT and different number of arcs in RA approach demonstrated the importance of non-coplanar delivery when larger GTV to PTV margins were used (10mm). With smaller PTV margins (2mm) both co-planar and non-coplanar delivery provided similar degrees of hippocampal sparing although a benefit for brainstem and optic nerve sparing was still noted with non-coplanar delivery (although PTV and OAR constraints were met by all techniques). A similar benefit was noted with 2 versus 3 non-coplanar arc plans.

## Discussion

Our comparisons suggest interventions to minimize GTV to PTV margins (accurate tumor volume delineation and image guidance) have a profound influence on the ability to spare intracranial OAR. Non coplanar techniques could be advisable when larger margins are used.

## References

- [1] Byrne TN: Cognitive sequelae of brain tumor treatment. *Curr Opin Neurol* 18:662-6, 2005
- [2] Eriksson PS, Perfilieva E, Bjork-Eriksson T, et al: Neurogenesis in the adult human hippocampus. *Nat Med* 4:1313-7, 1998
- [3] Cozzi L, Clivio A, Bauman G, et al: Comparison of advanced irradiation techniques with photons for benign intracranial tumours. *Radiother Oncol* 2006; 80:268-73.
- [4] Yartsev S, Kron T, Cozzi L, et al: Tomotherapy planning of small brain tumours. *Radiother Oncol* 74:49-52, 2005

# Volumetric modulated arc therapy in stereotactic body radiation therapy for metastases to abdominal lymph-nodes

L.Cozzi<sup>2</sup>, M. Bignardi<sup>1</sup>, A.Fogliata<sup>2</sup>, G. Nicolini<sup>2</sup>, E. Vanetti<sup>2</sup>, A. Clivio<sup>2</sup>, M. Scorsetti<sup>1</sup>

<sup>1</sup>Istituto Clinico Humanitas, Rozzano (Milan), Italy

<sup>2</sup>Oncology Institute of Southern Switzerland, Bellinzona, Switzerland

mail: [afc@ios.ch](mailto:afc@ios.ch)

## Introduction

A planning study was performed comparing volumetric modulated arcs, RapidArc (RA), fixed beam IMRT (IM) and conformal radiotherapy (CRT) with multiple static fields or short conformal arcs in a series of patients treated with hypofractionated stereotactic body radiation therapy (SBRT) for solitary or oligo-metastases from different tumors to abdominal lymph nodes.

## Material and Methods

Fourteen patients were included in the study. Dose prescription was set to 45 Gy (mean dose to CTV) in 6 fractions of 7.5 Gy. Objectives for CTV and PTV were: Dosemin>95%, Dosemax<107%. For organs at risk the following objectives were used: Maximum dose to spine <18Gy; V15Gy<35% for both kidneys, V36Gy<1% for duodenum, V36Gy<3% for stomach and small bowel, V15Gy<(total liver volume - 700 cm<sup>3</sup>) for liver. DVH were evaluated to assess plan quality.

## Results

Planning objectives on CTV and PTV were achieved by all techniques. RA improved PTV coverage (V95%=90.2±5.2% for RA compared to 82.5±9.6% and 84.5±8.2% for CRT and IM respectively). Most planning objectives for OARs were met by all techniques, except for duodenum, small bowel and stomach where in some patients the CRT plans exceeded the dose/volume constraints. MU/fraction were: 2186±211 for RA, 2583±699 for IM and 1554±153 for CRT.

## Discussion

SBRT delivery by RapidArc showed improvements in conformal avoidance with respect to standard conformal irradiation. Delivery parameters confirmed logistical advantages of Rapidarc, particularly compared with fixed beam IMRT.

## References

- [1] [Choi C, Cho C, Yoo S, et al.: Image-guided Stereotactic Body Radiation Therapy in Patients with Isolated Para-aortic Lymph Node Metastases from Uterine Cervical and Corpus Cancer. Int J Radiat Oncol Biol Phys. 2008 Epub
- [2] Macdermed DM, Weichselbaum RR, Salama JK. A rationale for the targeted treatment of oligometastases with radiotherapy. J Surg Oncol. 2008;98:202-6.
- [3] Cozzi L, Dinshaw KA., Shrivastava SK., Mahantshetty U., Engineer R., Deshpande DD., Jamema SV, Vanetti E., Clivio A., Nicolini G., Fogliata A. A treatment planning study comparing volumetric arc modulation with RapidArc and fixed field IMRT for cervix uteri radiotherapy. Radiother. Oncol. 2008; epub PMID 18692929
- [4] Fogliata A., Clivio A., Nicolini G., Vanetti E., Cozzi L. Intensity modulation with photons for benign intracranial tumours. A planning comparison of volumetric single arc, helical arc and fixed gantry techniques. Radiother. Oncol. 2008, epub PMID 18760851

# The first IMRT dosimetry intercomparison of the SGSMP using a thorax phantom with inhomogeneities

H.Schiefer<sup>1</sup>, G. Nicolini<sup>2</sup>, A. Fogliata<sup>2</sup>, W.W. Seelentag<sup>1</sup>, and M.K. Fix<sup>3</sup>

<sup>1</sup> Klinik für Radio-Onkologie, Kantonsspital St.Gallen, St.Gallen

<sup>2</sup> Oncology Institute of Southern Switzerland, Medical Physics, Bellinzona

<sup>3</sup> Division of Medical Radiation Physics, Inselspital, Bern University Hospital, and University of Bern  
mail: [johann.schiefer@kssg.ch](mailto:johann.schiefer@kssg.ch)

## Introduction

An audit performed by an independent external body is a fundamental step in any dosimetry quality assurance program. [1]. An issue often discussed is the ability of the planning systems to take into account inhomogeneities, especially in the thorax region. So, it has been decided to perform a national intercomparison in Switzerland dealing with IMRT in the thorax region.

## Material and Methods

The intercomparison has been organized by the team of the Cantonal Hospital of St.Gallen. The thorax phantom 002LFC (CIRS Inc.) has been used. To accommodate the TLDs, a standard slice has been modified with 54 drillings grouped in 7 anatomic regions. The CT scan has been carried out by the institutions themselves. For the planning process, dose constraints for different structures had to be considered. The applied CT dose has been measured with additional TLDs, attached to the phantom surface. Measurements have been done with TLDs, EDR2 films (Kodak) and ionisation chambers (4 positions). Measurements of an additional irradiation with a single field using TLDs and ionisation chamber allowed checking the absolute dosimetry and correcting for systematic errors. The TLD procedure has been described elsewhere [2]. Altogether 23 institutions participated with 24 machines. 30 planning-irradiation combinations have been evaluated. For the planning evaluation, the calculation algorithms have been classified as type a and type b algorithms. In contrast to type a algorithms, type b algorithms are 3D. They are able to treat the electron transport in an approximate way as well as the secondary photon transport in the medium.

## Results

*Machine output check:* The ratio between the measured to the stated dose has been  $1.007 \pm 0.010$  (ion chamber measurement and  $1.002 \pm 0.014$ , respectively (TLD measurement).

*Planning check:* Due to the limited number of participants, it is not possible to issue reliable statements on the properties of the applied calculation algorithms. Nevertheless, there are some trends to observe: Generally, „type b“ algorithms take inhomogeneities better into account than “type a” algorithms. In the lung region of the PTV, the difference of the calculated dose  $D_c$  to the measured dose  $D_m$  relative to the stated dose  $D_{\text{prescribed}}$ ,  $(D_m - D_c)/D_{\text{prescribed}}$ , is -0.4 % instead of -5.5 %. In regions outside the lung tissue type a algorithms show similar satisfying results as type b algorithms. Further results have been presented in [3] and will be published in detail.

## Discussion

The results of the intercomparison exceed the expectations. They suggest that cancer patients in Switzerland get a suitable radiation therapy in any of the centres offering this treatment modality. In the future, the IMRT intercomparison will be repeated regularly with modified objectives.

## References

- [1] Izewska J., Svensson H., Ibbott G.: Worldwide quality assurance networks for radiotherapy dosimetry. International Atomic Energy Agency. Standards and codes of practice in medical radiation dosimetry (2003) 2: pp. 139 – 55
- [2] Schiefer H., Seelentag W.W., Stucki G.: Ein nationaler Dosimetrievergleich durch Postversand von TLDs. Proceedings of the SGSMP Scientific meeting in Sion 2001, ISBN 3 906 401 34-0, S. 89 - 94
- [3] Schiefer H. and Seelentag W.W. Results of the IMRT dosimetry intercomparison 2008. SGSMP Bulletin Nr. 68 (2009) 1: pp 16– 19. <http://www.sgsmp.ch/bullA91.pdf>

# The influence of the bow tie filtration on the dose and image quality for the Elekta XVI coneBeam CT

L. Wissmann<sup>1</sup>, S. Peters<sup>2</sup>, W.W. Seelentag<sup>2</sup>

<sup>1</sup> Department of Physics, ETH Zürich, 8093 Zürich

<sup>2</sup> Klinik für Radio-Onkologie, Kantonsspital St.Gallen, St.Gallen

mail: [lukaswi@student.ethz.ch](mailto:lukaswi@student.ethz.ch)

## Introduction

Cone Beam Computer Tomography (CBCT) is used to control the position of the patient based on internal body structures. Thereby, the CBCT data set is fitted to the planning CT image. The accuracy of this alignment process strongly depends on the quality of the CBCT images. The radiotherapy department of the cantonal hospital St.Gallen operates two Elekta Synergy linacs equipped with an integrated CBCT. One linac is equipped with a bowtie filter which reduces the dose originating from the body surface and, in this way, reduces image artefacts. It was the aim of the presented study to evaluate the influence of the bowtie filter on the image quality and the dose to the patient.

## Material and Methods

Image acquisitions have been performed without and with the bowtie filter (mAs product 1.6 times larger than without filtration). For the dose measurements, CBCT images have been acquired using CT body and head phantoms (Capintec, INC, NJ, USA). Three different collimators have been applied: M10 ( $\varnothing = 41.7$  cm, length = 13.5 cm); S20 ( $\varnothing = 27.4$  cm, length = 27.7 cm); L20 ( $\varnothing = 50.7$  cm, length = 27.7 cm). The dose measurements have been performed in the centre ( $D_c$ ) and in four peripheral positions ( $D_{p,i}$ ,  $i = 1..4$ ) with a PTW31003 chamber and the PTW Unidos electrometer (PTW Freiburg). The CT dose index (CTDI) has been calculated based on the expressions

$$CTDI = 1/3 \times (D_c + 2/3 \times D_p); D_p = 1/4 \times (D_{p,1} + D_{p,2} + D_{p,3} + D_{p,4}).$$

For the determination of the image resolution, the CatPhan 500 CT phantom (The Phantom Laboratory, NY, USA) and the module CTP 528 (provided with line patterns showing 1 to 21 lines per cm) have been used. The modulation transfer function (MTF) has been derived as described by [1]. The homogeneity has been investigated by evaluating concentric 5 mm rings. Additionally, acquisitions of an Alderson Phantom (RSD, INC, CA, USA) have been evaluated.

## Results

The CTDI values are summarized in table 1.

	without filter	with filter	ratio
S20	$(1.10 \pm 0.03) \cdot 10^{-3}$ Gy	$(1.26 \pm 0.03) \cdot 10^{-3}$ Gy	114.1%
M10	$(2.99 \pm 0.03) \cdot 10^{-2}$ Gy	$(2.94 \pm 0.03) \cdot 10^{-2}$ Gy	98.5 %
L20	$(1.22 \pm 0.01) \cdot 10^{-2}$ Gy	$(1.14 \pm 0.01) \cdot 10^{-2}$ Gy	93.6 %

Table 1.: CTDI values for different collimators, with and without bowtie filter

The bowtie filter has no apparent influence on the image resolution. Only for the S20 collimator, the MTF shows larger values (for 5 to 9 lines per cm) than without filtration. The surface of the Capintec phantom, acquired with the bowtie filter, shows a sharper edge but also artefacts in the air due to an overcompensation effect. This is valid for all tested collimators, but more pronounced for larger collimators. The same observation can be done with the Alderson phantom. See further results in [2].

## Discussion

The influence of the bowtie filter on the applied dose is clearly smaller than 20 %. While the resolution is not affected markedly, the image quality is better especially for larger collimators.

## References

- [1] Ronald T. Droege and Richard L. Morin. A practical method to measure the MTF of CT scanners. Med. Phys., 9 (5):758–760, 1982.
- [2] Lukas Wissmann. Einfluss von Bow-Tie-Filtration auf Dosis und Bildqualität beim Elekta XVI ConeBeam CT. Term paper, ETH Zürich, 2009.

# DOSE CALCULATION FOR ORTHOVOLTAGE RADIOTHERAPY USING SWISS MONTE CARLO PLAN

D. Frauchiger, D. Terribilini, B. Isaak, P. Manser, D. Frei, W. Volken and M. K. Fix  
Division of Medical Radiation Physics, Inselspital and University of Berne, Switzerland  
mail: [daniel.frauchiger@insel.ch](mailto:daniel.frauchiger@insel.ch)

## Introduction

Dose calculation for low energy (kV) treatments are mainly based upon measured depth dose curves and output factors in water for the used energies and add-ons. Therefore, treatment planning is limited and interpretation of clinical outcome of the treated patients becomes very difficult because of not knowing the delivered 3D dose distributions. Due to difficulties in low energy dose calculations using analytical models, Monte Carlo dose calculations are preferred in this situation. The goal of this work is to enable dose calculations of an orthovoltage beam within the Swiss Monte Carlo Plan (SMCP)<sup>1</sup>.

## Material and Methods

To implement the geometry of the PANTAK DXT300 equipped with a COMET MXR-321 x-ray tube, the dimensions of all beam defining components were measured. The parts within the vacuum tube could not be measured and therefore the dimensions supplied by the manufacturer were used. The thickness of the Beryllium window and the anode angle were assumed to be 3 mm and 30°, respectively, as provided by the manufacturer. X-ray tube voltages were measured with the Keithley Triad System 35080B non invasive divider and the Mobile Filter Pack 50-135kV. Measured x-ray tube voltages were about 5% higher than the nominal voltages. The geometry was implemented in BEAMnrc<sup>2</sup> using the provided user interface. Geometry modules XTUBE, SLABS, CONS3R, CONESTAK and CHAMBER were used to define the X-ray tube with the energy depending filter.

A first phase space was generated after the exit window of the PANTAK machine for each of the available 8 energies (50 kV, 75 kV, 100 kV, 125 kV, 150 kV, 200 kV, 250 kV, 300kV). A second phase space was created after an add-on using the previous generated phase space data from the Pantak machine head as input (see figure 1). Having 8 energies and 7 add-ons meant to produce 43 phase spaces, 8 for each energy and 35 for each add-on at each energy. Using particles from the phase space below the add-on, dose calculations in a 30x30x30 cm<sup>3</sup> water tank were performed with the DOSXYZnrc code within SMCP. Simulation results were compared with measurements made with an ionization chamber (PTW 31010 0.125 ccm) as well as with a Diode (PFD Scanditronix) to obtain measurements near the surface for energies lower than 100 kV. Having checked the plausibility, the phase spaces were taken as input for the SMCP calculations on CT data.

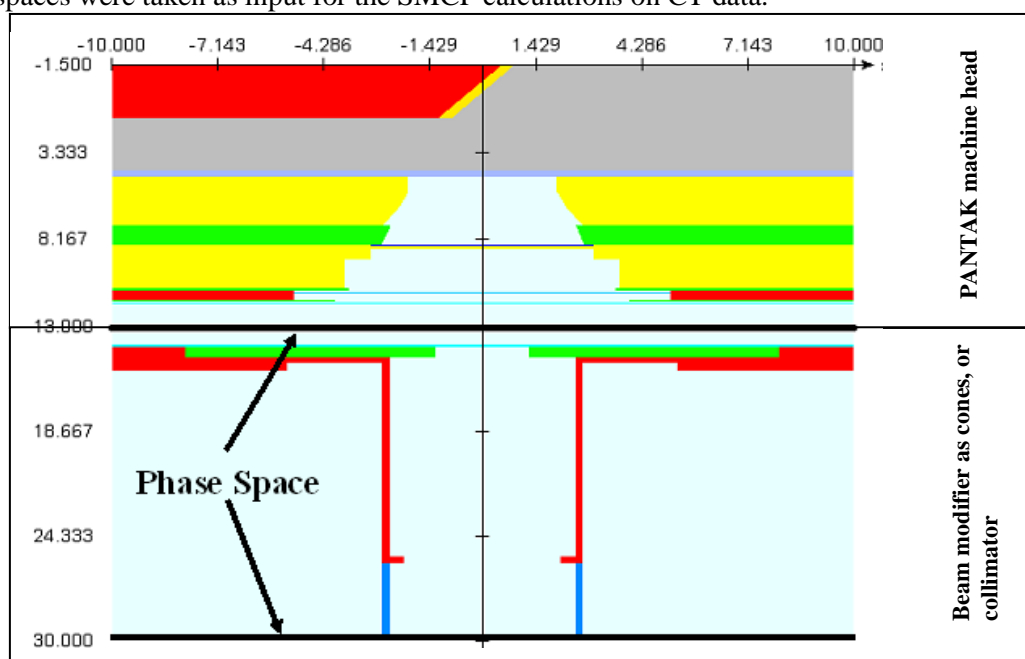


Figure 1: Scheme of the PANTAK DXT 300 implementation in BEAMnrc with the 5 cm cone

## Results

Calculated and measured depth doses and profiles for all add-ons agree within the 3% ( $2\sigma$ ) uncertainty. As an example the percentage depth dose (PDD) curve of the 300kV beam with the 2.5cm cone is shown in figure 2 and the corresponding PDD for the 5cm cone at 100kV is represented in figure 3. In figure 4 the PDD is calculated for the 2.5 cm cone at 100 kV within the SMCP framework and in figure 5 a crossplane-profile at 20 mm depth in water for the 5 cm cone at 50 kV is shown. Dose calculation grid size was  $2 \times 2 \times 2 \text{ mm}^3$  for all presented calculations. Dots represent MC calculations and the dashed line the measurement in figures 2 to 5.

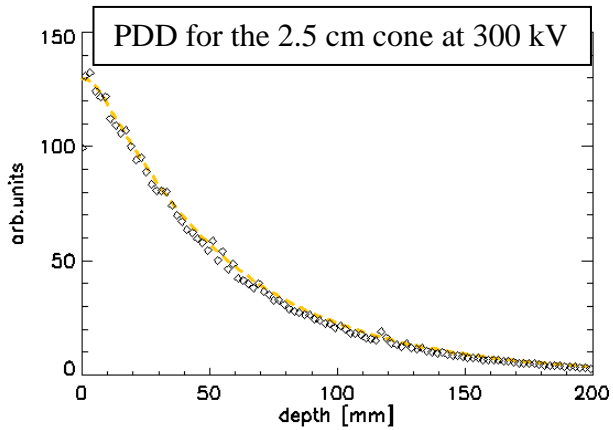


Figure 2: PDD for 2.5 cm cone at 300kV

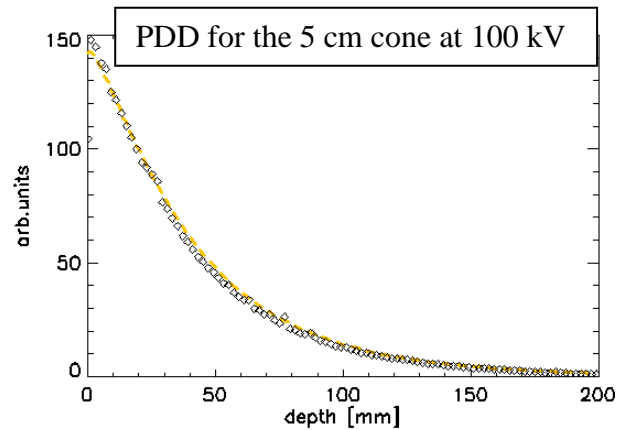


Figure 3: PDD for 5 cm cone at 100kV

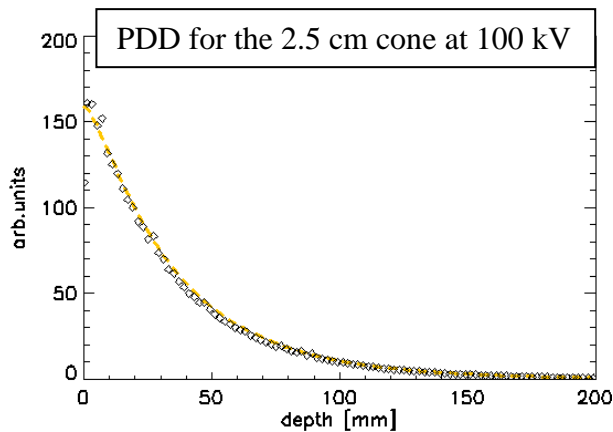


Figure 4: PDD for 2.5 cm cone at 100 kV

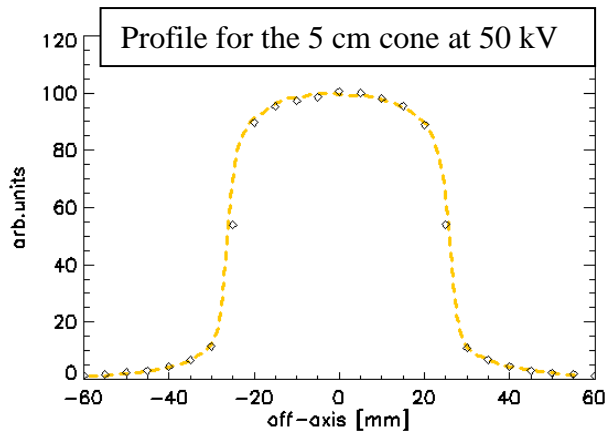


Figure 5: crossplane-profile in water for 5 cm cone at 50 kV in a depth of 2 cm

Figure 6 represents the resulting 3D dose distribution of a typical nose treatment using one field with a 5 cm cone at an energy of 100 kV calculated using SMCP. Due to calculating dose to medium bony structures absorbed about 4 times more energy than water equivalent tissue at this energy. This is also visible in the related dose volume histogram (DVH) shown in figure 7.

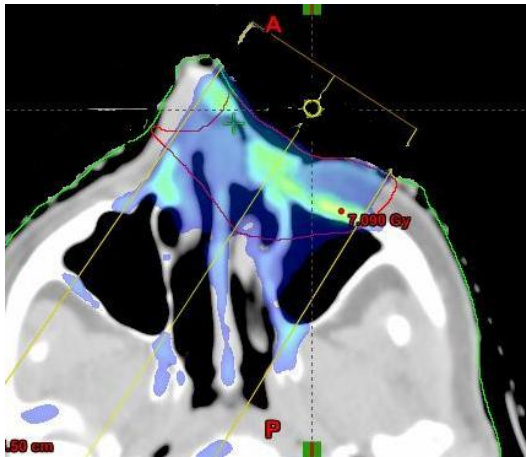


Figure 6: 3D dose distribution of a nose treatment

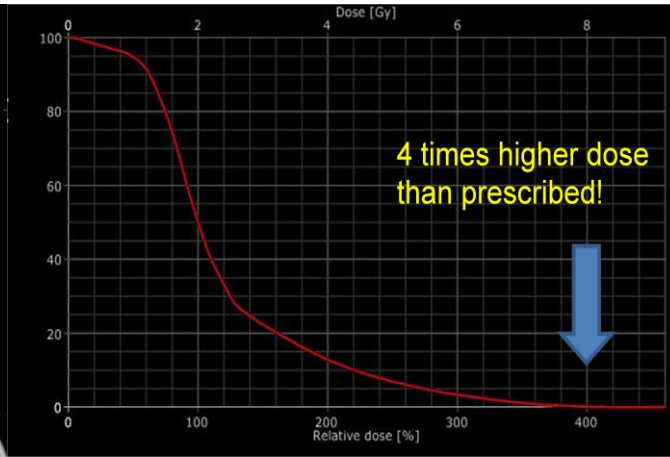


Figure 7: DVH of the dose distribution shown in figure 6

Figure 8 represents the resulting 3D dose distribution of an academic skull treatment using 5 fields with an energy of 100 kV each defined with an adjustable collimator calculated using SMCP. The surface of the skull receives a mean dose of 2 Gy, whereas bony structures receive again up to 5 times more dose due to dose to medium calculation and overlapping of the treatment fields.

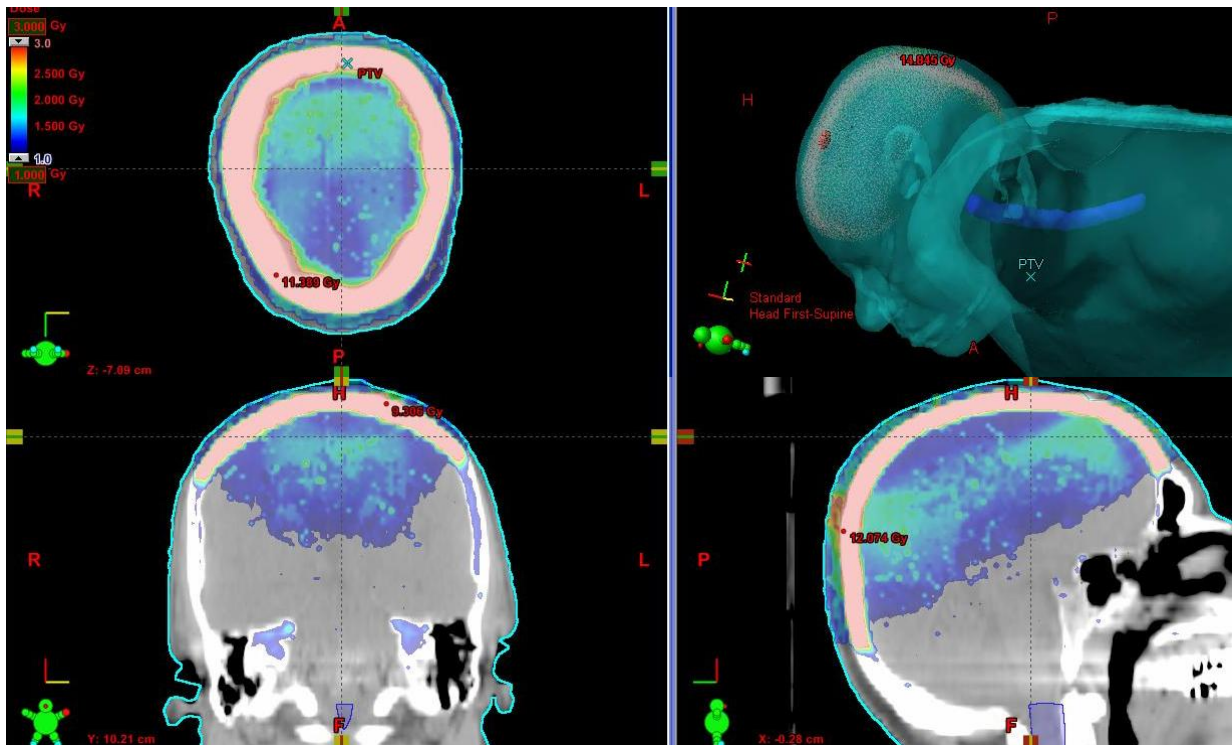


Figure 8: 3D dose calculation of an academic 5 field skull treatment using an adjustable collimator at 100 kV

## Discussion

3D dose calculations of an orthovoltage treatment have been performed using SMCP with phase space data derived using the BEAMnrc user code. To improve accuracy of simulations an optimization of the geometries is work in progress. To obtain better statistics, that means lowering the simulation uncertainties, the number of simulated particles have to be increased. Enabling the calculation of dose to water within SMCP will be considered if necessary. The interpretation of such dose calculations as shown is beyond the goal of this work but have to be discussed elsewhere.

## References

- [1] Fix M K et al, An efficient framework for photon Monte Carlo treatment planning, Phys. Med. Biol. 52, N425-N437, 2007
- [2] Kawrakow I, Rogers DWO, The EGSnrc Code System: Monte Carlo Simulation of Electron and Photon Transport, NRCC Report PIRS-701, 2003

# Independent 2D dose calculation of IMRT fields using MapCALC

A.-C. Schulte, M. Fix, P. Manser, R. Mini, D. Terribilini, D. Vetterli, D. Frauchiger  
Abteilung für Medizinische Strahlenphysik, Inselspital Bern  
mail: [anja-carina.schulte@insel.ch](mailto:anja-carina.schulte@insel.ch)

## Introduction

Quality assurance (QA) for IMRT is usually performed by comparing calculated 2D dose distributions with measurements using film, EPID, or 2D detector arrays, often in combination with an ionization chamber for absolute dose at one point. However, these methods are time-consuming and require access to the linear accelerator. We investigated the potential of a planar dose calculation algorithm for independent IMRT treatment verification, which would make additional patient-specific measurements redundant.

## Material and Methods

The algorithm uses an advanced two-source model [1] and has to be commissioned using Linac/MLC-parameters, dose profiles, and output factors measured in a specific dose plane. With this model planar dose and fluence maps of 1 mm<sup>2</sup> spatial resolution are calculated from patient plan data (incl. MLC leaf-map), exported from the treatment planning system (TPS). We used MapCALC, the commercialized algorithm by SunNuclear, and generated a model for a 6 MV Varian linac equipped with a millennium 120 MLC at an SSD of 90 cm and a dose plane depth of 10 cm. This model was then applied to calculate 2D dose maps of 10 clinical IMRT prostate plans (5 fields each) applying sliding window technique. The resulting dose maps were compared to the calculation results of the TPS (Eclipse) using gamma analysis. In addition, we tested the sensitivity of the algorithm to detect artificial errors, created in the MLC leaf maps of randomly selected prostate fields.

## Results

The average passing rates for the 3%/3 mm and 2%/2 mm criteria were 99.9%±0.3% (range: 98.3-100%) and 98.4%±1.8% (range: 92.0-100%), respectively, whereby a threshold of 10% was applied. On average, isocenter and maximum dose values of MapCALC and TPS agreed within (0.6±0.7) cGy and (1.6±2.1) cGy, respectively, which corresponds to (0.3±0.4)% and (1.0±1.1)% of the applied dose per fraction. Fig.1 shows the result of an exemplary comparison for an IMRT prostate field. The effect of an artificial lag of a single leaf on the dose map calculated by MapCALC is presented in Fig. 2.

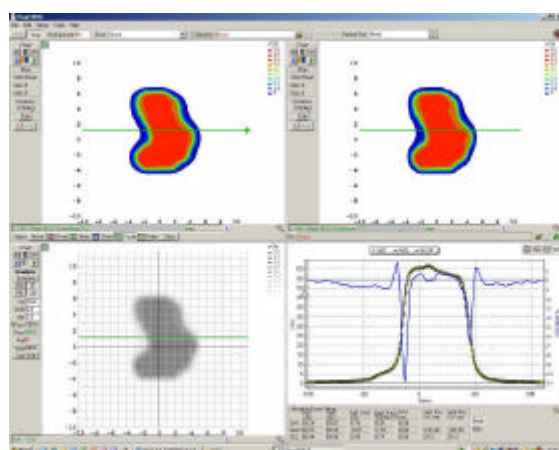


Fig.1: 2D dose plane calculated by MapCALC (top, left) and the TPS (top, right), the result of the gamma analysis (bottom, left) and corresponding profiles (bottom, right).

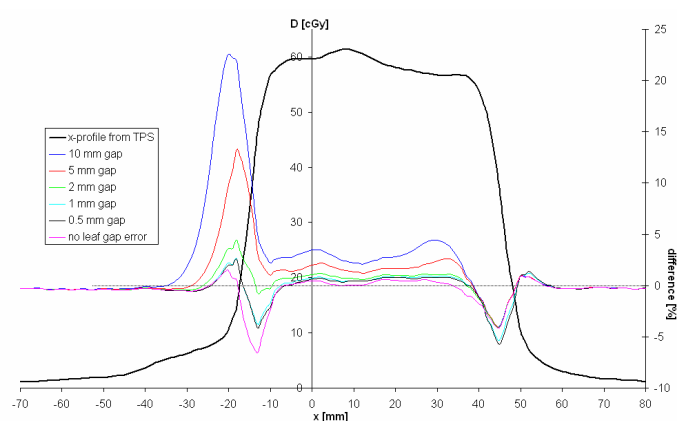


Fig.2: Dose planes with leaf gap errors ranging from 0.5 to 10 mm were calculated with MapCALC. The resulting profiles at the position of the respective leaf were subtracted from the corresponding dose profile of the original dose map calculated by the TPS (curve in black).

## Discussion

Our first tests show that MapCALC is a fast and reliable method for patient-specific 2D IMRT-QA of prostate plans. Accurate planar dose maps are calculated within seconds. Our work in progress is the evaluation of 2D dose distribution of more modulated fields - as e.g. in head and neck cases.

## References

[1] Yan, G.; Liu, C.; Lu, B.; Palta, J.R.; Li, J.G.: Comparison of analytic source models for head scatter factor calculation and planar dose calculation for IMRT. Phys Med Biol. 53(8) (2008), S. 2051 - 2067

# Implementing RapidArc on the Novalis Tx

P. Manser<sup>1</sup>, E.J. Born<sup>1</sup>, D. Schmidhalter<sup>1</sup>, D. Aebersold<sup>2</sup>, R. Mini<sup>1</sup>, M.K. Fix<sup>1</sup>

<sup>1</sup> Division of Medical Radiation Physics, Inselspital and University of Berne

<sup>2</sup> University Clinic for Radio-Oncology, Inselspital and University of Berne

mail: [peter.manser@insel.ch](mailto:peter.manser@insel.ch)

## Introduction

With the Novalis Tx (Varian Medical Systems and BrainLAB) high-precision radiation delivery is combined with high-precision imaging. RapidArc (Varian Medical Systems) is a recent method in radiation therapy enabling intensity modulated arc therapy. Several groups performed treatment plan comparisons which demonstrate that the quality of RapidArc based dose distributions is at least as good as for IMRT. In this work, we address the implementation, particularly the commissioning and quality assurance (QA) procedures, of RapidArc on the Novalis Tx.

## Material and Methods

The commissioning of RapidArc was based on ARIA 8.6 (Varian Medical Systems) and was pursued according to the procedures of the vendor. Machine related QA is performed by using portal dosimetry and is along with the paper from Ling et al. [1]. Patient specific quality assurance is based on the comparison of measured and calculated dose distributions on a phantom. For this purpose, either the Delta4 system (Scandidos) or portal dosimetry are used. Additionally, we extended our Swiss Monte Carlo Plan (SMCP) [2] in order to manage also RapidArc treatment plans.

## Results

The use of an electronic portal imaging device for machine and patient specific QA minimizes the efforts for QA. Patient specific QA using the Delta4 system demonstrates that RapidArc is not only efficient but also an accurate treatment modality. Monte Carlo based QA is performed for dedicated treatment plans. It is worth to note that due to its statistical nature, Monte Carlo calculation is more efficient for RapidArc treatments than for IMRT or 3DCRT.

## Conclusion

Clinical implementation of RapidArc on the Novalis Tx was successfully realized. QA procedures were conducted by comparing dose measurements with corresponding calculations. Results from Monte Carlo based QA are very promising and will hopefully replace the measurement based patient specific QA in the future.

## References

- [1] Ling CC., Zhang P., Archaumbault Y., Bocanek J., Tang G., LoSasso T., Commissioning and quality assurance of RapidArc radiotherapy delivery system, *Int. J. Radiat Oncol Biol Phys*, 72(2):575-81, 2008
- [2] M.K. Fix, P. Manser, D. Frei, W. Volken, R. Mini, E.J. Born, An efficient framework for photon Monte Carlo treatment planning, *Phys. Med. Biol.*, 52, N425-N437, 2007

## Qualification of PET-CT scanners for use in SAKK 56/07 multicentre trial

F. Camus<sup>1,2</sup>, J. O. Prior<sup>2</sup>, G. Allenbach<sup>2</sup>, L. Modolo<sup>1,2</sup>, T. Hany<sup>4</sup>, J. Müller<sup>5</sup>, J. Coulot<sup>6</sup>, A. Bischof Delaloye<sup>2</sup>, S. Leyvraz<sup>3</sup>, M. Montemurro<sup>3</sup>, F.R. Verdun<sup>1</sup>

<sup>1</sup>University Institute for Radiation Physics (IRA), Centre Hospitalier Universitaire Vaudois and University of Lausanne, Switzerland

<sup>2</sup>Nuclear Medicine, Centre Hospitalier Universitaire Vaudois and University of Lausanne, Switzerland

<sup>3</sup>Lausanne Cancer Centre, Centre Hospitalier Universitaire Vaudois and University of Lausanne, Switzerland

<sup>4</sup>Klinik für Nuklearmedizin, Universitätsspital Zürich, Switzerland

<sup>5</sup>Nuklearmedizin, Kantonsspital St.Gallen, Switzerland

<sup>6</sup>Médecine Nucléaire, Institut de Cancérologie Gustave Roussy, Villejuif, France

E-mail: [Fabrice.Camus@chuv.ch](mailto:Fabrice.Camus@chuv.ch)

### Introduction

Our PET Core Laboratory qualifies sites to participate in an oncologic multicenter trial assessing therapeutic response with hybrid PET/CT performed for the Swiss Group for Clinical Cancer Research (SAKK) in Switzerland (n = 6) and France (n = 4). Each site must meet entry criteria before the first patient enrolment and accuracy of scanner SUV calibration verified. The PET Core Laboratory quantitatively reviews PET images of uniform phantoms submitted by each centre. This validation is crucial to ensure that changes observed during therapy actually correspond to real changes. Precise and accurate determinations of SUV are a prerequisite for any multicenter trial.

### Materials & Methods:

In order to qualify for participation, each PET centre had to submit a PET/CT dataset from a water-filled uniform phantom containing 40-55 MBq (6283 mL) or 80 MBq (9293 mL) of F-18-FDG scanned according to each centre's standard oncologic protocol. The activity of the phantom has to be determined precisely by measuring the syringe activity before and after injection in a dose calibrator. The average standardized uptake value (SUV) and standard deviation (SD) should be measured in the reconstructed image along all transverse slices. The expected SUV should be 1.00 g/mL in all slices with acceptable values ranging from 0.90 to 1.10 g/mL to accommodate possible variations of SUVs across PET scanners and institutions.

### Results:

The average SUVs for uniform cylinder images for the different scanners evaluated are reported in the Table. In total, 13 PET scanners in 10 participating centres performed these uniform phantom measurements and 1/13 (8%) did not qualify for study participation. This last centre performed manufacturer's maintenance of its PET/CT and the measurements were subsequently within acceptable SUV ranges.

Table. Uniform Phantom Mean SUVs vs. Scanner Model (g/mL)

Scanner Model	Mean±SD	Range before inclusion	Range after recalibration
GE Discovery (n=6)	0.99 ± 0.08	0.91 – 1.15*	0.91–1.10
Siemens Biograph (n=5)	1.02 ± 0.07	0.93 – 1.06	–
Philips Gemini (n=2)	0.98 ± 0.08	0.90 – 1.03	–

\*The centre with out-of-limit SUV was notified and performed manufacturer's maintenance, including a recalibration of the PET/CT.

### Discussion

Minimizing methodological errors in SUV measurement is critical to achieve accurate quantification, which is of utmost importance in multicenter clinical trials. Our results show that SUV accuracy must be verified in each centre, and that all centres are able to qualify for accurate SUV calibrations after additional recalibration. The stability of SUV values would also need to be verified by periodic assessment of SUV calibration during the whole trial duration.

# Influence of an Air Gap between Bolus and Patient Skin on Electron Beam Dose Characteristics

G. Kohler

Radioonkologie, Universitätsspital Basel (USB)

mail: [kohlerg@uhbs.ch](mailto:kohlerg@uhbs.ch)

## Introduction

In electron beam therapy bolus is often used to conform as closely as possible to the target volume while avoiding critical structures in the depth. In most cases a flexible bolus can cover the skin without air gap. However, under certain conditions it is difficult –or even not possible– to avoid air gaps between bolus and patient without reducing treatment quality. In a special clinical case in our hospital (USB) bolus was used in the neck region in combination with a head fixation. The fixation grid was not in contact with the patient skin in the treatment region but the bolus was attached outside the grid resulting in an air gap behind the bolus. Such an air gap can affect dose and dose distribution [1]. The aim of the current investigation is to evaluate the effects of an air gap behind a bolus on dose and dose distribution characteristics.

## Material and Methods

Three electron beam energies of an Elekta medical linear accelerator were used: The lowest and the highest available energy as well as one between (6, 10, 20MeV). The applicator (closed walls,  $12 \times 8 \text{ cm}^2$ , 96cm distance from focus to applicator end) is the standard applicator for electron treatment in the neck region at the USB. A typical asymmetrical lead insert ( $4 \times 8 \text{ cm}^2$ ) was used (Fig 1). The tissue equivalent bolus (Superflab, Mick Radio-Nuclear Instruments, USA; thickness 1cm,  $1.02 \text{ g/cm}^3$ ) was attached either in front or behind an air gap (2, 4cm) with the same thermo plast grid (Posticast, Sinmed BV, Netherlands) as used for head fixation. Percent depth dose (PDD), dose profiles, and relative dose were determined in a water phantom (MP3, PTW, Germany).

## Results

Depth of maximum dose in the unblocked central field axis was nearly unaffected by the air gap and the position of the bolus (front, behind). The same is valid for the 50% field width in the depth of the central beam maximum. In contrast, dose in the central field axis was reduced up to 30% (Fig 2) with the bolus in front of the air gap compared to the setting with the bolus behind the air gap. Furthermore, penumbra broadened clearly when the bolus was placed in front of the air gap (Fig 3). Both dose reduction and penumbra broadening are more expressed at lower energies and larger air gaps.

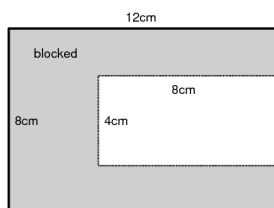


Fig 1: Scheme of the lead insert which is typically for the use in the neck region at the USB.

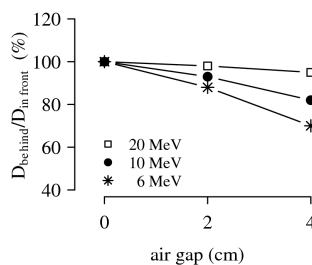


Fig 2: Relative dose in the center field axis with bolus placed in front of the air gap and behind.

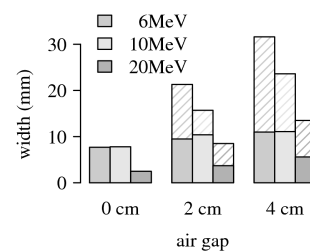


Fig 3: Penumbra width with bolus behind (filled) and in front (total height) of different air gap distances.

## Discussion

Even if PDD did not change remarkable due to the position of the bolus, dose decreased markedly at lower energies when the bolus is placed in front of the air gap instead behind. Furthermore a huge increase of the penumbra width was observed. The results show again how sensitive dose and dose distribution can be to small changes of the settings.

## References

- [1] Sharma SC, Johnson MW Surface dose perturbation due to air gap between patient and bolus for electron beams. *Med Phys.* (1993) 20:377-8.

# Absorption measurements for a carbon fiber couch top and its modelling in a treatment planning system

G. Kunz, F. Hasenbalg, P. Pemler<sup>1</sup>

<sup>1</sup> Klinik für Radio-Onkologie und Nuklearmedizin, Stadtspital Triemli Zürich

E-mail: guntram.kunz@triemli.zuerich.ch

## Introduction

Full carbon couch tops are widely used for radiotherapy treatments on linear accelerators. In contrast to their predecessors which were constructed with metal bars they have almost no limitations in choosing beam angles in treatment planning. In this work we have measured the absorption for the new Varian Exact IGRT couch top<sup>®</sup> for different setups. With the latest version of our treatment planning system (TPS), it is possible to model the couch top as a supporting structure with different options for parameter settings. We investigated the quality of the modelling of the couch top in the TPS and the influence on clinical dose distributions were analysed.

## Material and Methods

The couch top, of which the surface consists of carbon fiber and which is filled with foam [1], was CT-scanned (120 kV) together with the phantom setup used for dose measurement. Within the TPS (Eclipse V 8.6) a model of the couch top was added as a structure to the CT slices and was included in the dose calculation. The 3 different predefined thicknesses of the couch top model, thin (50 mm), thick (75 mm) or medium (62.5 mm) were added and evaluated. For absorption measurement we irradiated a cylindrical, isocentrically placed PMMA phantom (diameter 20 cm, length 12 cm) varying gantry angle, photon energy (6, 15 MV), field size (4 cm, 10 cm) and position at the couch top (thin and thick part). Further we irradiated a 1 mm spaced moving gap dMLC field (6 MV) under different gantry angles. By defining HU values for the couch top surface and the inner material of the couch top the model has been fitted to the measurement. With the thickness and the mass density of the carbon fiber and the given relation between mass density, electron density and the resulting HU value from the CT, we could confirm the HU value of the carbon fiber in the model. We compared the farmer chamber measurement to the TPS dose calculation with the original scanned couch top and with the couch top model. In a 5 field IMRT prostate plan we investigated the influence of the couch top on the dose distribution.

region	length [mm]	overall height [mm]
thin end / head	400	50
transition zone	350	50 .. 75
thick end / feet	1250	75

Tab. 1: Size of the couch top

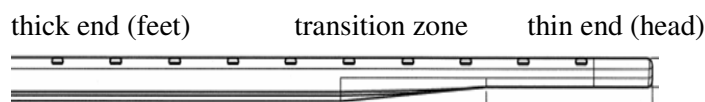


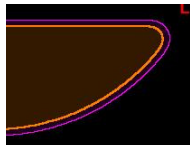
Fig. 1: Couch top design

components	mass density [g/cm <sup>3</sup> ]
cover/surface: carbon fiber	1.4 ± 0.2
inner material (foam): polymethacrylimide (Rohacell 51 <sup>®</sup> )	0.06 ± 0.01

Tab. 2: Real couch top composition

region	carbon fiber thickness	
	top [mm]	bottom [mm]
thin end / head	0.85	1.05
transition zone	0.85	1.05
thick end / feet	1.25	1.25 .. 3.05
edge	2 .. 3.5	

Tab. 3: Carbon fiber thickness

localization	real couch top	Eclipse couch top model
surface/ carbon fiber	0.8 to 3.5 mm	constant thickness; 4 mm
height	depending on region	constant
height at transition zone	50 ..75 mm	62.5 mm
edge & grooves for positioning tools		
whole couch top	deflection	no deflection

Tab. 4: Comparison between real couch top and Eclipse couch top model design

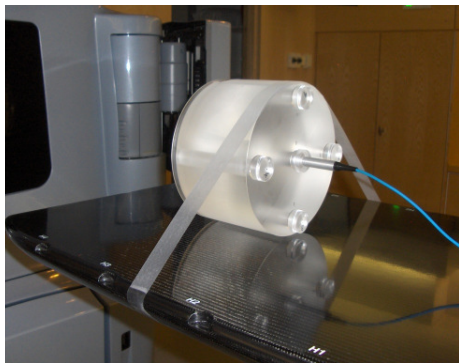


Fig. 2: Setup for the couch top absorption measurements: Isocentrically placed thimble chamber in a cylinder phantom (radius 10 cm).

## Results

The outline of the Eclipse couch top model and the real couch top are nearly identical in transversal projection. The passage from the thin to the thick part is approximated with the medium thickness (62.5 mm). The thickness of the carbon fiber in the model is constant over the whole couch top in opposition to the real situation. Therefore the calculation of the HU value of the carbon fiber for the model yields in the feet end to a lower HU value than in the head end (Tab. 6, 7). But by taking HU = - 680 for the carbon surface and HU = - 950 for the foam of the couch top the agreement between measurement and calculations is within 1% both thick end and thin end of the couch top. The calculation with the real scanned couch top deviates from the measurement because of the rough spatial resolution of the dose algorithm in comparison to the small thickness of the carbon surface. For a 4x4 cm<sup>2</sup> the absorption is roughly 0.3% higher than for the 10x10 cm<sup>2</sup> field, for 6 MV the absorption is about 1% higher than for the 15 MV. For clinical situations, where the lateral couch position is variable (e.g. prostate), the deviation may be larger because the dorso-lateral fields are passing through the couch only partially.

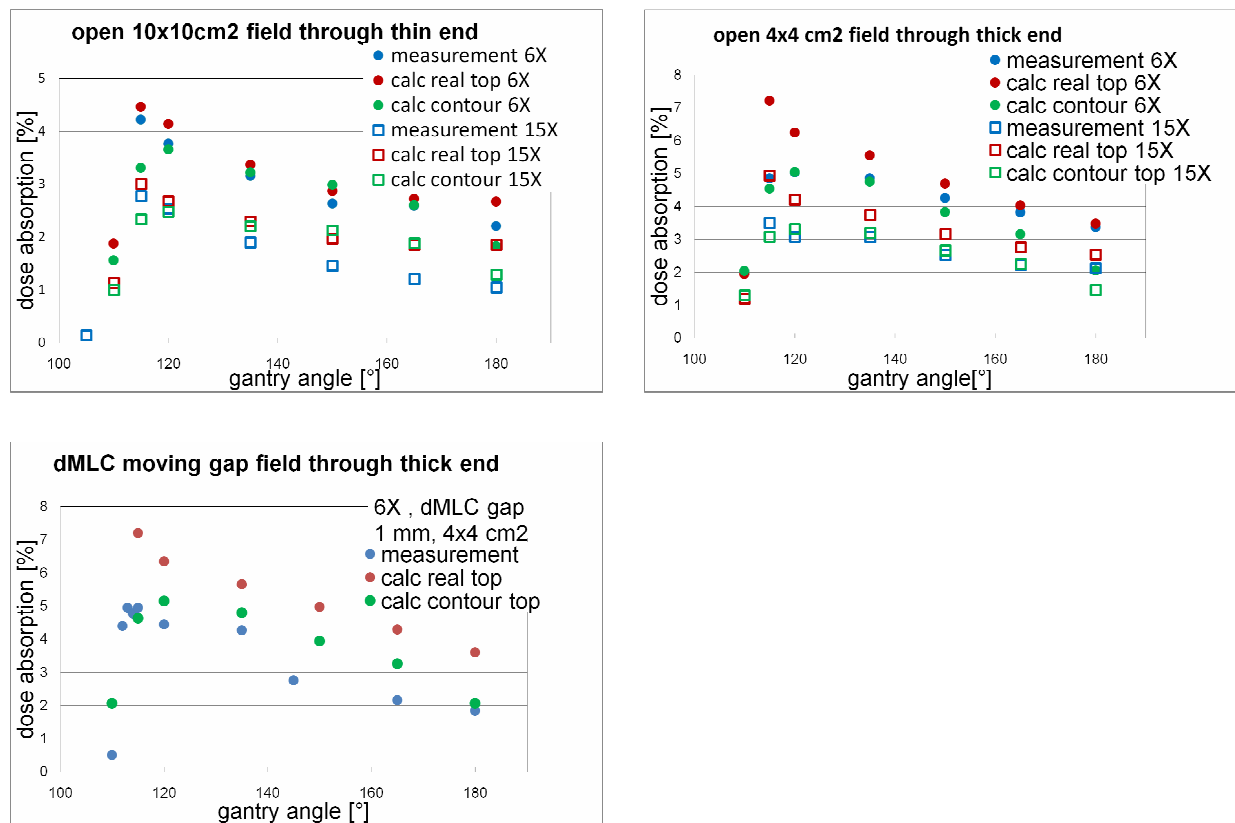


Fig. 3: Couch top absorption; comparison between measurement, top model contour and real scanned couch top

Absorption	thin part		thick part	
photon energy\gantry angle	180°	115°	180°	115°
6 MV	2.4%	3.5%	3.3%	4.5%
15 MV	1.2%	2.5%	2.2%	3.5%

Tab. 5: Couch top absorption by gantry angle 180° and 115° (nearly maximal value, worst case)

contour	HU ( $\sigma$ )	determination
internal	-950 (5)	<b>measured</b> in Eclipse
surface	-680	<b>fitted</b> to optimal agreement between measurement & planning (because of small surface thickness & rough spatial resolution )

Tab. 6: Determined HU values for the couch top

position	real surface thickness [mm] (top + bottom side)	model surface thickness [mm] (top + bottom side)	model surface density [ $\text{g}/\text{cm}^3$ ] (real density*real thickness/model thickness)	calculated HU of the carbon fiber surface	water equivalent thickness [cm]
head end, transition zone	$0.85 + 1.05 = 1.9$	$4 + 4 = 8$	$1.4 * 1.9 / 8 = 0.32$	$-710 \pm 70$	<b>0.58</b> $0.58 \dots 0.72$
feet end	$1.25 + 1.25 = 2.5$	$4 + 4 = 8$	$1.4 * 2.5 / 8 = 0.43$	$-620 \pm 70$	<b>0.83</b>

Tab. 7: Calculation of the HU for the carbon fiber (irradiation form gantry angle  $180^\circ$ ); real surface density (carbon fiber) =  $(1.4 \pm 0.2) \text{ g}/\text{cm}^3$ ; (assumption: constant relation between mass density and electron density and HU value for the carbon fiber)

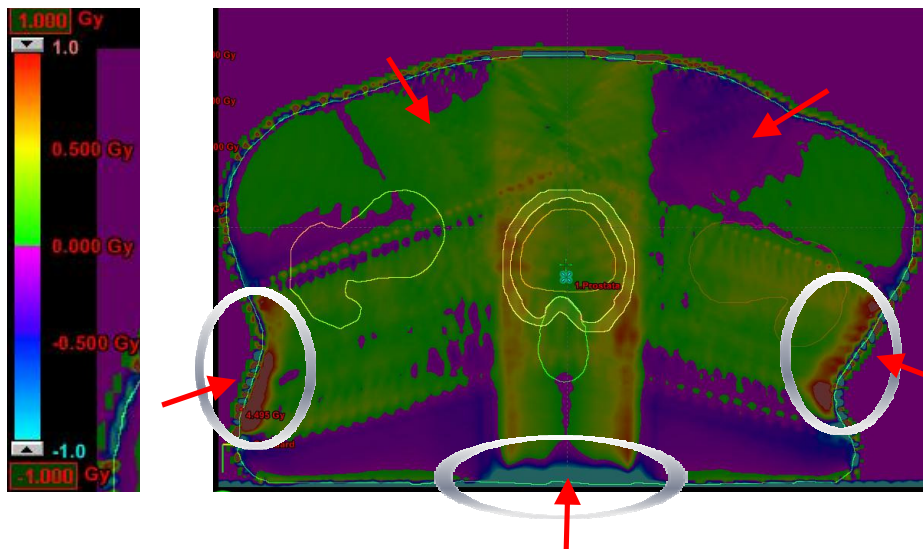


Fig. 4: Difference plan of two 5-field IMRT prostate plans with the same MU and fluence (Dose(PTV) = 70 Gy); difference plan = plan without couch – plan with couch (thick end); difference region: beam entrance of the field and near couch surface (build up)

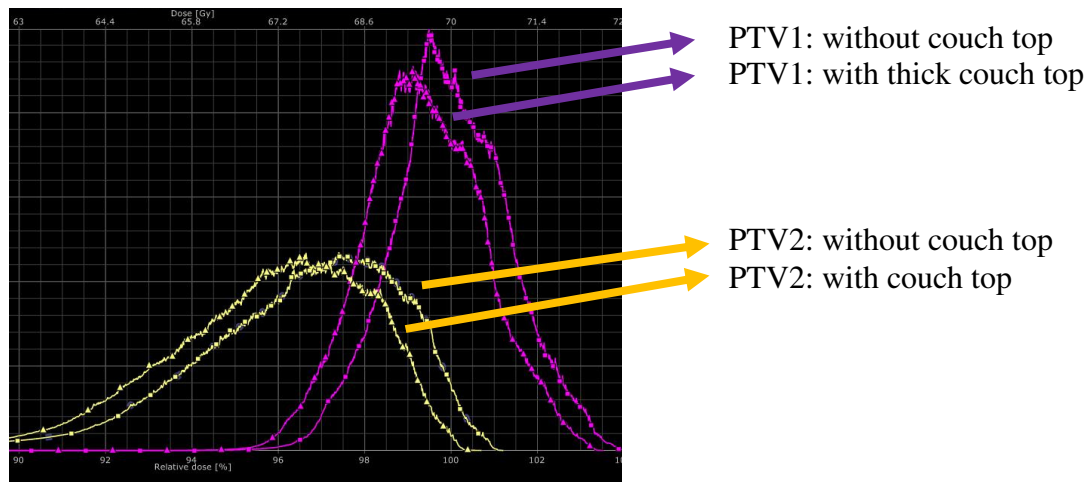


Fig. 5: Differential DVH for the high dose PTV (70 Gy) and the low dose PTV (54) for the two 5-field IMRT prostate plans (two plans with the same MU and fluence); triangle: plan including the thick end of the couch top; square: plan without couch; PTV1 (pink): 100% vs 99.4%; PTV2 (yellow): 96.4% vs 95.6%

## Discussion

Advantages of the couch top are the stiff material consisting of only two components and the low absorption. The different thicknesses and the 35 cm long passage from the thin to the thick part of the couch top and the constant thickness of the surface in the model in opposition to the real carbon fiber surface may be disadvantages. An advantage of the Eclipse couch top model is the possibility to adapt the Hounsfield Units of the surface and the inner material. As in some clinical situations, the treated volume is located in the transition zone between thick and thin end (e.g. head and neck), the model is only an approximation. For a higher precision, exact modelling of the couch top and absolute indexing of the patient position on the couch top in lateral and longitudinal direction would be necessary.

## References

[1] Exact IGRT Couch, User and Maintenance Guide, Varian Medical Systems, P/N 100026454-14, Dec. 2008

# Investigation of 6 MV static beams within the Swiss Monte Carlo Plan

V. Magaddino<sup>1,2</sup>, P. Manser<sup>2</sup>, D. Frei<sup>2</sup>, W. Volken<sup>2</sup>, D. Schmidhalter<sup>2</sup>, L. Hirschi<sup>2</sup>, M.K. Fix<sup>2</sup>

<sup>1</sup> University of Naples "Federico II", and INFN, Naples, Italy

<sup>2</sup> Division of Medical Radiation Physics, Inselspital – University of Berne, Switzerland

mail: [michael.fix@ams.unibe.ch](mailto:michael.fix@ams.unibe.ch)

## Introduction

Monte Carlo (MC) based dose calculations can compute doses with an accuracy that surpasses that of the conventional algorithms used in radiotherapy, especially in regions of tissue inhomogeneities and surface discontinuities. Currently only very few commercial treatment planning systems (TPSs) support photon MC treatment planning. This is mainly due to the lack of an accurate model of the accelerator radiation source, and long computing time needed to get reasonable statistical accuracy in the calculated dose distributions. The Swiss Monte Carlo Plan (SMCP) [1] developed at the Division of Medical Radiation Physics, Inselspital and University of Berne, overcame these problems by automation of the procedures needed for dose calculation and evaluation. This makes the MC environment very flexible and suitable for photon MC treatment planning. Aim of this study is the investigation of 6 MV beams within the framework of the SMCP.

## Material and Methods

For this study dose distributions for 6 MV were simulated in a water phantom using the following parameters: a phase space source; the VMC++ code [2] for the full radiation transport through the individual beam modifiers, such as jaws, wedges and block; the VMC++ code to compute the dose distribution in the phantom for the selected fields with a voxel size of 0.2 cm and a statistical uncertainty of about 0.5%. Simulated depth dose curves and profiles for open fields and fields with beam modifiers (wedges and block), ranging from 3x3 to 30x30 cm<sup>2</sup>, were compared with the corresponding measurements using dose difference and gamma analysis. For the commissioning of the block, its density has been used as parameter to match transmission measurements. For the wedged beams (15°, 30°, 45° and 60°) the density and the thickness of the wedges have been adjusted within the range specified by the manufacturer to match the according measurements for the largest field size available. The validation was performed for smaller field sizes down to 5x5 cm<sup>2</sup>.

## Results

Results for all open fields showed an excellent agreement between measurements and simulations, for the chosen dose difference criterion of  $\pm 1\%$  of  $D_{\max}$  and the distance to agreement criterion of  $\pm 1$  mm. The tuning of all wedges lead to an agreement with the corresponding measurement within 1% and 1mm. Similar results have been achieved for the block. For the validation of the tuned wedges, more than 99% of all voxel have a  $\gamma < 1$  using a 1%/1mm criterion.

## Discussion

The comparison of calculated and measured dose distributions lead to optimization of the simulation parameters such as density and shape of the beam modifiers. The SMCP has been validated so far for a photon beam of 6MV and static fields, but further studies will be carried out for the validation of the SMCP for additional beam energies and dynamic fields.

## References

- [1] M. K. Fix, P. Manser, D. Frei, W. Volken, R. Mini, and E. J. Born. An efficient framework for photon Monte Carlo treatment planning. *Phys. Med. Biol.*, Vol. 52, 2007, pp. N425-37.
- [2] I. Kawrakow, M. Fippel, and K. Friedrich. 3D dose calculation using a Voxel based Monte Carlo algorithm (VMC). *Med. Phys.* 23 (4), 1996.

# Low energy electron beam dose calculation using eMC

M.K. Fix<sup>1</sup>, D. Frei<sup>1</sup>, W. Volken<sup>1</sup>, H. Neuenschwander<sup>2</sup>, E.J. Born<sup>1</sup>, P. Manser<sup>1</sup>

<sup>1</sup> Division of Medical Radiation Physics, Inselspital – University of Berne, Switzerland

<sup>2</sup> Clinic for Radiation-Oncology, Lindenhofspital Berne, Switzerland

mail: michael.fix@ams.unibe.ch

## Introduction

In Eclipse (Varian Medical Systems) the electron Monte Carlo (eMC) dose calculation algorithm is based on the macro MC method [1, 2] and is able to accurately predict dose distributions for high energy electron beams. However, there are some limitations for low energy electron beams such as 4 and 6 MeV. The aim of this work is to improve the accuracy of the dose calculation for 4 and 6 MeV electron beams of Varian linear accelerators using eMC.

## Material and Methods

The eMC algorithm implemented in Eclipse uses the initial phase space multiple source model (IPS) as particle generator [3] and the macro MC method for the dose calculation [1, 2]. The IPS consists of 4 sub-sources: a *main diverging source* representing electrons and photons coming from the scattering foil; an *edge source of electrons* which accounts for electrons produced at the edges of the applicator or insert; a *source of transmitted photons* through the applicator or insert and a *second diverging source* which takes into account all the photons and electrons not included in the aforementioned sources. Figure 1 shows a schematic view of the 4 sub-sources.

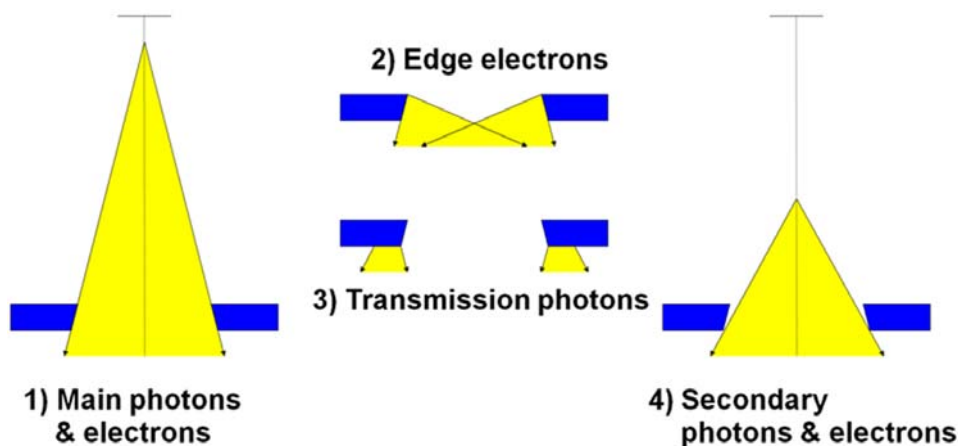


**Figure 1:** Schematic representation of the four sub-sources used by the IPS model [3]: 1) main diverging sub-source of electrons and photons, 2) sub-source of edge electrons, 3) sub-source of transmitted photons and 4) second diverging sub-source of electrons and photons.

In order to improve the accuracy of the dose calculations for low electron beams, the original eMC implementation has been modified with respect to both the beam model and the transport code for the dose calculation. In this improved version of the beam model all three scrapers of the applicator are taken into account. Based on the geometric information of the scraper positions it is determined for each sampled electron from the main diverging source whether or not it intersects within a scraper. If there is an intersection, the electron is rejected otherwise the particle is transported downstream for the dose calculation. In order to improve the accuracy of the energy spectrum for the electrons of the main diverging source, the resolution of the mono-energetic depth dose curves used during beam configuration has been increased.

The modification of the transport code for the dose calculation has been performed by reducing the maximum allowed size of the sphere used for the electron transport according to the energy of the initial electron. Overall, spheres between 1 mm and 5 mm are available. Thresholds between 4 and

7.5 MeV have been introduced so that if the energy of the incident electron is below such a threshold the maximum size of the possible sphere is reduced. This scheme is illustrated in figure 2.

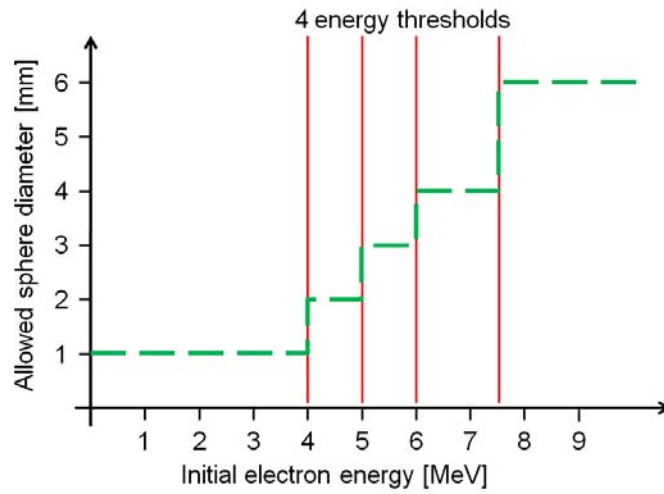


**Figure 2:** The maximal allowed sphere sizes used in the dose calculation as a function of the initial energy of the electron. The energy thresholds are shown as red lines. The maximum allowed sphere size is gradually reduced with reduced initial energy illustrated as broken green line.

The impact of these changes in eMC is investigated by comparing calculated dose distributions for 4 and 6 MeV electron beams with applicators ranging from 6x6 to 25x25 cm<sup>2</sup> of a Varian Clinac 2300C/D with the corresponding measurements.

## Results

In figure 3 calculated absolute depth dose curves together with the corresponding measurements are shown for the 4 MeV beam and a 10x10 cm<sup>2</sup> applicator. On the left the results are depicted using the original implementation of the eMC and on the right the improved version of eMC is used. The agreement with the improved eMC is within 1.5%, whereas the original eMC leads to dose differences of up to 6%.

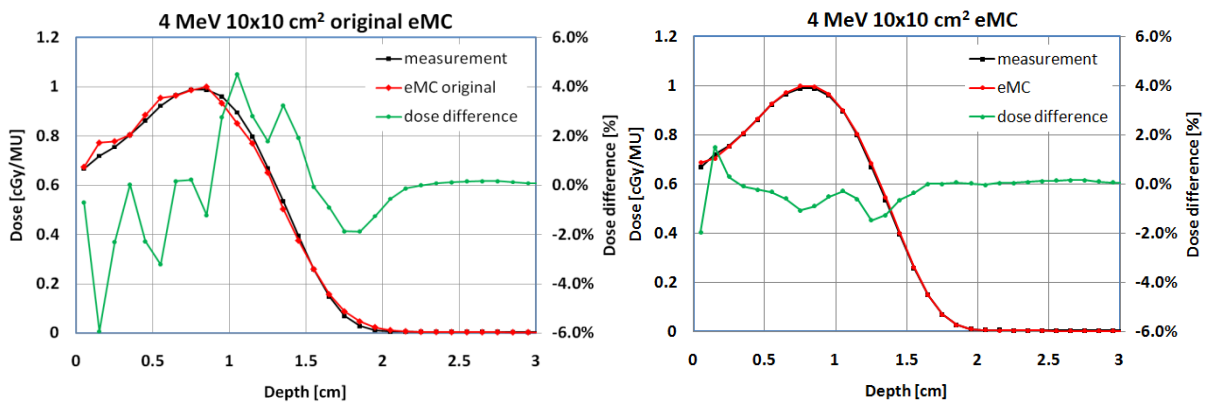


**Figure 3:** Calculated and measured absolute depth dose curves in water comparison for a 4 MeV electron beam with a 10 x 10 cm<sup>2</sup> applicator together with the corresponding dose differences using the original (left) and improved (right) eMC.

The analogous data for the 4 MeV beam and a 25 x 25 cm<sup>2</sup> applicator is shown in figure 4 demonstrating the increased accuracy when using the improved version of eMC. Overall, the agreement between measured and calculated absolute depth dose curves using the improved eMC is

within 1.5% for 4 and 6 MeV energies and all applicators considered, whereas the original eMC leads to dose differences of up to 6%.

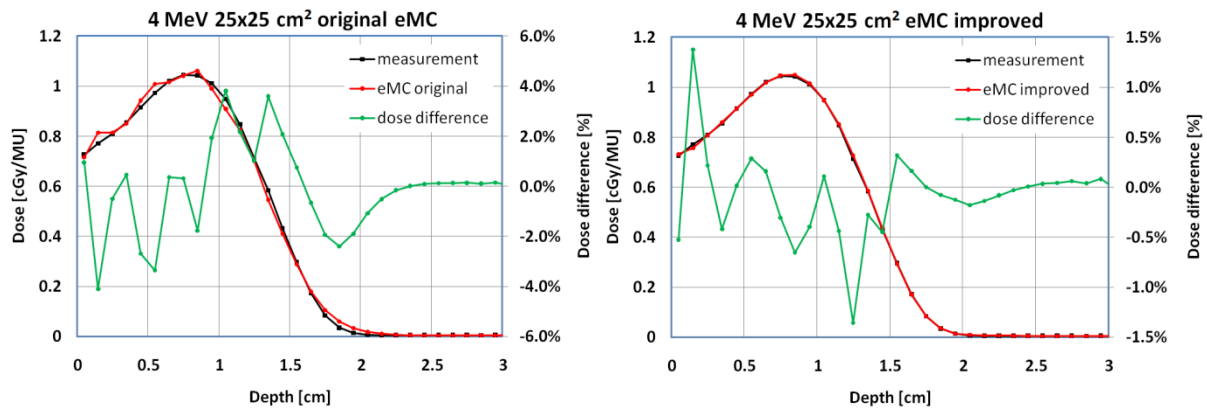


**Figure 4:** Calculated and measured absolute depth dose curves in water comparison for a 4 MeV electron beam with a 10 x 10 cm<sup>2</sup> applicator together with the corresponding dose differences using the original (left) and improved (right) eMC.

Figure 5 depicts examples for calculated and measured absolute dose profiles at several depths in water. The original eMC version leads to dose differences of up to 8% for low electron beams and applicators larger than 15x15 cm<sup>2</sup>. Those differences are reduced to about 2% for all dose profiles investigated when the improved version of eMC is used.

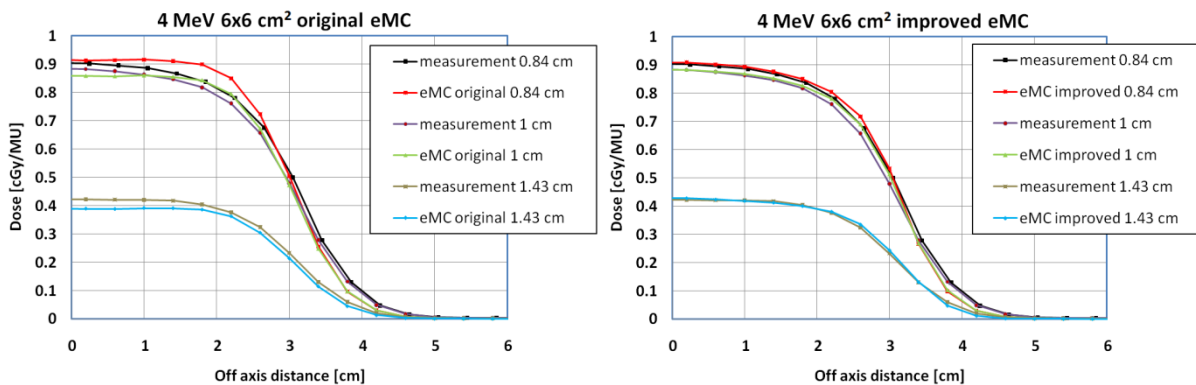


**Figure 5:** Calculated and measured absolute dose profiles at several depths in water comparison for a 4 MeV electron beam with a 6 x 6 cm<sup>2</sup> applicator using the original (left) and improved (right) eMC.

## Discussion

In this work several enhancements were made in the original eMC beam model and dose calculation algorithm. It has been shown that these modifications lead to significant improvements in the accuracy of the dose calculation for 4 and 6 MeV electron beams of Varian linear accelerators. This work was supported by Varian Medical Systems.

## References

- [1] H. Neunschwander and E. J. Born, "A macro Monte Carlo method for electron beam dose calculations," *Phys Med Biol* **37** (1), 107-25 (1992).
- [2] H. Neunschwander, T. R. Mackie, and P. J. Reckwerdt, "MMC--a high-performance Monte Carlo code for electron beam treatment planning," *Phys Med Biol* **40** (4), 543-74 (1995).
- [3] J. J. Janssen, E. W. Korevaar, L. J. van Battum, P. R. Storchi, and H. Huizenga, "A model to determine the initial phase space of a clinical electron beam from measured beam data," *Phys Med Biol* **46** (2), 269-86 (2001).

# Monte Carlo Dose Calculation on Deforming Anatomy

M. Peterhans<sup>1</sup>, P. Manser<sup>2</sup>, D. Frei<sup>2</sup>, M.K. Fix<sup>2</sup>

<sup>1</sup> Institute for Surgical Technology and Biomechanics ISTB, University of Bern

<sup>2</sup> Division of Medical Radiation Physics, Inselspital and University of Bern

mail: Matthias.Peterhans@istb.unibe.ch

## Introduction

For radiation therapy of tumours in abdomen and thorax, accurate dose calculation is challenging because of organ motion. Such motion includes changes in size, shape and position of the organ, and can be caused by patient motion, organ activity (breathing, digestion) and by changes in the organ itself (tumour growth, shrinking). When calculating radiation dose for moving targets, the resulting dose distributions change over time due to the dynamic anatomical situation. Previous work using analytical dose calculation algorithms on different images of a 4D-CT dataset [1] by means of dose warping approaches [2] showed dosimetric errors especially in regions with high dose gradients. An alternative approach is tracking the motion of the corners of each voxel. The aim of this work is the development, implementation and validation of a Monte Carlo (MC) methodology using motion tracking for each voxel in a patient dataset to calculate dose depositions on deformed voxel grids.

## Material and Methods

Tracking the motion of the corners of each voxel leads to a deforming voxel grid (changes in voxel shape and density) which preserves correspondence between voxels in the different image volumes of the 4D-CT dataset [3]. Using this approach, we have implemented a dose calculation algorithm for irregularly-shaped voxels within the Swiss Monte Carlo Plan (SMCP) framework [4]. Using computer vision methodology, the deformed voxels are represented as triangular surfaces. MC particle transport and dose deposition are calculated on this modified voxel definition. The validation methodology first establishes the equivalence with existing algorithms for a static scenario and then investigates the aspects of particle path calculation and handling of density changes on three specifically developed computational phantoms. Dose calculation is performed for pencil beams of electrons and photons of 6 and 10 MeV.

## Results

Comparison with existing algorithms on a non-deformed voxel grid shows equivalent results. By calculating a dose deposition on a phantom with irregular voxels which are contained in a larger, regular grid, correctness of the particle path calculation is shown. The handling of voxel density changes is investigated on the third phantom and comparison with an analytical dose summation method shows similar results.

## Discussion

Based on the validation results, we conclude that our implementation provides correct dose calculation on deformed voxel grids. The representation of organ deformation through deforming voxels avoids interpolation problems and temporal sampling of the deformation vector fields allows for real 4D-MC dose calculation. The combination of the presented algorithms and non-rigid image registration methods enables accurate dose calculation for moving anatomy and could be used for dose planning in advanced radiation therapy treatments.

## References

- [1] P.J. Keall, J.V. Siebers, S. Joshi, and R. Mohan: Monte Carlo as a four-dimensional radiotherapy treatment-planning tool to account for respiratory motion, *Phys. Med. Biol.*, Vol. 49, 2004, 3639-48.
- [2] M. Rosu, I.J. Chetty, J.M. Balter, M.L. Kessler, D.L. McShan, and R.K. Ten Haken: Dose reconstruction in deforming lung anatomy: dose grid size effects and clinical implications, *Med. Phys.*, Vol. 32, 2005, 2487-95.
- [3] E. Heath and J. Seuntjens, A direct voxel tracking method for four-dimensional Monte Carlo dose calculations in deforming anatomy, *Med. Phys.*, Vol. 33, Feb. 2006, 434-45.
- [4] M.K. Fix, P. Manser, D. Frei, W. Volken, R. Mini, and E. J. Born. An efficient framework for photon Monte Carlo treatment planning. *Phys. Med. Biol.*, Vol. 52, 2007, N425-37.

# Recurrence landscapes of uterine cervix carcinoma – A 3-D analysis of topography and spatial frequency distribution

U.-D. Braumann<sup>1</sup>, J. Einkenkel<sup>2</sup>, N. Manthey<sup>2</sup>, U. Wolf<sup>3</sup>, G. Hildebrandt<sup>3</sup>, A. Liebmann<sup>3</sup>, M. Höckel<sup>2</sup>

<sup>1</sup> Interdisziplinäres Zentrum für Bioinformatik, Universität Leipzig

<sup>2</sup> Universitätsfrauenklinik (Triersches Institut), Universität Leipzig

<sup>3</sup> Klinik und Poliklinik für Strahlentherapie, Universität Leipzig

mail: [braumann@izbi.uni-leipzig.de](mailto:braumann@izbi.uni-leipzig.de)

## Introduction

We introduce a method to accomplish a representative three-dimensional mapping of recurrence locations after primarily treated cervical carcinoma. Such collective-based mapping is of utmost importance for our present research on local tumour spread within the female pelvis [1]. In particular, we are interested in the analysis of differences depending on the primary treatment (surgical vs. radio-(chemo-)therapy).

## Material and Methods

51 patients with loco-regional recurrences of cervical carcinoma have been delineated based on T2-weighted NMRI. Following, the recurrence outlines were projected onto a reference pelvis data set using a landmark-based linear transform. Underlying data for this reference pelvis was taken from the cryosection data set of the “visible woman” part of “The Visible Human Project”, National Library of Medicine [2]. Depending on the primary treatment, two separate maps (“recurrence landscapes”) were built up just by superimposition of the respective projected recurrence locations. Such recurrence maps can be analysed concerning extent, shape, frequency distribution and topographical assignment.

## Results

For the primary therapy, 34 cases have undergone a hysterectomy (3: simple; 31: radical), while 17 cases received a radio-(chemo-)therapy. Recurrence landscapes obtained from patients with primary radio-(chemo-)therapy (i) exhibit smaller overall volumes (see Figure 1) compared to those obtained from patients with primary radiation therapy (whereas the individual recurrence volume distributions do not differ), (ii) show a arched instead of a rather (semi-)circular contour (in the transversal plane), and (iii) possess a rather centrally localised map maximum instead of two or more lateral maxima.

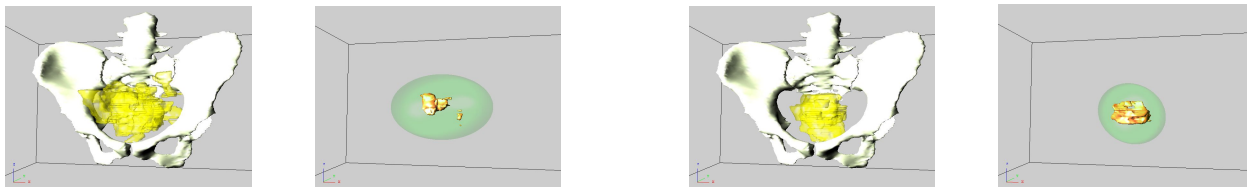


Figure 1: Overall entries (yellow) and 50%-level surface (orange) of the maps for surgically treated (left pair) vs. the radiated branch (right pair). Green ellipses illustrate  $3\sigma$  surfaces assuming multivariate normal map distributions.

## Discussion

The localisation of loco-regional recurrences of cervical carcinoma, besides tumour-biological factors, is decisively determined by (i) the preceding therapy and (ii) the topographical relations of the pelvic intestines. In accordance with the concept of a compartment-related tumour spread within the pelvis, the obtained shapes in the recurrence maps support the hypothesis of an incomplete resection within the embryologically defined uterovaginal (Müllerian) compartment during conventional radical hysterectomies. Further on, the results also rectify a modification of the prescribed dose distribution within a modern intensity-modulated radiation therapy during the primary cervical carcinoma treatment.

## References

- [1] Höckel, M.; Horn, L.-C.; Manthey, N.; Braumann, U.-D.; Wolf, U.; Teichmann, G.; Frauenschläger, K.; Dornhöfer, N.; Einkenkel, J.: Resection of the embryologically defined uterovaginal (Müllerian) compartment and pelvic control in patients with cervical cancer: A prospective analysis. *The Lancet Oncology*. Vol. 10, No. 7, July 2009, pp. 683 - 692
- [2] [http://www.nlm.nih.gov/research/visible/visible\\_human.html](http://www.nlm.nih.gov/research/visible/visible_human.html)

# A novel calibration approach to clinical PET/CT imaging.

T. Weitzel<sup>1</sup>, T. Beyer<sup>2</sup>, F. Corminboeuf<sup>1</sup>, T. Krause<sup>1</sup>

<sup>1</sup>University Clinic for Nuclear Medicine, Inselspital Bern University Hospital, 3010 Bern, CH

<sup>2</sup>cmi-experts GmbH, Pestalozzistr. 3, 8032 Zürich, CH

mail: [Thilo.Weitzel@insel.ch](mailto:Thilo.Weitzel@insel.ch)

## Introduction

Quantitative <sup>18</sup>F-FDG Positron Emission Tomography (PET) has become a routine imaging modality for diagnosis and for therapy response assessment in clinical oncology. Through the use of standardized uptake values (SUV) metabolic or functional information on PET images can be evaluated semi-quantitatively. SUV's, or changes thereof have been shown to yield diagnostic and prognostic information.

However, it is well-known that SUV's are affected by the limited spatial resolution of PET systems. SUV calculations of small lesions depend particularly on a proper calibration of the PET using a suitable phantom imaged under a reproducible study protocol.

Standard PET calibration may include a phantom containing a set of hollow spheres that have to be filled with <sup>18</sup>F solution of known radioactive activity. Such calibration is a rather lengthy procedure and requires a knowledgeable user on-site. Furthermore this process is costly and the user is exposed to radioactivity during this work. Here, we propose a novel calibration phantom for reproducible system calibration for a single or multiple sites.

## Material and Methods

Our proposed PET calibration phantom consists of a 20 cm cylindrical plastic phantom with two concentric circular arrangements of 6 spherical reference sources each. All spheres are filled with a homogeneous activity of about 0.1MBq/ml of <sup>68</sup>Ge-resin (T<sub>1/2</sub>~270d). The spherical moulds were produced from epoxy resin using rapid prototyping techniques. The wall thickness of each sphere is 1 mm.

The 6 sources placed in the outer circle mimic the standard arrangement used in conventional phantoms with source diameters ranging from 10 mm to 31 mm (0.5 ml to 16 ml). An additional set of 6 smaller sources with diameters ranging down to 2.5 mm is employed for the inner circle.

The spheres can be mounted in the empty cylinder, or in the cylinder filled with a uniform background activity to assess lesion recovery in air and soft tissue (water), respectively.

<sup>68</sup>Ge decays to short-lived <sup>68</sup>Ga, which is a positron emitter. The mean free path (FWHM) of positrons emitted from <sup>68</sup>Ge in water is 1.6 mm compared to only 1 mm for positrons emitted by <sup>18</sup>F.

In order to validate our approach to a long-lived and reproducible calibration phantom based on <sup>68</sup>Ge for clinical PET we compare the recovery coefficients of the <sup>68</sup>Ge-resin filled phantom with a standard <sup>18</sup>F-filled phantom for the same 6 standard spherical lesions. All measurements were repeated for a range of acquisition times and simulating lesions in water (soft tissue) and air (lungs). First recovery measurements of this work-in-progress were performed on a whole-body PET/CT (Biograph HiRez16, Siemens).

## Results

Recovery measurement in water showed no significant difference for <sup>18</sup>F- and <sup>68</sup>Ge-based phantoms.

Recovery measurements in air indicated a slightly degraded image quality for the <sup>68</sup>Ge-based phantom caused by positrons from the very surface of the spheres escaping to air and the subsequent extended annihilation distribution pattern. However, this effect had no influence on the recovery measurements.

Supplemental measurements on the smaller spheres of the solid-state phantom in air and water proved the effects of positron range on recovery factors to be limited to spheres well below 10 mm diameter.

## Conclusion

We present a novel approach to PET calibration using an efficient and user-friendly phantom filled with longer lived radioisotope. Our approach does not require repeated refilling or handling of open radioactivity and thus limits individual set-up errors and costs.

First validation of the new calibration phantom yields reproducible results and indicates adequate recovery estimates for lesions as small as 10 mm. Frequent PET quality control and a base recovery estimation can be facilitated using this solid-state phantom as presented, thus supporting PET quality control measures according to directive L-09-03 from BAG.

# **Pre-treatment verification of RapidArc treatment plans: comparison between Epiqa and Seven29 2D ion chamber array with Octavius phantom**

J Hrbacek<sup>1</sup>, M Zamburlini<sup>1</sup>, J Krayenbühl<sup>1</sup>, S Klöck<sup>1</sup>

<sup>1</sup> Klinik für Radio-Onkologie, UniversitätsSpital Zürich  
mail: Mariangela.Zamburlini@usz.ch

## **Introduction**

The purpose of this study was to compare two quality assurance methods for verification of RapidArc treatment plans. The first method verified the dose distribution in two orthogonal planes using a 2D chamber array Seven29 (PTW, Freiburg) combined with dedicated octagonal Octavius phantom (PTW, Freiburg). The second method was a verification of the “collapsed” dose distribution derived from EPID integrated images.

## **Materials and methods**

In order to measure the collapsed dose distribution, an integrated image was acquired with EPID positioned in the isocenter for 20 clinical RapidArc treatment plans. Using Epiqa (Epidos), a commercial solution of GLAaS algorithm, the acquired images were converted into dosemaps. The same treatment plans were also used for the irradiation of the tandem 2D array + phantom, with horizontally and vertically oriented 2D array.

All three planar measurements were compared with the reference dose distributions calculated in Eclipse using AAA 8.2.23. The gamma score with 3% dose difference and 3 mm distance to agreement criteria was used to express the agreement.

## **Results and discussion**

The collapsed plan based verification shows to be more sensitive than the 2D array based verification, due to its high resolution. In 4 out of 20 investigated patient plans the gamma score of the 2D array verification was poor. The low score was clearly a result of the imperfection of the detector (strong angular dependence for oblique irradiation).

# How sensitive is the collapsed plan?

J Hrbacek<sup>1</sup>, J Bocanek<sup>2</sup>, T Dossenbach<sup>1</sup>, G Nicolini<sup>3</sup>, A Fogliata<sup>3</sup>, S Klöck<sup>1</sup>

<sup>1</sup> Klinik für Radio-Onkologie, UniversitätsSpital Zürich

<sup>2</sup> Varian Medical Systems, Zug

<sup>3</sup> Oncology Institute of Southern Switzerland, Bellinzona

mail: Jan.Hrbacek@usz.ch

## Introduction

Epiqa is software that converts an EPID integrated images into planar dose distributions using the principle of the GLAaS algorithm [1]. The software can be utilised also for the verification of RapidArc fields. During irradiation of a RapidArc field, EPID follows the gantry motion and therefore the gantry appears to be static in respect to the detector. Planar dose distribution captured by EPID during RapidArc plan delivery has a specific character and cannot be related to any plane in a patient's body. We refer to it as the "collapsed" RapidArc dose distribution

The presented theoretical study tries to demonstrate the sensitivity of the *collapsed dose distribution* to errors introduced into real clinical patient plans and compares it to the changes in *patient dose distribution*.

## Materials and methods

For three qualitatively different clinical RA plans with (prostate, oesophagus, skull) the *patient* and the *collapsed* dose distribution has been calculated in Eclipse using AAA 8.2.23 with calculation grid of 2.5 mm.

The plans were exported from treatment planning system and their leaf aperture and dose meterset have been altered on the level of control points. The modified plans have been imported back to the TPS and the patient and the collapsed dose have been recalculated.

The original and modified *patient dose distributions* have been compared in coronal, transversal, and sagittal plane in terms of relative local dose changes. In the same fashion, the *collapsed dose distributions* of the original and modified plan have been compared.

## Results

The changes introduced into the investigated plans had an influence on the *patient dose distribution* as well as the *collapsed dose distribution*. The qualitative evaluation (frequency histograms) reveals that the collapsed dose distribution was more sensitive to the given type of introduced changes.

## References

[1] Nicolini G.; Vanetti E.; Clivio A.; Fogliata A.; Korreman S.; Bocanek J.; Cozzi L. The GLAaS algorithm for portal dosimetry and quality assurance of RapidArc, an intensity modulated rotational therapy, Rad. Oncol. 3 (2008) 24.

# QA for rapid arc treatment using the SGSMP IMRT – dose intercomparison facility

Karl Loewenich<sup>1</sup>, Jan Hrbacek<sup>1</sup>, Hans Schiefer<sup>2</sup>, Tino Streller<sup>1</sup>, Jérôme Krayenbuhl<sup>1</sup>, Stephan Klöck<sup>1</sup>

<sup>1</sup>Abteilung für Medizinphysik, Klinik für Radio - Onkologie, Universitätsspital Zürich

<sup>2</sup>Abteilung für Medizinphysik, Klinik für Radio - Onkologie, Kantonsspital St. Gallen.

mail: [jan.hrbacek@usz.ch](mailto:jan.hrbacek@usz.ch)

## Introduction

At the USZ RapidArc treatments are delivered with the Varian Trilogy linac since February 2009. QA is routinely done on a single patient basis with in-house equipment (Epiqa/Octavius). We took advantage of SGSMP IMRT – dose intercomparison facility [1] to have an external QA audit for checking the RapidArc delivery chain. The measurement was done twice – before and after the introduction of the new version of AAA dose calculation algorithm for Eclipse treatment planning system. The present study summarizes obtained results.

## Material and Methods

Treatment plans for the CIRS thorax phantom (supplied by the Klinik für Radio-Onkologie of the Kantonsspital St. Gallen) were produced with the Eclipse treatment planning system using Progressive Resolution Optimizer (PRO) and Analytical Anisotropic Algorithm (AAA) version 8.2.23 and 8.6.14. Contouring, irradiation and dose measurements in the phantom were performed according to the prescriptions given in the “intercomparison-2008-instructions” [2].

## Results

TLD's inserted in the phantom allow to compare the dose calculated by the planning system with measured dose in 54 positions of a specific slice. Predictions of the older AAA (8.2.23) were in a reasonable overall agreement (on the average less than 2% deviation) with the TLD-measured values. However, a maximum deviation of about 4 % occurred in the region where the PTV extended into the lung. With the new version of the AAA (8.6.14) the deviations between calculated and measured values were generally smaller and never exceeded 2%.

## Discussion

With the latest version of the AAA of Eclipse treatment planning system reliable dose calculation is achieved.

## Reference

[1] Schiefer H, Seelentag WW, Results of the Pilot study to the IMRT dose intercomparison 2008. STSMP Bulletin 2/2008 66:14-16

[2] <http://www.sgsmp.ch/intercomp/intercomparison-2008-instructions.pdf>

# Comparison of image quality between a digital panorama X-ray unit with a CdTe-CMOS detector and panorama X-ray units with other types of digital detectors

Stephan Scheidegger<sup>1</sup>

<sup>1</sup>Zürcher Hochschule für Angewandte Wissenschaften, Winterthur (Zurich University of Applied Sciences at Winterthur)

## Abstract

An investigation of the image quality of 5 panoramic X-ray units was carried out for this paper. Measurement of the MTF clearly shows good resolution for the Art Plus unit ( $MTF(50\%) = 5.61 \text{ lp / mm}$ ) compared to the average of all 5 of the units ( $3.44 \pm 1.55 \text{ lp / mm}$ ). To investigate image noise, the ratio was calculated between average gray scale value and standard deviation in a  $32 \times 32$  matrix ( $R_{32 \times 32}$ ). Compared to the other units, identical regions in the image are less noisy for the Art Plus unit ( $R_{32 \times 32} = 92.28$  and  $R_{32 \times 32} = 19.40 \pm 11.00$  for the other units). Also image displacement of a series of images was determined for the Art Plus and the Pro Max unit. The displacements were between 1-5 Pixels for both.

## 1. Introduction

Progress in digital detector development is playing an increasingly important role in the area of dental X-ray methods [1]. In dealing with digital detectors for X-ray radiation, the challenge is to find the most efficient way of transforming X-ray quanta into an electronic signal. In the case of CCD detectors, this is accomplished by a matrix of light sensitive photodiodes. Conventional CCD and CMOS detectors use a fluorescence layer to transform X-rays into visible light. The thicker the fluorescence layer is, the better will be the optical efficiency. However, spatial resolution is reduced due to scattering of light in the fluorescence layer.

One new development is CdTe detector technology. Here, a CdTe layer replaces the fluorescence layer. X-ray quanta release electrically charged particles in this layer, which then flow in an electric field in the direction of a diode matrix. Because there is no transformation into visible light taking place, there is no additional optical scattering. This leads to the higher resolution.

In this article, a comparison between the image quality of a digital panorama X-ray unit with a CdTe detector (ART Plus<sup>1</sup>) and other more standard digital panorama units is presented. Qualitative comparisons and ratings of the image quality of film and digital panorama photos have been performed where experienced observers rate image quality visually [2,3]. In this article, quantitative measurement (modulation transfer function MTF) will be emphasized and image noise and image displacement will be investigated.

---

<sup>1</sup> Oy AJAT Ltd, Espoo, Finland

## 2. Materials and Methods

### *Creating a test image*

Test images were used for comparing image quality. For the sake of practical relevancy, a special anthropomorphic bone phantom was used. This makes possible a qualitative as well as a quantitative evaluation of the X-ray image. The phantom was positioned identically for each of the devices and the tube voltages kept as similar as possible (Tab.1). All the images were stored (8 bit resolution) and analyzed in the same manner. The test images were analyzed with Matlab<sup>2</sup> using the *Image Tool Box*

Tab.1. The devices used and the exposure parameters for the test images

Unit	Tube voltage U / kV	Charge Q / mAs
ART Plus	70	94.5
Sorodex Cranex Novus	70	63
Kodak 9000	70	68
Sirona Orthophos	71	112
Planmeca ProMax	70	96

### *Determining image resolution*

For determination of the modulation transfer function MTF, a sharp and piecewise straight edge of a tooth was used. Tooth enamel is very radio-opaque so the tooth edge functions approximately as a step function. A small exactly defined area identical for all panoramic images was cut out of the X-ray images (Fig.1).

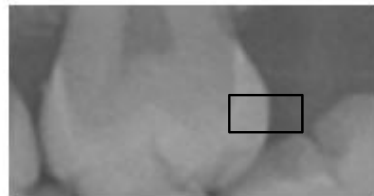


Fig. 1. Area of tooth used for determining the MTF (black frame)

### *Determining image noise*

In an additive model, the image  $I(x, y)$  (with image coordinates  $x$  and  $y$ ) is given by the picture information (projection of the object image  $P(x, y)$ ) plus the noise component  $N(x, y)$ :  $I(x, y) = P(x, y) + N(x, y)$ . It can be assumed that the pixel values for the noise component will have a statistical distribution around zero. This distribution is characterized by a standard deviation. Olsen [4] compared six methods for estimating the deviation from white noise in real images. Filtering the image information (i.e., separation of image contents) beforehand proved to be

---

<sup>2</sup> V. 7.5, The Mathworks Inc.

especially advantageous for this. The better filtering methods are being sought that would separate the image noise from the diagnostic content of the image itself as completely as possible [5].

The comparison of the devices in Tab.1 was made using a single image. The standard deviation as well as the variance can be estimated for a region of a real image having a distribution of intensity that should be as homogenous as possible. Local estimates of average intensity and variance can be improved by combining with measurements at other locations [6]. For all the test images, sections without any anatomical structures (analogous to an empty image) were chosen. Of course, structures in the panoramic picture were smeared due to motion blur. For this reason, the chosen areas of the pictures were investigated for systematic features of darkening. In addition, the Fourier transformation was calculated for each area in order to identify possible correlations in the intensity distribution. Several sections of various sizes (128 x 128, 64 x 64 and 32 x 32 – image matrix) of each image were also compared to each other. The following expression was used for quantifying image noise:

$$R_{N \times M} = \frac{1}{s \cdot N \cdot M} \cdot \sum_{n=1}^N \sum_{m=1}^M I(x_n, y_m) \quad (1)$$

Here,  $s$  is the estimate of the standard deviation  $\sigma$  of the gray scale values ( $x$  and  $y$  are the image coordinates). Calculating  $R_{N \times M}$  at chosen locations in the image gives only fragmentary insight because the places that show homogenous distribution of intensity can only be found in certain areas of blackening. For this reason, an additional image was taken with a cylindrical water phantom for verification (diameter 20 cm). Such images display an adequately homogenous local intensity distribution. However, due to movements of tube and detector (translation and rotation), regions of varying intensity are formed over the whole picture because the path length of the x-rays through the phantom changes.

Another difficulty is mechanical instability which can lead to shifts in the positions of the structures in the image. These shifts are especially important when they occur during the actual taking of a picture and result in changes to the relative positions of structures within the image. Such shifts were determined for two of the devices being investigated by calculating the difference image  $\Delta I(x, y) = I_2(x, y) - I_1(x, y)$  of pictures taken in succession.

### 3. Results

#### *Resolution*

Fig. 2 shows the MTF for the ART Plus unit. Various characteristic values can be read from the curve. The MTF(80%) value lies above 3 lp/mm. According to the information given by the manufacturer, the value MTF(>75%) is at 2 lp/mm, which is clearly satisfied here. The MTF(50%) value results in a frequency of 5.61 lp/mm and for MTF(30%), the resulting image frequency is 6.26 lp/mm. For MTF(50%), the average value plus/minus standard deviation is equal to  $3.44 \pm 1.55$  lp/mm for

all five devices. For MTF(30%), it is equal to  $4.86 \pm 1.24$  lp/mm. For the ART Plus, the result is above the average value plus standard deviation in both cases.

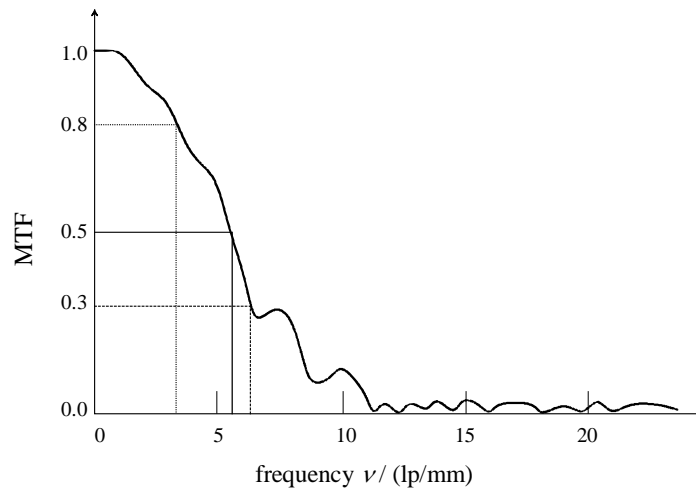


Fig.2. MTF for the ART Plus unit, measured in the section shown in Fig.1.

#### *Image noise*

In order to calculate the value  $R_{N \times M}$ , four image sections (32x32 pixels) were chosen that were identical in every picture of every device. The results scatter enormously (standard deviation of the average value of  $R_{32 \times 32}$  is  $34.92 \pm 33.83$ ). The resulting value for all the units without ART Plus was  $19.40 \pm 11.00$ . ART Plus's value ( $R_{32 \times 32} = 92.28$ ) lies distinctly above all the others. In areas of similar average intensity, the  $R_{32 \times 32}$  values for the images made with the water phantom show comparable values (1.25% deviation). As expected, the  $R_{32 \times 32}$  values are correlated with the gray scale average.

#### *Image shift*

A series of 10 pictures was taken one after another with two devices (Art Plus and Pro Max). Two successive x-ray images were then used to calculate the difference image  $\Delta I(x, y)$ . Shifts are especially clear to see at the edges. Since only horizontal displacements can be observed in the images, the tooth edge in Fig.1 was very suitable for determining these shifts. Fig.3 shows a cut through the difference image in the  $x$  direction at the location of the edge. A pattern results that is characteristic to the form of this edge. This pattern can be described by the distribution of difference values with a maximum and a half-width. The shift has been simulated in Fig.4 where we see that maximum and half-width can be assigned to a shift by a certain number of pixels. The half-width is useless for small shifts but the maximum can be used very well. This behavior is reversed for large shifts. Both units showed the greatest shift (and consequently, the highest value for the maximum) between the first and second pictures.

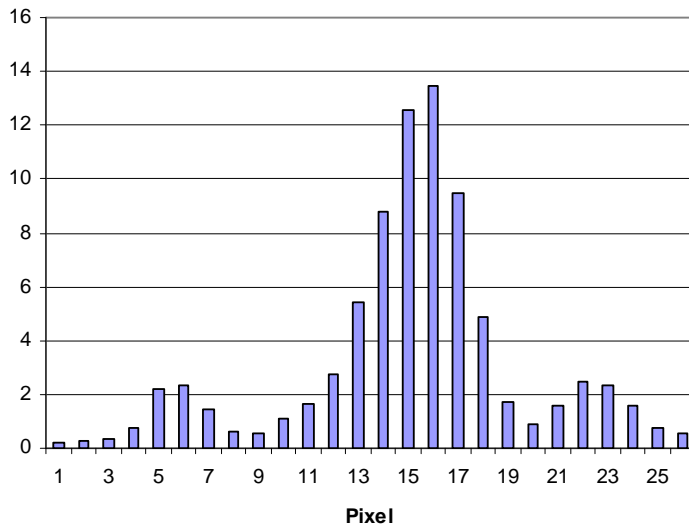


Fig.3. Horizontal section (in the  $x$  direction) through the difference image  $\Delta I(x, y)$ : The difference was produced between two images taken in series by the Art Plus. The section goes through an edge of a tooth in the marked area of Fig.1.

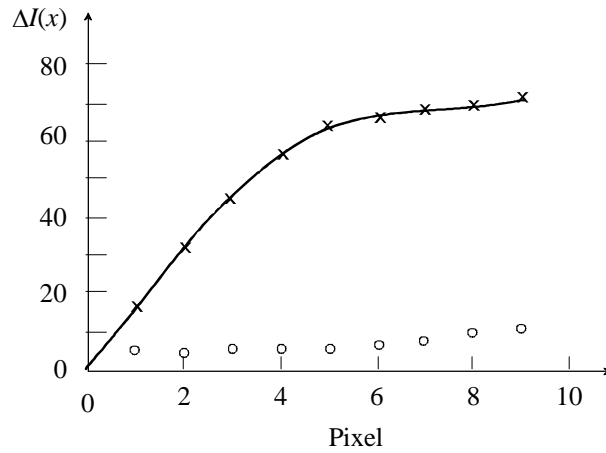


Fig.4. Relation between the maximum value (crosses) and the half-widths (circles) of the distribution, and shift (by a certain number of pixels), respectively, in the vicinity of the edge (Fig.1) in the difference image (Art Plus unit): The solid line is described by the function  $f(x) = 0.0253x^4 - 0.4818x^3 + 1.1458x^2 + 15.2648x + 0.0245$ .

The highest maximum value for the Art Plus unit was 59, which according to Fig.4, is equivalent to a shift of 4 to 5 pixels. The maximum for Pro Max was 62.27, which also just about equals 4 to 5 pixels. However, the fact that pixel size between the two units differs by a factor of 1.08 should be taken into account as well as the slight variations of edge form due to differences in resolution. The pictures that followed afterward showed noticeably smaller shifts. The maxima in the difference

images of the Art Plus lay between 12 and 18 (shift of 1 pixel) and for the Pro Max, between 14 and 22 (shift of also about 1 pixel). While the shifts in the images produced by Art Plus always occurred in an either right or left direction across the entire image, the Pro Max also exhibited symmetrical displacements about the center axis.

#### 4. Discussion and Conclusions

The visual impression was confirmed by the measured data. The Art Plus's CdTe-CMOS detector displays a high picture resolution compared to the other devices. In the case of image noise, the Art Plus distinguished itself, even though the  $R_{32 \times 32}$  values can be used only for a rough appraisal. In this context it should be mentioned that  $R$  is dependent of the level of the gray value. Because it was not the areas with identical blackening that were compared but the locations in the image that were identical, the results are significant only to a limited degree. The differences in image noise are therefore also dependent upon the representation of the image as regards the gray scale values, although the histograms weakly vary with respect to the most frequent value. In Addition, the applied charge ranges between 63 mAs and 112 mAs. For the devices with high image quality, there may be a potential for dose optimization.

An interesting peculiarity having to do with image noise in every picture is the fact that the random variations (spots) extend over more than one pixel. When noise is caused by the detector's electronics, we should be able to find stochastic gray scale values changing from pixel to pixel. In the case of quantum noise, on the other hand, the fluorescence layer influences the gray scale modulation by scattering the light. Since the electrically charged particles released by the Art Plus's CdTe detector are directed toward the detector matrix without any transformation into light taking place, higher modulation frequencies should be expected. Other causes may be application of image filters (or noise filters) that smear the modulations. Some devices (Orthopos and Pro Max) give the impression that a combination of edge-sharpening filter and noise filter (in the sense of a pretreatment of the image) were used. The applied dose for the images differs remarkably between the tested devices (Tab.1). The low dose used for images taken with the Kodak 9000 or Cranex Novus device may affect resolution when applying extensive noise reduction. In this case, not the intrinsic resolution of the detector but the resolution of the entire system (possibly including automatic image pretreatment) is depending on the applied dose. In regard to an optimization of dose and required image quality, further investigations should address this problem.

With the exception of the first two pictures in each series, the image shifts measured in the Art Pro and Pro Max devices are small and amount to only a few pixels (a mechanical displacement of the skull phantom can be ruled out).

#### References

- [1] Van der Stelt, P.F. (2005): Filmless imaging: The uses of digital radiography in dental practice. *J. Am. Dent. Assoc.*, **136**(10), 1379-1387

- [2] Molander, B., Gröndahl, H.G., Ekestubbe, A. (2004): Quality of film-based and digital panoramic radiography. *Dentomaxillofac. Radiol*, **33**, 32-36
- [3] Gijbels, F., De Meyer, A.M., Bou Serhal, C., Van den Bossche, C., Declerck, J., Persoons, M., Jacobs, R. (2000): The subjective image quality of direct digital and conventional panoramic radiography. *Clin. Oral. Invest.*, **4**, 162-167
- [4] Olson, S.I. (1993): Noise Variance Estimation in Images. In: *8<sup>th</sup> Scandinavian Conference on Image Analysis*.
- [5] Goebel, P.M., Belbachir, A.N., Truppe, M. (2005): Noise estimation in panoramic x-ray images: An application analysis approach. *Proc. HACIPPR 2005 (IEEE)*, 996-1001
- [6] Gravel, P., Beaudoin, G., De Guise, J.A. (2004): A Method for Modeling Noise in Medical Images. *IEEE Transactions on Medical Imaging*, **23**(10), 1221.

# Validation of a Monte Carlo model for peripheral dosimetry and dose calculations in a full-body voxelised phantom with regards to secondary cancers

A. Joosten<sup>1</sup>, F. Levi<sup>2</sup>, S. Baechler<sup>1</sup>, O. Matzinger<sup>3</sup>, W. Jeanneret-Sozzi<sup>3</sup>, R.-O. Mirimanoff<sup>3</sup>, F. Bochud<sup>1</sup>, R. Moeckli<sup>1</sup>

<sup>1</sup> University Institute for Radiation Physics, CHUV and University of Lausanne

<sup>2</sup> Cancer Epidemiology Unit and Cancer Registries of Vaud and Neuchâtel, Institute of Social and Preventive Medicine, CHUV, Lausanne

<sup>3</sup> Department of Radiation Oncology, CHUV, Lausanne  
mail: andreas.joosten@chuv.ch

## Introduction

Secondary cancers after successful treatment of the initial cancer is becoming of increasing concern in the radiation oncology community due to longer survival times and new treatment techniques spreading low doses over larger volumes of healthy tissue. The comparison of risks associated with different treatment techniques (conventional, steep-and-shoot IMRT, arc therapy) with regards to secondary cancer induction is controversial due to uncertainties in risk estimations [1]. Current models for low doses (< 2 Gy) are based on atomic bomb survivors and data for higher doses (> 2 Gy) is sparse [2]. There is a clear need to collect more data from long-term cancer survivors and stratify the risk as a function of dose. Since doses ranging from 100 mGy up to > 50 Gy are susceptible to induce cancer [3], an accurate dosimetry in the full body of the patient is required to ascertain radiation risks. This can be achieved with Monte Carlo (MC) methods.

## Material and Methods

The linear accelerator Siemens Primus was modelled for 6MV beams with BEAMnrc MC code. The MC simulations were compared with measurements of the Primus in a water tank with special emphasis on out-of-beam doses up to 25 cm from the field edge. Peripheral dose measurements were also performed on 3 other linear accelerators operating at 6MV in order to validate the MC model as a generic model to be used in epidemiological studies. A four-field breast cancer treatment was simulated with MC in a full body voxelised phantom.

## Results

Comparison of MC simulations with different measured linacs shows that the MC out-of-field doses are within the variability of measured linear accelerators up to 25 cm from the beam edge. The variability between machines was 15% for a 20x20 field and increased up to 100% for a 5x5 field. These discrepancies are acceptable considering the large range of doses (3 orders of magnitude) and uncertainties involved in second cancer risk assessment.

A single MC model for 6MV linacs has thus been validated for peripheral dosimetry with regards to secondary cancer induction. This validation allowed us to perform dose calculations in a full-body voxelised phantom. Dose-Volume Histograms were extracted for several organs.

## Discussion

A Monte Carlo model has been validated for full-body dose calculations. Such a model allows accurate calculation of low doses (< 2 Gy) and associated risks with these low doses which is not possible with a commercial treatment planning system.

## References

- [1] Hall, E.J.; Wu, C.S.: Radiation-induced second cancers: the impact of 3D-CRT and IMRT. *Int. J. Radiat. Oncol. Biol. Phys.* **56** (2003), 83 – 88
- [2] Schneider, U.; Walsh, L.: Cancer estimates from the combined Japanese A-bomb and Hodgking cohorts for doses relevant to radiotherapy. *Radiat. Environ. Biophys.* **47** (2008), 253 - 263
- [3] Suit et al: Secondary carcinogenesis in patients treated with radiation: a review of data on radiation-induced cancers in human, non-human primate, canine and rodent subjects. *Radiat Res.* **167** (2007), 12 - 42

# Reliability and use of the HiArt detector for 3D dose reconstruction in tomotherapy

K. Schombourg<sup>1</sup>, F.O. Bochud<sup>1</sup>, R. Moeckli<sup>1</sup>

<sup>1</sup>University Institute for Radiation Physics, CHUV and Lausanne University

Mail: Karin.Schombourg@chuv.ch

## Introduction

The HiArt built-in detector of the tomotherapy is used for patient imaging, but it also records the transmitted dose during the entire treatment. Our aim was to determine whether the Xenon-filled ion chambers of the detector are reliable for 3D dose reconstruction and whether a calibration of the signal is possible.

## Materials and Methods

The transmitted signal on the detector was extracted from the built-in detector using the TQA (tomotherapy quality assurance) tools. A calibration of the signal was done using an independent measure with the A1SL ion chamber and gafchromic films. Short term, i.e. on a typical treatment time scale, and long term stability of the signal was checked by measurements over 2 months. The variability with beam hardening and scatter amount was also checked. To reconstruct the delivered dose to a solid water phantom an iteration algorithm was used. This algorithm, presented at the SSRPM 2007 meeting, was upgraded by using 3D Monte Carlo simulated energy deposition kernels. The dose reconstruction was performed for different MLC configurations.

## Results

Our measurements showed that the Xenon-filled chambers are reliable for the measurement of the transmitted beam on a long term basis, i.e. the variations from day to day was under 1%. The transmitted signal could be converted into a dose using independent measurements. The iterative algorithm estimated the delivered energy fluence and the 3D dose distribution was computed with a precision within 3%/3mm.

## Discussion

The signal measured on the Xenon-filled ion chambers is reliable on a long term basis and a conversion into a dose could be done. The dose delivered to a solid water phantom could be reconstructed with a satisfying precision for the check of the delivered dose. This is a first step for adaptive radiotherapy.

# Passive Tracking of the Devices during MR-guided Interventions

S.Patil<sup>1</sup>, O. Bieri<sup>1</sup>, K. Scheffler<sup>1</sup>

<sup>1</sup>Division of Radiological Physics, University of Basel Hospital, Basel  
e-mail: oliver.bieri@unibas.ch

## Introduction:

In endovascular MR-guided interventions, passive tracking of the surgical devices utilizing paramagnetic markers is a challenging task [1, 2]. In this work, we describe two novel methods that are based on morphing SSFP and echo-dephased SSFP generating positive contrast within close vicinity of the marker.

## Material and Methods:

The basic template of morphing SSFP is based on SSFP-echo sequence. In combination with long TR, low flip angle and in the presence of local gradients induced by paramagnetic markers, the sequence morphs itself to a balanced SSFP sequence. The second novel method is based on inversion of the polarities of pre-phasing as well as dephasing gradients of the balanced SSFP sequence.

A custom-built phantom with 11 mm diameter tubes to model the blood flow in large vessels and to insert the guide wire was used. The tubes were immersed in a gadolinium (Gd)-doped water and were surrounded by a 2% agarose gel doped with 0.5 mM copper sulphate ( $\text{CuSO}_4$ ) concentration to closely resemble the relaxation times of fat tissues. All the measurements were done on a Siemens Espree 1.5T scanner.

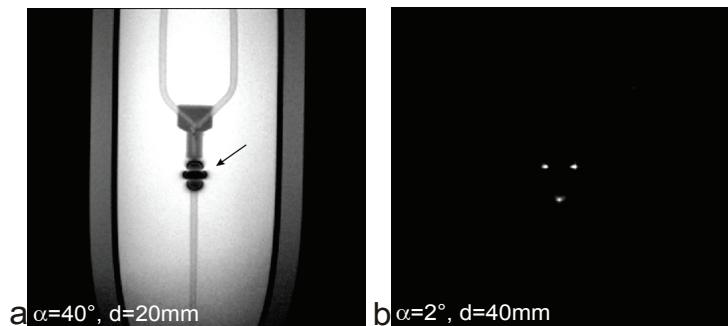


Figure 1: a) SSFP-echo image showing black void. b) Morphing SSFP image showing positive contrast within the vicinity of the marker

## Results:

An image of the experimental set-up with a guidewire inserted in a tube is shown in Fig. 1a using SSFP-echo sequence. In this image signal loss due to field perturbations of the paramagnetic marker is clearly visible. Figure 1b shows the image obtained using morphing SSFP technique.

Figure 2a displays the localizer image using GRE sequence displaying black void due to marker. Figure 2b depicts the positive contrast within the close vicinity of the paramagnetic marker obtained using echo-dephased SSFP.

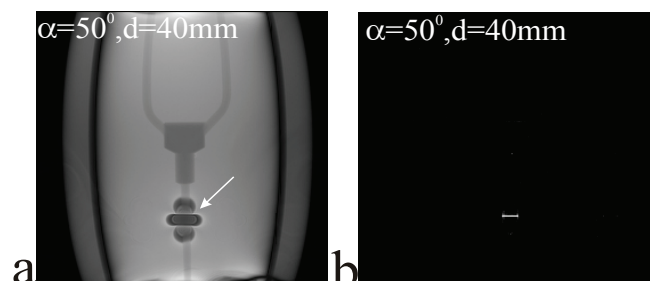


Figure 2: a) GRE image showing black void. b) Echo-dephased SSFP image showing positive contrast within the vicinity of the marker

## Discussion:

We have given evidence, that the proposed new methods of morphing SSFP and echo-dephased SSFP is able to produce positive contrast from susceptibilities, while keeping a vanishing background signal. Both methods are promising new concepts for fast detection of positive contrast for passive tracking of interventional devices.

## References:

- [1] Seppenwoolde et al., MRM 50:784-790, 2003.
- [2] Stuber et al., MRM 58:1072-1077, 2007.

# Assessing Extracranial Tumors using Diffusion-Weighted Whole-Body MRI

C. Lenz<sup>1</sup>, M. Klarhöfer<sup>1</sup>, K. Scheffler<sup>1</sup>, L. Winter<sup>2</sup>, G. Sommer<sup>2</sup> (mail: claudia.lenz@unibas.ch)

<sup>1</sup>Division of Radiological Physics, University of Basel Hospital, Basel

<sup>2</sup>Department of Radiology, University of Basel Hospital, Basel

## Introduction

Diffusion-weighted imaging (DWI) is a well established technique in MRI. Especially the application to intracranial diseases (i.e. cerebrovascular accidents) became important in the last two decades [1]. Apart from that, there is growing interest in the application of DWI to patients with extracranial pathology. One feasible measurement technique, referred to as diffusion-weighted whole-body imaging with background body signal suppression (DWIBS), was introduced in 2004 by Takahara et al. [2]. In this work, preliminary results from the application of DWIBS to extracranial tumors are presented.

## Theory

In comparison to free diffusion, the water diffusion in biologic tissues is hindered due to interactions with cell membranes and macromolecules. The degree of restriction correlates inversely with the tissue cellularity and the integrity of cell membranes, leading to more restricted water diffusion in tissues with high cellular densities, i.e. tumor tissues. In DWI, the degree of water motion is found to be proportional to the degree of signal attenuation, whereby tumors show particular high signal magnitudes [3].

## Material and Methods

Patients were measured on a 1.5T Siemens MRI scanner. Free-breathing DWIBS was acquired at 5-7 different image stations using either a coronal or an axial STIR ss-EPI sequence with parameters TR=7800 ms, TE=58 ms, b=0, 800 s/mm<sup>2</sup>, matrix=192, slice thickness=5 mm, FOV=50x31 cm<sup>2</sup>. Total scan time for the DWIBS of one patient was 17 min.

## Results

Figure 1 shows an example of an inverse grey scale DWIBS image in a patient with lesions from multiple myeloma. Signals from normal tissue such as fat, muscle, blood vessels and bowel are suppressed. However, other normal structures, i.e. the spinal cord, liver, kidneys and spleen remain visible due to the restricted water motion. Furthermore and most important, hypercellular structures, such as tumor lesions (arrows) become clearly visible as hyperintense spots.

## Discussion

DWIBS is an encouraging new, non-invasive technique for assessing extracranial tumors. At the moment, several studies are planned at the University of Basel Hospital, one of them comparing the two methods DWIBS and positron emission tomography (PET). Other studies have shown that DWIBS shows considerable promise for detecting and characterizing tumors and evaluating treatment response [4-6].

## References

- [1] Bammer, Eur J Radiol 2003;45:169-184.
- [2] Takahara et al. Radiat Med 2004;22:275-282.
- [3] Koh et al., AJR Am J Roentgenol 2007;188:1622-1635.
- [4] Koh et al., Magn Reson Med Sci 2007;6:211-224.
- [5] Vilanova et al., Eur J Radiol 2008;67:440-447.
- [6] Kwee et al., Eur Radiol 2008;18:1937-1952.



**Fig.1:** Example of diffusion-weighted whole-body imaging with background body signal suppression in a 49-year-old patient with lesions from multiple myeloma (arrows). Image is displayed using an inverse grey scale.

# Improving the QA for geometric accuracy for stereotactic radiotherapy with a Linac

H. Petermann

Institut für Radio-Onkologie, Universitätsspital Basel

mail: [hpetermann@uhbs.ch](mailto:hpetermann@uhbs.ch)

## Introduction

Cranial Stereotactic irradiation using an add-on micro-MLC was introduced at the Universitätsspital Basel in 2009. From the beginning irradiation of very small lesions (<1cm) was intended. Introducing the QA program it turned out soon, that accuracy and reproducibility of QA procedures used so far were not sufficient to fulfil the needs for stereotactic treatment, i.e. submillimeter accuracy. Therefore developments to improve the geometrical accuracy had to be introduced.

## Material and Methods

1) First the fixation procedure of the add-on micro-MLC (DMLC, ELEKTA) was modified. Additionally to the delivered screws appropriate alignment pins are used to reduce the tolerance of the position of the micro-MLC versus the head of the linear accelerator (ELEKTA Synergy Platform). Reproducibility of fixation is reduced from about 0.4 to below 0.2 mm.

### 2) Star Films

Primary need of the stereotactic irradiation is the perfect coincidence of laser and radiation field at any possible gantry, collimator and table angle. Therefore the quality of star films is of great concern. Radiographic films are used, laser position is marked by a needle. Marking the laser line several pinpricks are done using a magnifying glass (magnification 3x). After development and scanning of the film, the image file is imported to a free-ware image manipulation program (GIMP, version 2.6; [www.gimp.org](http://www.gimp.org)). Using this program lines indicating the central beams can easily be drawn and repositioned; the maximum zoom factor of 1600% allows very precise evaluation of the position and dimension of the centre of the star films.

### 3) Winston Lutz Test

The usual regular QA process in stereotactic irradiation is the Winston-Lutz Test. A radio-opaque ball is aligned to the laser coordinate system. A small field is irradiated and the relative position of the ball to the field boundaries is assessed for different angles of gantry, collimator and table. The point limiting the precision of this test, is the alignment of the Winston-Lutz tool to the laser, which is done by manually moving the table to the desired position. High quality images of a digital camera allow to determine the alignment of ball and laser to 0.1 mm. Misalignment during the test can be corrected in the subsequent analysis.

## Results

The improved techniques lead to a more accurate determination of the geometric QA parameters. Using image manipulation software the process can be redone by one or several operators. Reproducibility of the single processes is 0.2 mm or lower. Reproducibility of the entire QA is 0.3 mm or lower.

## Discussion

Improvements of QA processes lead to highly reproducible results with maximum uncertainty of 0.3 mm. Therefore deviations can be reliably detected at an early stage. Using these methods, irradiation of very small fields can be done with high geometrical accuracy, limiting factors are the positioning of the linear accelerator (i.e. gantry sag) and of the patient.

# Radiation therapy dosimetry in Switzerland

Damian Twerenbold  
Bundesamt für Metrologie METAS  
mail: damian.twerenbold@metas.ch

## Introduction

The current status of calibration and verification of radiation therapy dosimeters for high energy photons, electrons and soft x-rays in Switzerland is reviewed. Experimental results of absolute dosimetry using the METAS water calorimeter at the scanned proton beam at PSI are presented and the procedure for calibrating the TLD dosimeters for the planned SGSMP electron comparison in 2010 will be described.

## Methods and Results

In Switzerland, the reference ionization chambers used as dosimeters for measuring absorbed dose to water in high energy photon, electron and x-ray radiation therapy are calibrated and verified on a four year basis at METAS and IRA, following the IAEA TRS 398 protocol [1]. The primary standard for absorbed dose to water for photons is water calorimetry [2] and for absorbed dose to water for electrons it is Fricke dosimetry. The dosimeters are calibrated at the respective beam radiation quality of high energy photons and electrons using the METAS microcyclotron accelerator.

Owing to the fact that the number of proton therapy facilities is increasing, the International Commission on Radiation Units and Measurements (ICRU) has recommended in their Report nr.78 of 2007 that calorimeters should be used as primary standard for proton dosimetry or, alternatively, for verifying the proton calibration coefficients of TRS 398. METAS has collaborated with PSI in order to investigate the feasibility of water calorimetry for dosimetry of scanned proton beams [3]. Within the uncertainties limited by statistics, the measurements confirm the TRS 398 proton calibration coefficients.

The SGSMP dosimeter intercomparison planned for the year 2010 will be a TLD dosimetry comparison of the electron beam dosimetry performed at the Swiss radiation therapy centres. The TLDs provided by the Kantonsspital St.Gallen will be calibrated at METAS using Fricke dosimetry.

## References (12 pt, bold)

- [1] Absorbed Dose Determination in External Beam Radiotherapy, An International Code of Practice for Dosimetry Based on Standards of Absorbed Dose to Water, Technical Reports Series No. 398, IAEA, Vienna, 2000.
- [2] Medin, J.; Ross, C.K.; Stucki, G.; Klassen, N.V.; Seuntjens J.P.: Phys. Med. Biol. 49 (2004), pp. 4073-4086.
- [3] Gagnebin, S.; Twerenbold, D.; Bula, Ch.; Hilbes, Ch.; Meer, D.; Pedroni, E.; Zenklusen, S.: PSI Scientific Report 2006 (2007), pp. 60-61.